



저작자표시-비영리-변경금지 2.0 대한민국

이용자는 아래의 조건을 따르는 경우에 한하여 자유롭게

- 이 저작물을 복제, 배포, 전송, 전시, 공연 및 방송할 수 있습니다.

다음과 같은 조건을 따라야 합니다:



저작자표시. 귀하는 원저작자를 표시하여야 합니다.



비영리. 귀하는 이 저작물을 영리 목적으로 이용할 수 없습니다.



변경금지. 귀하는 이 저작물을 개작, 변형 또는 가공할 수 없습니다.

- 귀하는, 이 저작물의 재이용이나 배포의 경우, 이 저작물에 적용된 이용허락조건을 명확하게 나타내어야 합니다.
- 저작권자로부터 별도의 허가를 받으면 이러한 조건들은 적용되지 않습니다.

저작권법에 따른 이용자의 권리는 위의 내용에 의하여 영향을 받지 않습니다.

이것은 [이용허락규약\(Legal Code\)](#)을 이해하기 쉽게 요약한 것입니다.

[Disclaimer](#)

Ph.D DISSERTATION

# Impedance Spectroscopy Analysis for Organic Light-Emitting Diodes

유기 발광 소자에 대한  
임피던스 분광 분석 방법에 대한 연구

BY

HYUNJONG KIM

FEBRUARY 2019

DEPARTMENT OF ELECTRICAL ENGINEERING AND  
COMPUTER SCIENCE  
COLLEGE OF ENGINEERING  
SEOUL NATIONAL UNIVERSITY

Ph.D DISSERTATION

# Impedance Spectroscopy Analysis for Organic Light-Emitting Diodes

유기 발광 소자에 대한  
임피던스 분광 분석 방법에 대한 연구

BY

HYUNJONG KIM

FEBRUARY 2019

DEPARTMENT OF ELECTRICAL ENGINEERING AND  
COMPUTER SCIENCE  
COLLEGE OF ENGINEERING  
SEOUL NATIONAL UNIVERSITY

# Impedance Spectroscopy Analysis for Organic Light-Emitting Diodes

유기 발광 소자에 대한  
임피던스 분광 분석 방법에 대한 연구

지도교수 홍 용 택

이 논문을 공학박사 학위논문으로 제출함

2019 년 2 월

서울대학교 대학원

전기 정보 공학부

김 현 중

김현중의 공학박사 학위논문을 인준함

2019 년 2 월

위 원 장 : 정 윤 찬 (인)

부위원장 : 홍 용 택 (인)

위 원 : 김 수 환 (인)

위 원 : 정 재 욱 (인)

위 원 : 정 승 준 (인)

# **Abstract**

## **Impedance Spectroscopy Analysis for Organic Light-Emitting Diodes**

HYUNJONG KIM

DEPARTMENT OF ELECTRICAL ENGINEERING AND  
COMPUTERSCIENCE

COLLEGE OF ENGINEERING  
SEOUL NATIONAL UNIVERSITY

In this dissertation, the method of analyzing the characteristics of organic light-emitting diodes using impedance spectroscopy was studied. Generally, the organic light-emitting device has a structure in which organic materials necessary for light emission are thinly laminated between a TCO (Transparent Conductive Oxide) and a metal electrode. Due to chemical vulnerability of organic materials as

well as the complexity with their hetero-junction, it is necessary to investigate the characteristics of fabricated an organic light-emitting diodes in a non-destructive manner rather than destructive manner. Classically, a method of measuring a current-voltage curve using a current-voltage meter and measuring a luminescence using luminance meter is used to evaluate the characteristics of the OLEDs. However, in order to investigate details at intrinsic interface state or carrier dynamics of OLEDs, it is require measuring the impedance response under operating condition.

Impedance spectroscopy (IS) covers all impedance responses in the frequency range from milli hertz to megahertz, while focusing primarily on capacitance in solid-state electronics. This makes it possible to construct a high-resolution equivalent circuit and analyze each measured impedance. Each impedance is measured by applying ac small signal after determining the dc operating voltage. The dc operating voltage and ac small signal should be strategically chosen to describe the behavior of the device.

In Chapter 1, an overview of the Impedance Spectroscopy Analysis is introduced and the background of the impedance measurement method is explained. Then the motivation for applying this impedance analysis method to OLEDs is explained and the methods of analyzing the characteristics of OLEDs through impedance spectroscopy are discussed.

Chapter 2 reviews previously reported papers about impedance analysis methods of OLEDs and explains the limitations of these papers. In particular, the contributions of the diffusion capacitance that they underestimate are very important to prevent errors when characterizing of OLEDs. To explained diffusion capacitance the Laux & Hess model is applied. This model can explain the impedance response to the residual current and even demonstrate the negative capacitance phenomenon. The analytical results using the Laux & Hess model[1] were verified to describe the characteristics of the OLEDs during operation and an approximate and fitting process for the analytical method of this model is proposed.

In Chapter 3, ITO/a-NPD[N,N'-Bis(naphthalen-1-yl)-N,N'-bis(phenyl)-2,2'-dimethylbenzidine]/Alq3[Tris-(8-hydroxyquinolato)aluminum]/LiF/Al type OLEDs were fabricated and investigated using the improved impedance analysis method proposed in Chapter 2. First, according to the structural (thickness) change, the physical analysis was performed quantitatively by changing the impedance response. The measured impedance at high frequencies represents the interface and bulk characteristics in the OLEDs, and the impedance at low frequencies explains the dynamics of carriers in the OLEDs.

In addition, the impedance changes due to OLEDs degradation are analyzed. Using the proposed Impedance Spectroscopy Analysis method in this paper, the

origin of degradation can be accurately and effectively separated from the state change of the interface and the bulk. The results strengthen the existing interpretation of the interface trap effect of HTL/EML and showed that it can be traced with the rate of change of the extracted impedance value.

Chapter 4 briefly introduces the program tool for analyzing the OLEDs used in this paper, and attached an appendix for derived the formula. And I will discuss the possibility of applying this Impedance Spectroscopy Analysis to mass products industry in the future.

**Keywords:** OLEDs, Impedance Spectroscopy Analysis (IS), Equivalent Circuit Modeling, Degradation, Negative Capacitance, Diffusion Capacitance

**Student Number:** 2014-30311



# Contents

<b>Abstract</b> .....	<b>i</b>
<b>Contents</b> .....	<b>v</b>
<b>List of Figures</b> .....	<b>viii</b>
<b>List of Tables</b> .....	<b>xiii</b>
<b>Chapter 1 Introduction</b> .....	<b>1</b>
1.1 Motivation.....	1
1.1.1 History of Organic Light Emitting Diodes .....	6
1.1.2 OLEDs Hetero Structures.....	8
1.1.3 OLEDs life time .....	11
1.2 Materials.....	15
1.2.1 Alq <sub>3</sub> .....	16
1.2.2 HAT-CN .....	17
1.2.3 $\alpha$ -NPB .....	18
1.2.4 DCM.....	19
1.3 Equipment & Instrument.....	20
1.3.1 Thermal Evaporator.....	20
1.3.2 Impedance Measurement Equipment for OLEDs .....	23
<b>Chapter 2 Analytic Theory of OLED Impedance Spectroscopy</b> .....	<b>26</b>

2.1 Problems of Previous Reported Impedance Spectroscopy to extract parameter on OLEDs .....	28
2.2 Complex Capacitance Concepts for IS.....	31
2.2.1 $\epsilon$ ARC .....	31
2.2.2 ZARC .....	34
2.2.3 Negative Capacitance.....	38
2.2.4 Equivalent circuit strategy for OLEDs .....	43
2.3 Theory .....	45
2.3.1 Impedance Spectroscopy.....	45
2.3.2 Small-Signal Model.....	49
2.3.3 Complex Plane Diagram .....	51
2.3.4 Equivalent Circuit Modeling.....	54
2.3.5 Superposition of various Impedance Component.....	58
2.3.6 Debye relaxation plot( $\epsilon$ -plot) .....	60
2.4 How to extract reasonable parameter from impedance spectroscopy.....	64
<b>Chapter 3 Experiments .....</b>	<b>71</b>
3.1 Thickness modification OLEDs .....	72
3.1.1 Analysis of the Interface of the OLEDs .....	76
3.1.2 Analysis of the Carrier Distribution of OLEDs.....	78
3.2 Thickness ratio modification.....	80
3.2.1 Relation between efficiency and M-plot .....	82
3.3 DCM doping ration Modification.....	84
3.3.1 Correlation between Current-Voltage-Efficiency and Impedance Response .....	84
<b>Chapter 4 Discussion .....</b>	<b>90</b>
4.1 Consideration of Effects of Interface Properties .....	90
4.2 Consideration of Effects of Bulk properties .....	92

4.3 Negative Capacitance relation with efficiency analysis .....	93
4.4 Mobility Measurement Using Impedance analysis .....	96
<b>Chapter 5 Conclusion .....</b>	<b>101</b>
<b>Appendix .....</b>	<b>109</b>
<b>Bibliography .....</b>	<b>116</b>
<b>Publications.....</b>	<b>122</b>
<b>초 록 .....</b>	<b>127</b>

# List of Figures

Figure 1.1 A dateline highlighting 30 key moments in the evolution of OLEDs[8].....	7
Figure 1.2 Schematic hetero-structure of conventional OLEDs. The abbreviations represented by each organic layer are as follows; HTL : Hole Injection Layer, HTL : Hole Transport Layer, EML : Emissive Material Layer, ETL : Electron Transport Layer, EIL : Electron Injection Layer.....	10
Figure 1.3 Energy band diagram of conventional OLEDs.....	11
Figure 1.4 Degradation process of OLEDs.....	13
Figure 1.5 (a) SEM images of defected ITO after diode fabrication and testing in atmosphere condition and (b) SEM images of fully defected ITO due to voltage[17].....	14
Figure 1.6 Optical image of dark-spot formation and growth (a) before stress (b) after 14.5 hours (c) after 78.5 hours; (d) voltage drop; (e) luminance drop; (f) decrease of current efficiency of the OLEDs with the structure ITO(150nm)/ a-NPB(60nm)/Alq3(70nm)/LiF(5nm)/Al(100nm) in constant current which has been measured in atmosphere condition .	15
Figure 1.7 The chemical structures of Alq <sub>3</sub> .....	16
Figure 1.8 The chemical structures of HAT-CN .....	17
Figure 1.9 The chemical structures of $\alpha$ -NPB .....	18
Figure 1.10 The chemical structures of DCM.....	19
Figure 1.11 A thermal evaporator located at the Inter-University	

Semiconductor Research Center of Seoul National University. ....	22
Figure 1.12 Schematic diagram of completed OLEDs. Two shadow masks were used for organic material (middle fluorescent square pattern) and for electrode (gray pattern). ....	23
Figure 1.13 Measurement process for Impedance Analysis .....	25
Figure 2.1 Example of the capacitance analysis of (a) MOS (b) diode (source from Máté Jenei lecture note at Aalto University) .....	27
Figure 2.2 Frequency vs Capacitance plot and their equivalent circuit model reported by Nowy et al. [38].....	30
Figure 2.3 Cole-cole plot and their equivalent circuit model reported by Pingree et al. [29].....	30
Figure 2.4 (a) Time dependence of the polarization, (b) Debye equivalent circuit (c) complex plane plot of the complex permittivity .....	32
Figure 2.5 (a) Distribution of relaxation times .....	33
Figure 2.6 Equivalent circuit when interface is formed perpendicular to current direction (a) And the reactance value (b) and complex plane plot of $Z(c)$ for the three components on the left side of the equivalent circuit (d).....	36
Figure 2.7 Comparison of Equivalent Circuit Representation of eARC (a) and Equivalent Circuit Representation of ZARC. It shows that according to changes in $\alpha$ and $\psi$ value how to change CPE value. ....	37
Figure 2.8 The one-dimensional double layered OLEDs, The depletion width is $W = w_{HTL} + w_{EM}$ . The total diode length is $c+a$ . Hole is injected at $-a$ and electron is injected at $c$ . $b$ is chosen to be the location where $n(b)=p(b)$ .....	39
Figure 2.9 The charge injected into the diode affects the depletion capacitance and diffusion capacitance. At this time, the charges that are discharged to the outside in the unit time and the recombination charge cause the decrease of the capacitance.....	42

Figure 2.10 Graph of C-V characteristics of OLEDs.....	42
Figure 2.11 Energy band diagram which explain the negative capacitance phenomenon of OLEDs .....	43
Figure 2.12 Equivalent circuit model combining charge transfer model and interface model .....	44
Figure 2.13 Capacitance graph of OLEDs. The role of each equivalent circuit model is explained by dividing the area. ....	45
Figure 2.14 Number of journal articles on impedance spectroscopy identified on October 3, 2016 using <a href="http://www.sciencedirect.com/search">http://www.sciencedirect.com/search</a> engine In Elsevier(Journal article only).....	47
Figure 2.15 A brief history summary of Impedance spectroscopy.....	47
Figure 2.16 Schematic flow process for impedance spectroscopy measurement process .....	48
Figure 2.17 Complex Plane Diagram of a complex equation(2.3.6). The diameter of the semicircle is determined by the reciprocal values of A and B, and the position of the center of the semicircle is determined by the sign of A and B.....	53
Figure 2.18 Complex plane of Z and Y of resistance and capacitance circuits.....	55
Figure 2.19 Complex plane of Z and Y of resistance and capacitance circuits.....	56
Figure 2.20 Cole-cole plot of impedance(Z) of parallel circuit compound with resistance and capacitance. ....	56
Figure 2.21 Real(blue line) and imaginary(red dot line) value of impedance .....	57
Figure 2.22 Superposition of the impedance. Impedance response with a parallel combination of capacitance and capacitance connected in series. The shape of the impedance response appears as overlapping sub-circles and the parameters can be extracted in the minimum error range using the complex nonlinear least squares (CNLS)	

algorithm[50].	60
Figure 2.23 Time dependence of the polarization after the application of an electric field to an insulator at $t=0$ [46].	62
Figure 2.24 Frequency response of dielectric mechanisms. (ref : Application Note 1217-1, "Basics of measuring the dielectric properties of materials," Hewlett Packard literature number 5091-3300E, 1992.)	62
Figure 2.25 The Debye equivalent circuit.	63
Figure 2.26 Complex plane plot of the frequency dependence of the complex permittivity modeled by the circuit of Figure 2.1.2.[46].	63
Figure 3.1 Schematic diagram of OLEDs Structures used in this section .	73
Figure 3.2 I-V-L characteristic of the OLEDs.	74
Figure 3.3 Current Efficiency and Power Efficiency characteristic of the OLEDs	74
Figure 3.4 Response of Complex plane of M plot	75
Figure 3.5 Response of Complex capacitance of $\epsilon$ plot plain.	78
Figure 3.6 Capacitance response of the OLEDs with Frequency Sweep....	80
Figure 3.7 Schematic diagram of OLEDs Structures used in this section .	81
Figure 3.8 M-plot representation for each device. It can be seen that the ratio of the thickness ratio to the diameter of the sub-semicircle coincides.	83
Figure 3.9 Schematic diagram of OLEDs Structures used in this section .	86
Figure 3.10 Microscope image of the DCM doped OLEDs	86
Figure 3.11 CIE x, y value of the chromaticity diagram DCM doped OLEDs	87
Figure 3.12 I-V-L characteristic of the DCM doped OLEDs.	87
Figure 3.13 Current Efficiency and Power Efficiency characteristic of the DCM doped OLEDs	88
Figure 3.14 C-V characteristic of OLEDs (a) not doped (b) doped near HTL/EML interface (c) intermediate EL (d) near cathode	88

Figure 3.15 The structure of the device is maintained through the M-plot characteristics, but it can be seen that different layers appear in the intermediate frequency band. (a) Not doped (b) doped near HTL/EML interface (c) intermediate EML (d) near cathode.....	89
Figure 4.1 C-V graph showing the decrease in fixed charge of organic / organic interface at low frequency (100Hz) and the resulting decrease in efficiency .....	91
Figure 4.2 Capacitance response at 2V near turn on voltage. Rs can be read at transient frequency ( $f_r$ ).....	92
Figure 4.3 OLEDs of the same structure made of the same process with different electrical properties. The M-plot shows that the device structure is the same, but the efficiency is different. This can be understood in advance through the low-frequency analysis of the negative capacitance value.....	95
Figure 4.4 Mobility extraction from SCLC current characteristics. By adding a small signal to the SCL current, mobility can be obtained from the minimum value of the admittance value .....	96
Figure 4.5 Maximum frequency per voltage for mobility extraction using $\Delta G$ method.....	97
Figure 4.6 Mobility extraction value using $\Delta G$ method. Mobility proportional to square of field extracted.....	98
Figure 4.7 The lag phase shift of the negative capacitance.....	100
Figure 5.1 An equivalent circuit model and extraction strategy for which frequencies should be observed in frequency - capacitance graph ...	106
Figure 5.2 The voltage and frequency range that should be measured to determine the characteristics of OLEDs. The length of the ellipse tells the sweep range, which means that the longer the ellipse, the larger the voltage range must be swept.....	107



# List of Tables

Table 2.1 Relations Between the Four Basic Immittance Functions <sup>a[46]</sup> .....	48
Table 3.1 Information on fabricated OLEDs .....	82
Table 4.1 The average transient time value and the composite OLED SCLC mobility .....	100
Table 5.1 The effect of degradation, the observation method and the domain which easily informs characteristic according to degradation factor	108

# Chapter 1

## Introduction

### 1.1 Motivation

In display market, over the past several decades, a variety of technologies have emerged and disappeared and numerous technologies still engage in a heated competition in display market day by day. New emerging technologies are applied to the industrial field much faster than in the past to meet needs of sophisticated and demanding consumers.

After the widespread use of liquid crystal display (LCD) technology, which has enjoyed an era beyond CRT (Cathode Ray Tube) technology, OLEDs (organic light emitting diodes) technology has emerged. First practical OLED device was

built by Ching W. Tang and Steven Van Slyke at Eastman Kodak in 1987. [2] They succeeded in lowering operating voltage and improving efficiency using a very thin multilayer structure with hole transport layer (HTL) and electron transporting layer (ETL), which contributes to the application of OLED technology to displays. OLED displays can be easily fabricated into thin films which emit themselves, which become a major cause that OLED technologies lead the display industry in these days. OLEDs can be fabricated onto any suitable substrate by thermal evaporation, by an inkjet printer or by screen printing and have greater contrast ratio, wider viewing angle, very fast response time compared to LCDs. However, due to the low chemical stability against environment (water, air and etc.) and stimuli (electric, heat, interactions between materials and etc.), problems of degradation of lifetime and efficiency have been steadily pointed out.

The efforts of many researchers have led considerable advances in OLEDs with higher efficiency and longer lifetime compared to the earlier days of the OLED display industry, and as competition among the display companies getting fiercer, the small differences in the results of the research have had a significant impact on the price competitiveness of the market. In addition, higher performance OLED displays are now required to cope with next generation displays, for example applications that will be integrating OLED in the future include very large scale TV, clothing with embedded displays, augmented reality/virtual reality (AR/VR) devices,

helmets, wristbands, jewelry/watches, lighting, and automotive infotainment systems.

These researches about efficiency and lifetime include the improvement of organic materials for increasing the efficiency and stability of luminescent, the development of the structural stacking optimization technology to control the hole-electron charge balance, as well as the development of sealing technology. Among the above, because the sealing technology is a technique for minimizing the external environmental impact, so those who research the device itself are more interested in the first and second things mentioned above. The problem is that as a result of individual studies, even if advanced materials are developed or the optimized structure is designed, the actual completed OLED is a laminate structure of organic thin films, and therefore, the interfacial physics It is very sensitive to chemical changes as well as the influence of numerous environmental variables in the process, and the field applied to the OLED during driving. Therefore, the characteristics of the combined OLED often have a different result than the predicted value. In order to investigate the lifetime characteristics, it is necessary to explain the continuous degradation process inside the device. If the inside and the outside of the OLED are investigated during the degradation process, the influence of the device damage and degradation of the device Since the influences can only act together, it is difficult to explain the process of degradation. Therefore, most studies on degradation to date

have been limited to visual inspection of external devices such as changes in I-V-L characteristics and efficiency, or changes in luminescence area over time for finished devices. This approach is very simple, but provides only very limited information on the complex electrochemical interactions taking place at the interface and inside of a stacked OLED. Therefore, we need a technique to evaluate the inside of the device in a non-destructive manner. In this dissertation, we analyze the OLED by introducing Impedance Spectroscopy as a non-destructive method.

Measuring Impedance Spectroscopy is simple. All impedance measurements in this experiment were performed on OLEDs fabricated using Agilent E4980. Each OLED has an alternating current signal of 50 mV under a fixed dc bias. The impedance response was recorded while sweeping the frequency from 20Hz to 2MHz. The dc bias was selected from -5V to the forward voltage which not severe stress on OLEDs, and was selected tightly, especially near the turn-on. The impedance measured in this way was analyzed with the current-voltage-luminance graph measured by HP4155C.

Impedance response can be an advantage or a disadvantage that it is very sensitive to changes in the state of OLEDs. That is, unless external environmental factors are completely controlled, the impedance data is easily contaminated by the increase of parasitic components. In addition, OLEDs manufactured in laboratories

have problems in uniformity and stability. Therefore, it is necessary to repeatedly measure as many samples as possible to obtain the most reliable data, and an encapsulation process is necessary to eliminate the deterioration factor from the outside of the OLEDs. In addition, although the equivalent circuit model of impedance is presented in a wide variety of existing papers, it is necessary to establish a more fundamental physical model because the equivalent circuit model due to different operation according to voltage is less accurate. For this analysis, it is necessary to test OLEDs of various structures, and it is aimed to remove the trivial variables of the impedance of the OLEDs of the same structure and establish an equivalent circuit model by finding reliable information. This study not only presents a relatively simple method for evaluating OLED performance, but it is also suitable for supporting physicochemical analysis through OLED electrical analysis, which further expands the OLED industry and is complex and mass-produced.

### **1.1.1 History of Organic Light Emitting Diodes**

In the early 1950, electroluminescence in organic materials at high alternating voltages was first observed by André Bernanose[3-5]. After a decade of this appearance, Martin Pope reported that the injection of electrons and holes into the electrode contacts is closely related with the work function differences between electrodes and organic materials and first observed direct current (DC) electroluminescence[6]. In 1965, double injection recombination electroluminescence, which is the basis concept for current OLED driving way, reported by W. Helfrich and W. G. Schneider for the first time using hole and electron injecting electrodes[7]. Finally, in 1987, Ching W. Tang and Steven Van Slyke at Eastman Kodak built two-layer OLEDs with separate hole transporting and electron transporting layers to lower operating voltages and improve efficiency[2], and which structure is now widely employed in state-of-art OLED displays technology. Ching W. Tang's research means how to arrange materials with different work functions lead to determine the performance of the device, so that his study have been a great inspiration for many material development researchers and process development engineers and led to explosive growth in the OLED displays industry.

Figure 1.1 summarizes a dateline highlighting 30 key moments in the

evolution of OLEDs [8].

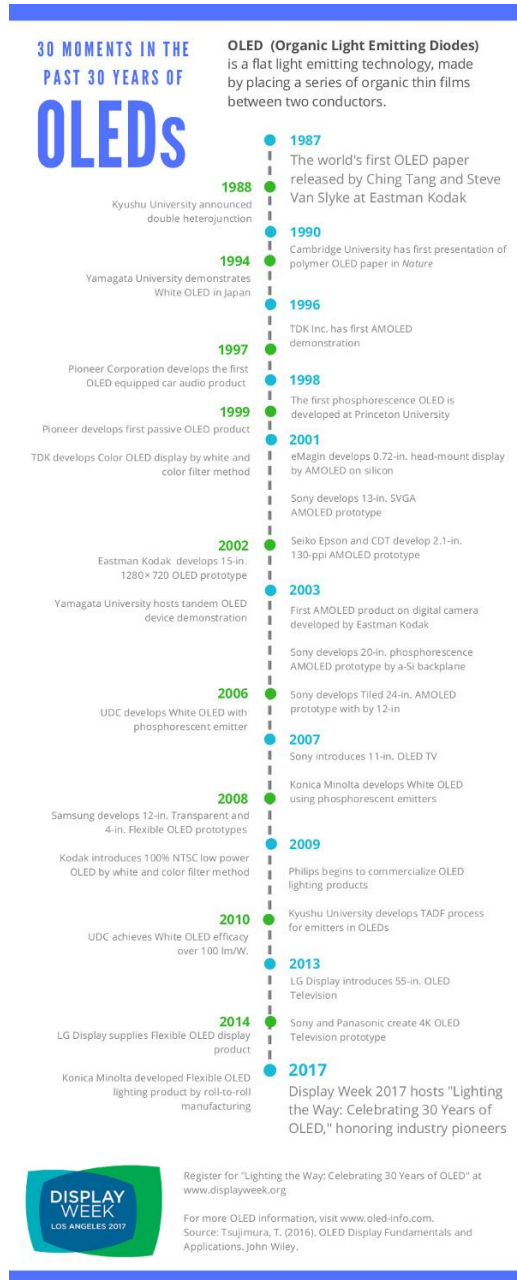


**Figure 1.1** A dateline highlighting 30 key moments in the evolution of OLEDs[8]



## 1.1.2 OLEDs Hetero Structures

As mentioned above, conventional OLEDs have a structure in which organics having different work functions and band gap are stacked in a sandwich manner by the efforts of Ching W. Tang. The advantage of this structure is that the holes injected from the anode and electrons injected from the cathode can be easily formed excitons and recombined only at the target organic layer having the desired band gap energy. Choosing the appropriate materials and structures is fundamental to design high performance OLEDs with high efficiency at low voltages. Therefore, it is necessary to understand the concept of solid state band theory in order to produce OLEDs suitable for the purpose.

In general, ITO (Indium Thin Oxide), whose work function is in the range of 4.7 to 5.2 eV[9], is preferred so that holes can be well injected at the Homo (Highest Occupied Molecular Orbital) level of the organic material. However, since ITO requires a high-temperature and high-vacuum sputtering process, PEDOT: PSS (poly (3,4-ethylenedioxythiophene) polystyrene sulfonate), which is a conductive polymer capable of low temperature treatment, can be used. And Li, Ca, and Ba having a small work function should be selected as the cathode, but they are coated on aluminum having a relatively large work function because of high reactivity. Figure

1.2 depicts the Schematic hetero-structure of OLEDs.

The organic material should be selected to reach the EML (Emitting Material Layer) at the same rate as the holes and electrons injected from the anode and cathode. To make realize this, it is necessary to adjust the energy barrier difference of each organic material appropriately. As can be seen in Figure 1.3, the HOMO or LUMO level should be designed to accept carriers in adjacent layers sequentially, and an additional blocking layer may be needed to ensure that carriers arriving at the EML have enough time to form excitons and allow recombination.

Of course, precisely aligning the properties of OLEDs is very hard because material measurement information (i.e., work function, energy band, defect distribution, controlled environment factors and etc.) cannot be perfectly accurate. Furthermore, it is impossible to design OLEDs with optimal conditions even if all of the material information is known correctly. There are factors that are difficult to predict with respective material information alone. This is due to the electrochemical correlations that occur at the interfaces due to the interactions in the hetero-junction of organic materials. There are many unexpected interfacial traps at the hetero-junction boundary, and dipoles can be formed by van der Waals force between molecules and electrode [10-12]. This can vary greatly depending on process conditions and can lead to unexpected behavior of OLEDs.

In this paper, we focus on analyzing the operation of the device which is difficult to predict due to the existence of many hetero-junctions of organic matter through the impedance analysis method. From the information that can be derived from the impedance response of the device, to understand the operation mechanism of the system.

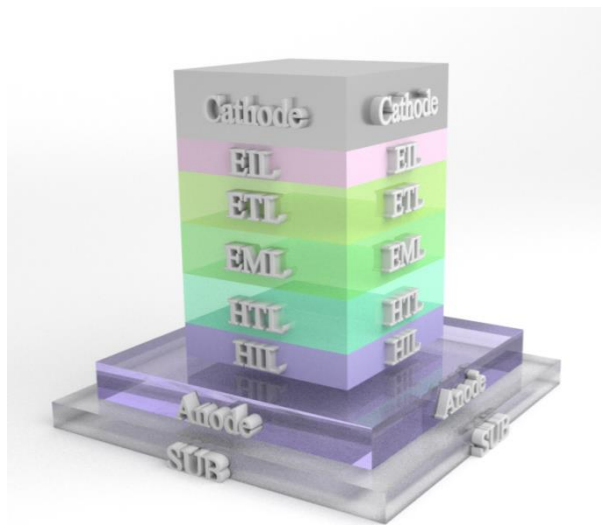


**Figure 1.2** Schematic hetero-structure of conventional OLEDs. The abbreviations represented by each organic layer are as follows; HTL : Hole Injection Layer, HTL : Hole Transport Layer, EML : Emissive Material Layer, ETL : Electron Transport Layer, EIL : Electron Injection Layer

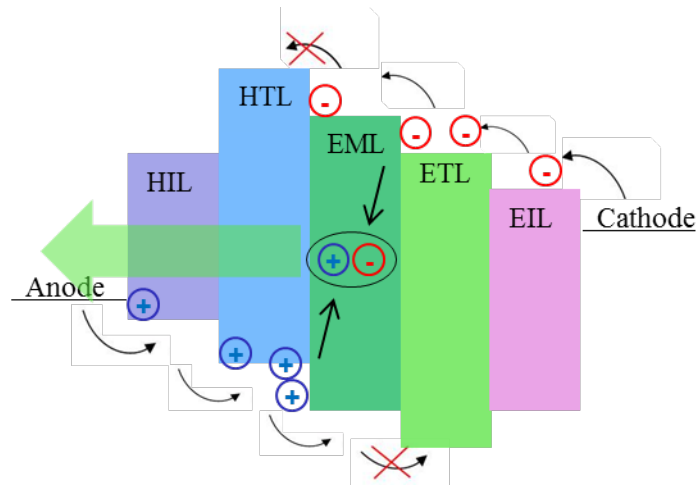


**Figure 1.3** Energy band diagram of conventional OLEDs.

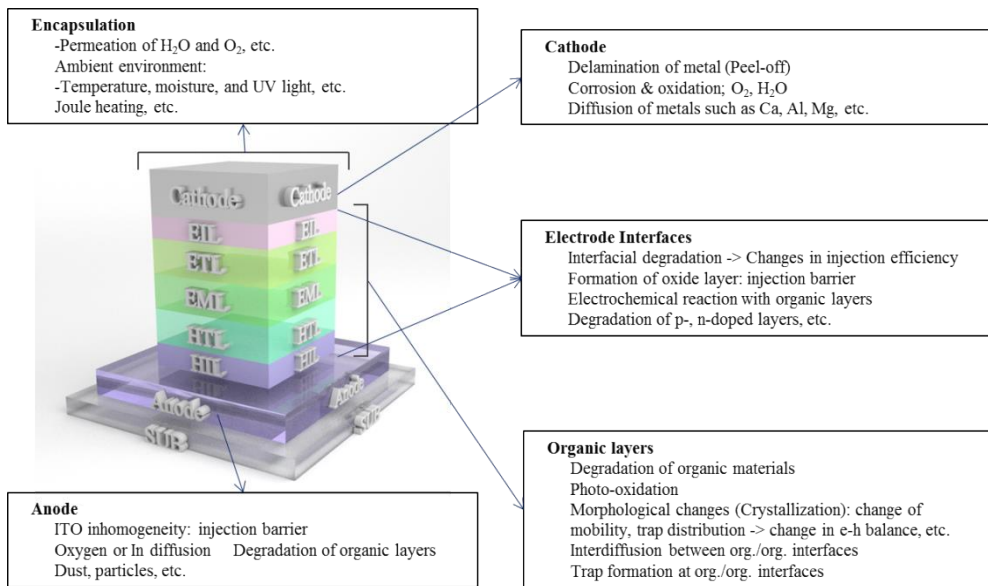
### 1.1.3 OLEDs life time

OLEDs are rapidly applied to the display industry because they can be fabricated into a thin film structure using thermal deposition or spin coating, which are relatively simple processes, and can display a desired color at low driving voltage by controlling the work function between the energy band differences of the materials. However, the use of organic material compounds is itself a disadvantage. Because organic material devices easily react with moisture, oxidation, and heat, the OLEDs fabricating process must be elaborately handled in a controlled atmosphere with very low oxygen and moisture levels and an encapsulation process is absolutely required after manufacturing OLEDs products. Even if the sealing

process is perfect, although that is impossible, OLEDs materials, electrodes and their interfaces may be degraded due to electrical stress during operation. These drawbacks not only shorten the life time of the display but also cause blurring which degrades uniformity of OLEDs display. This disadvantage has been a vital weakness when OLEDs compete with competition displays. Therefore, for OLED researchers, efforts to slow down the degradation process were the most challenging subject.

OLEDs degradation factors can be divided into environmental factors and intrinsic factors. Environmental factors are caused by the light, oxygen and moisture of the OLED. Organic materials in the excited state readily react with oxygen and moisture, creating a new chemical structure and degrading the emission properties in these regions. Without sealing process, OLEDs are exposed to atmospheric conditions directly, their lifetime is limited. Operating the OLEDs in air reduces the EL intensity by 99% in about 150 minutes [13]. Intrinsic factors are focus in change of chemically formation. Emissive species can be removed from devices if the excited states are chemically irreversible. It can act as quench centers for excitons formed on nearby unaffected site. Crystallization of organic materials is another intrinsic factor that degrades the organic layer which has the low glass transition temperature because of heat generated from the injection barrier [14]. Organic materials have a weaker and weaker molecular bond than non-organic materials, so ion migration is easier. Moving ions such as Al, Ca, Sn, and Mg that penetrate from

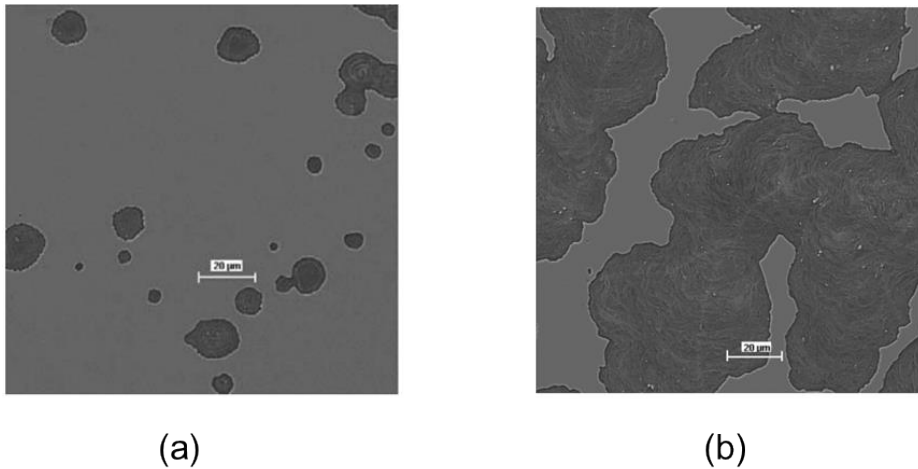
the electrode affect the effective field inside the device [15]. OLEDs degradation can be identified by measuring the amount of decrease in current at a constant biased voltage versus time or by measuring the decrease in luminance at a constant current and decrease of the emissive device area due to the evolution of the non-emission region or the dark spots can be identified visually [16]. In Section 1.1.2, we have mentioned that it is possible to grasp the state of the interface, which cannot be predicted, from the hetero-junction structure of OLEDs. At the same time, as mentioned here, we will examine the change of the interface according to the degradation through the impedance analysis.



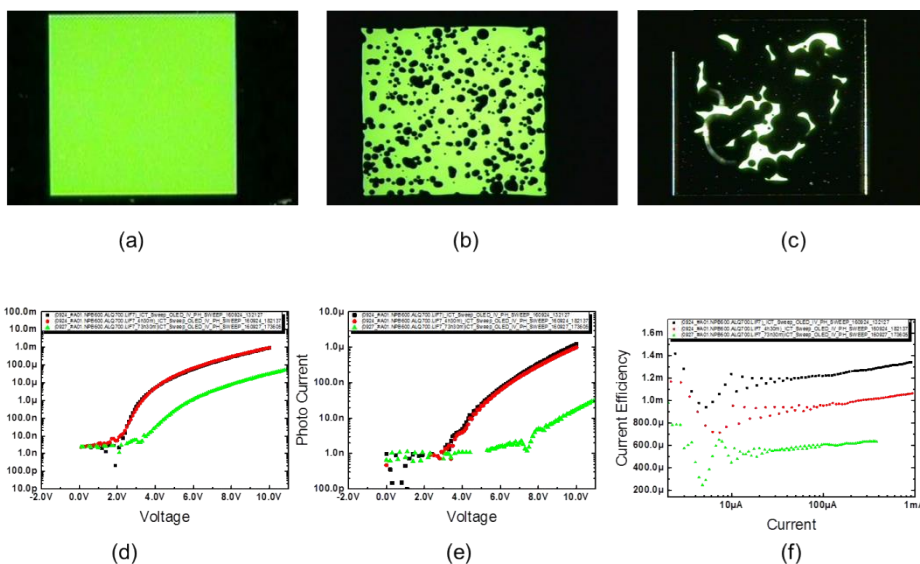
**Figure 1.4** Degradation process of OLEDs

Figure 1.4 shows the degradation process of OLEDs in an easy-to-view manner.

In addition, Figure 1.5 shows the difference in the state of the electrode (ITO) when the air is simply exposed and when the voltage is applied. And the optical image of the emitting OLEDs and its voltage drop under severe conditions are shown in Figure 1.6.



**Figure 1.5** (a) SEM images of defected ITO after diode fabrication and testing in atmosphere condition and (b) SEM images of fully defected ITO due to voltage[17]



**Figure 1.6** Optical image of dark-spot formation and growth (a) before stress (b) after 14.5 hours (c) after 78.5 hours; (d) voltage drop; (e) luminance drop; (f) decrease of current efficiency of the OLEDs with the structure ITO(150n)/ a-NPB(60n)/Alq3(70n)/LiF(5n)/Al(100n) in constant current which has been measured in atmosphere condition

## 1.2 Materials

This section briefly describes the material used in this paper and why it was selected. The best known OLED materials and structures were chosen to closely measure the varying impedance depending on the type of OLEDs, and each material's information was used to describe the equivalent circuit and charge



dynamics.

### 1.2.1 Alq<sub>3</sub>

Tris(8-hydroxyquinoline)aluminum(III)(Alq<sub>3</sub>) is green-light emitting and electron transport material for OLEDs [18]. Alq<sub>3</sub> is a material announced by Kodak in 1987 and its luminous efficiency is more than 15Cd/m<sup>2</sup>. It was so historic material that it was used in the first reported bi-layer OLEDs of Ching W. Tang [2], and it increased chemical stability with methyl derivatives [19]. In this paper, Alq<sub>3</sub> was chosen for the ETL and EML layers.

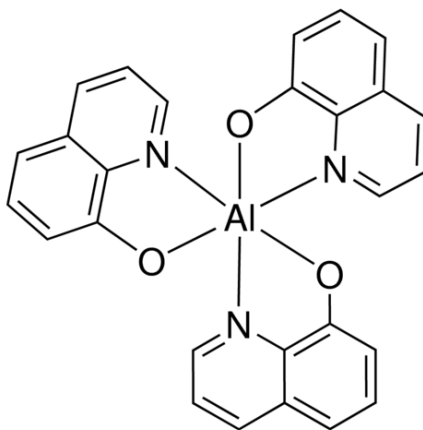


**Figure 1.7** The chemical structures of Alq<sub>3</sub>

### 1.2.2 HAT-CN

1,4,5,8,9,11-hexaazatriphenylene-hexacarbonitrile (HAT-CN) is hole injection layer material that changes the electrical properties of electrodes due to its strong electron-withdrawing property[20]. In this paper, HAT-CN were used for the purpose of measuring the efficiency decrease because the electron-hole balance in of Alq3-based OLEDs is worsen when the hole injection characteristics increase

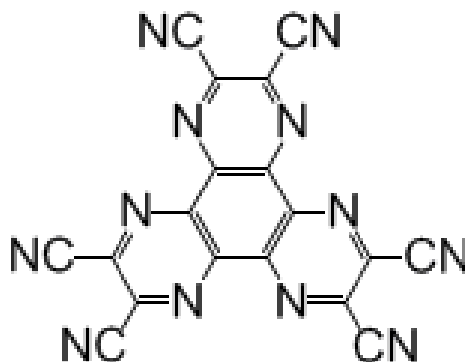


**Figure 1.8** The chemical structures of HAT-CN

### 1.2.3 $\alpha$ -NPB

2,2'-Dimethyl-N,N'-di-[(1-naphthyl)-N,N'-diphenyl]-1,1'-biphenyl-4,4'-diamine ( $\alpha$ -NPB) is hole transporting material for OLED devices.  $\alpha$ -NPB is also a material announce by Kodak and used in the first reported bi-layer OLEDs of Ching W. Tang [2]. This material is also used as a high performance host material for OLEDs devices showing increased device efficiency. Maximum luminance efficiency was 4.4 cd/A at 9 V for the fluorescent device and 24.4 cd/A for phosphorescent device[21].

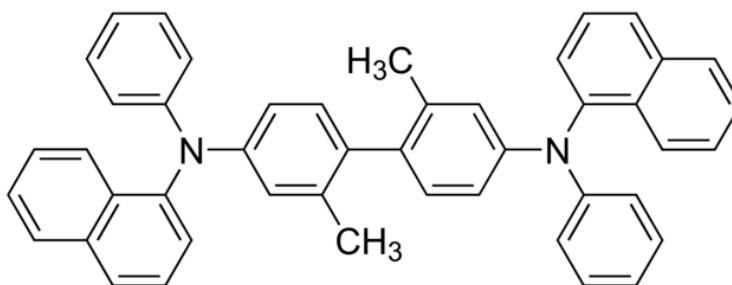


**Figure 1.9** The chemical structures of  $\alpha$ -NPB

## 1.2.4 DCM

In 1989, Dr. Tang reported that when two light emitting materials were mixed and deposited, the device efficiency increased and the color change occurred [22]. The material doped in  $Alq_3$  is 4-(Dicyanomethylene)-2-methyl-6-(4-dimethylaminostyryl)-4H-pyran (DCM). This material was used in this paper to investigate the change in impedance due to the doping of OLEDs.

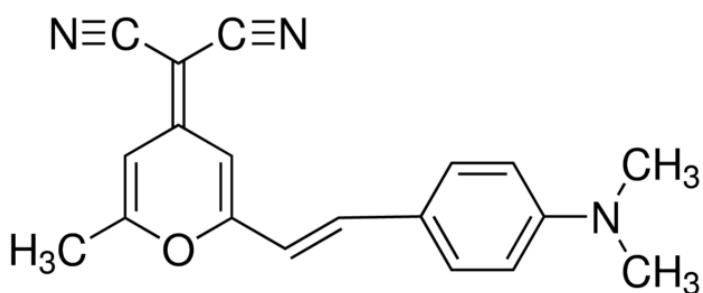


**Figure 1.10** The chemical structures of DCM

## 1.3 Equipment & Instrument

### 1.3.1 Thermal Evaporator

OLEDs were fabricated using a thermal evaporator at the Inter-University Semiconductor Research Center of Seoul National University (ISRC) (Figure 1.11). This thermal evaporator was donated to Samsung Display in 2014. The globe box filled with nitrogen is installed on the side, and the substrate and the organic material can be prepared and inserted into the loading chamber from globe box. There is an O<sub>2</sub> plasma generator which can cleaning ITO surface of a commercial glass substrate which ITO was patterned by 150nm thick. Each material is loading on a crucible at deposit chamber and is deposited sequentially using deposition software which programed the deposition sequence. And the organic material is deposited in a desired thickness automatically according to the information about tooling value in advance. Figure 1.11 shows the schematic diagram of completely fabricated OLEDs. ITO is coated at 150 nm on the center of the glass substrate, and PR is coated so that only 4 mm<sup>2</sup> areas of pixels can be contacted with organic material. After the surface treatment of ITO using O<sub>2</sub> plasma, the organic material is deposited only in the square

region of 100mm<sup>2</sup> through the shadow mask, and finally the cathode and the anode line are deposited at the same time. All deposition processes were performed less than 10<sup>-7</sup> torr and at room temperature. After all the deposition was done, encapsulation of OLEDs was performed in a globe box filled with nitrogen. A small glass cup with a desiccant sticker was placed over the OLEDs fabricated for encapsulation and an epoxy-based adhesive containing ultraviolet curing agent was used. In-capped OLEDs were exposed to the ultraviolet light using UV lamp with 365nm wavelength for about 15 minutes to cure the adhesive.



**Figure 1.11** A thermal evaporator located at the Inter-University Semiconductor Research Center of Seoul National University.

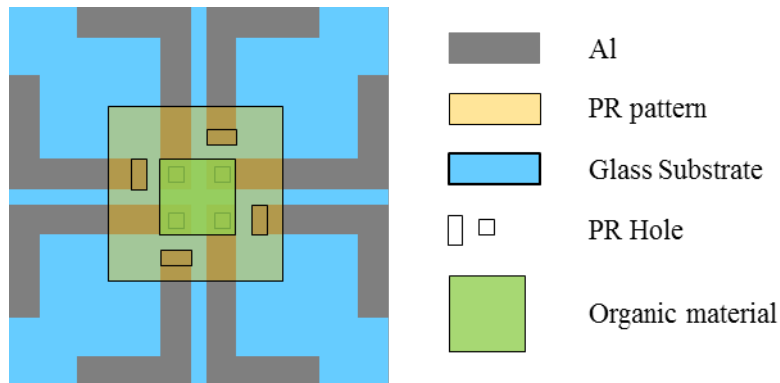


**Figure 1.12** Schematic diagram of completed OLEDs. Two shadow masks were used for organic material (middle fluorescent square pattern) and for electrode (gray pattern).

### 1.3.2 Impedance Measurement Equipment for OLEDs

The measurement system was designed to measure the impedance for OLEDs of different thicknesses and materials. OLEDs measurements illustrate the method of measuring the impedance of OLEDs in Figure 1.13. First, after the fabrication of the OLEDs, the spectrum and efficiency of the OLEDs are measured by synchronizing the Keithley 2400 SourceMeter with the Minolta-CS-2000 spectroradiometer to evaluate the performance of the OLEDs. Second, using the HP 4155B connected to the probe station to minimize external noise



I-V-L characteristics were measured. At this time, the luminance was measured using a photodiode capable of measuring only the relative value. Third, the impedance was measured while sweeping the frequency up to 20 Hz -2 MHz using the Agilent E4980 connected to the probe station. Each impedance was measured while varying the DC voltage according to the operating range of the OLEDs, and the ac signal was 50mV (rms) was used. Fourth, a constant current drive was performed using a Polaronix M6000. Impedance measurements of OLEDs were periodically re-measured at arbitrary time intervals, and the change in impedance of OLEDs due to degradation could be monitored.

The final result is to extract each parameter through a program that minimizes the error by applying the CNLS algorithm.

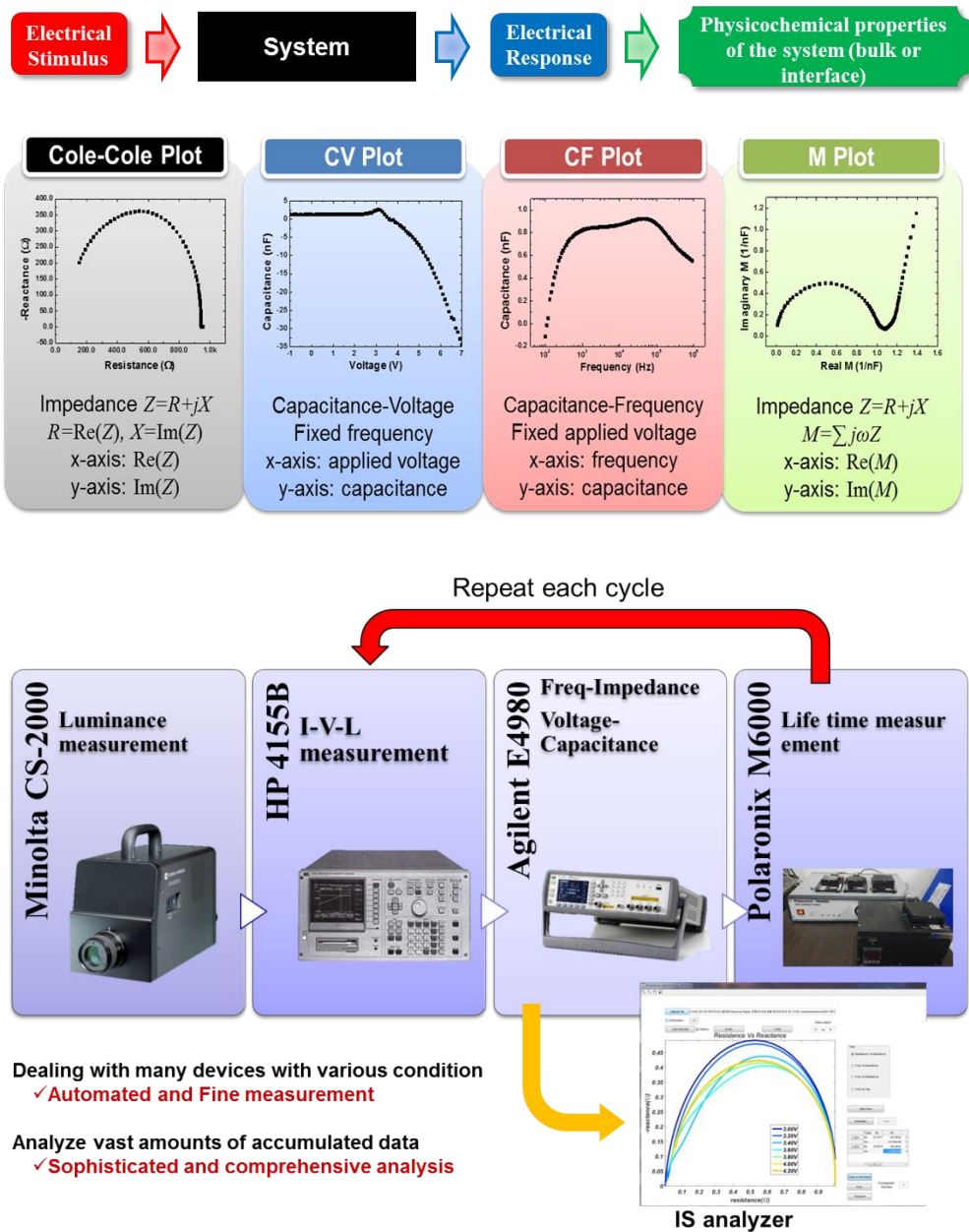


Figure 1.13 Measurement process for Impedance Analysis

## **Chapter 2**

# **Analytic Theory of OLED Impedance Spectroscopy**

As mentioned in Chapter 1, impedance analysis can be the most powerful method of characterizing completed OLEDs. Classic I-V-L characterization methods or efficiency measurements do not accurately convey OLEDs' interface or bulk information.

Impedance spectroscopy for OLEDs can be approached in a similar way to the small signal analysis model already used in solid-state physics, which is well known in the semiconductor field. For example, MOS capacitance analysis is powerful enough to provide a theoretical foundation for MOSFETs [23]. By using this method, the state density of the interfacial trap between the insulator and the active semiconductor can be known [24], and the flat band voltage and threshold voltage

can be estimated more accurately compared with the I-V curve[25]. The diode small signal analysis model can know the doping profile information of the diode through the capacitance value at both ends of the diode[24], and also can calculate the power loss in the integrated circuit in terms of system integrate(SI), or find out the allowable limit frequency of the system [26].

OLEDs behave like MOS (Metal Oxide Semiconductor) in certain ranges because they are a diode and have a hetero-junction. Therefore, it can be said that it corresponds to both of the above mentioned. However, the methodological approach of measuring the impedance of OLEDs is not fully understood and the way of analysis is different according to the voltage applied to both ends.

Therefore, in this chapter, we try to propose the impedance analysis method of OLEDs analytically.

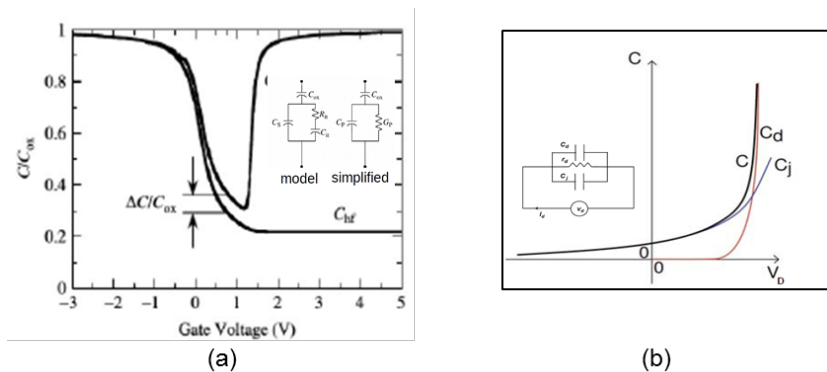


**Figure 2.1** Example of the capacitance analysis of (a) MOS (b) diode (source from Máté Jenei lecture note at Aalto University)

## **2.1 Problems of Previous Reported Impedance Spectroscopy to extract parameter on OLEDs**

Since the interfacial states of OLEDs and the charge transport in bulk have a significant influence on the performance of OLEDs, many researchers have attempted to interpret the completed OLEDs through impedance. However, the impedance response of OLEDs is very complex and has very different active properties depending on the driving voltage, which make it difficult to obtain noble results. Moreover, OLEDs are very unstable when in caps are not perfect. Each researcher has a similar or different interpretation at the same time, and there are many questions about its practicality. As a simple example, the leakage current of OLEDs depends on external environmental factors (temperature, light intensity), and the interface characteristics vary considerably from process to process. In case of the forward bias condition, carrier transports as well as interface characteristics have a great influence on the capacitance response. In addition, a strong negative capacitance appears at low frequencies [27-33], and it is also necessary to be very careful to set the amplitude of the small signal when measuring the impedance of the OLEDs. When OLEDs are driven for a long time, the I-V-L shift of OLEDs may occur in real time during the measurement.

In the papers reported previously, it is most often regard as the series

combination of the simplest R and C parallel circuits [34-38]. Sometimes there is confusion in distinguishing between conduction currents and displacement currents, and to represent negative contribution at low frequency, inductance sometimes can be added in equivalent circuit, but which is just suitable for simple calculations, is not reasonable because violates conservation of energy law due to absent of induced magnetic field in OLEDs device [39-42].

When the actual capacitance values are extracted according to the equivalent circuits assumed by the researchers, the physical interpretation can be greatly distorted by using the extracted values if there are errors in the assumptions.

Figure 2.2[38] and Figure 2.3[29] shows the difference between the equivalent circuit model and the experimental impedance response in past papers of OLEDs analysis using impedance spectroscopy. In most cases, the error of impedance is ignored in the low frequency, so that impedance response of equivalent circuit and experimental impedance response of the OLEDs device shows a considerable difference. These models overlook the distribution of mobile carriers within OLEDs, which ultimately do not seem to account for the physical phenomena of OLEDs. Therefore, this section starts with the most general analytical approach for impedance analysis.

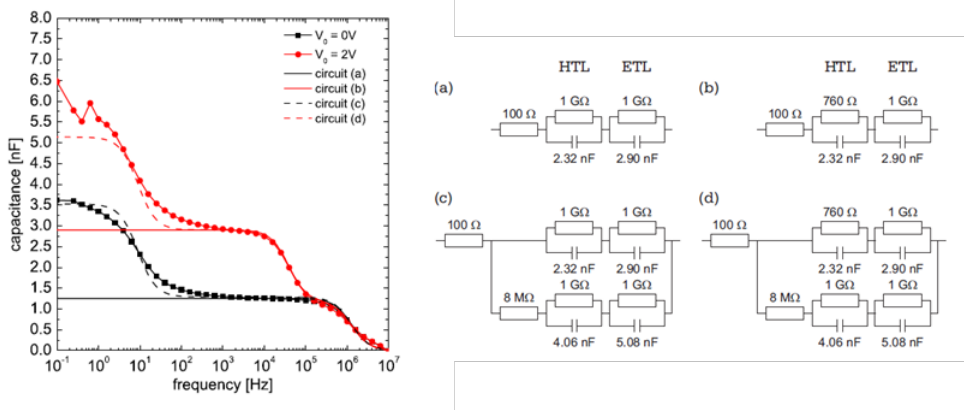


**Figure 2.2** Frequency vs Capacitance plot and their equivalent circuit model reported by Nowy et al. [38]

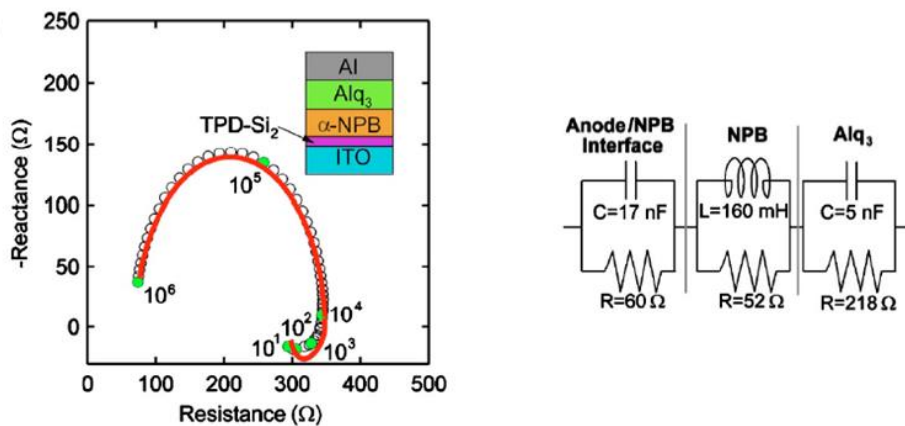


**Figure 2.3** Cole-cole plot and their equivalent circuit model reported by Pingree et al. [29]

## 2.2 Complex Capacitance Concepts for IS

To understand the impedance, it is necessary to know how the permittivity of any device is described. In the general Gauss's law, the sum of the electric field of the closed surface becomes the source of the dielectric constant.

$$\oint_s \mathbf{E} \cdot d\mathbf{a} = \frac{Q}{\epsilon} \quad (2.2.1)$$

Electric displacement field is sum of displacement field of free space and polarization moment

$$\mathbf{D} = \epsilon \mathbf{E} = \epsilon_0 \mathbf{E} + \mathbf{P} \quad (2.2.2)$$

Because a material cannot polarize spontaneously in response to an applied field, polarization can be convolution of the electric field so that the permittivity can be complex number. Using Fourier transform

$$D e^{-j\omega t} = \epsilon(j\omega) E_0 e^{-j\omega t} \quad (2.2.3)$$

### 2.2.1 $\epsilon$ ARC

According to Debye's expression, the expression of the complex



permittivity  $\varepsilon(j\omega)$  is written as

$$\varepsilon - \varepsilon_\infty = \frac{(\varepsilon_s - \varepsilon_\infty)}{1 + j\omega\tau} \quad (2.2.4)$$

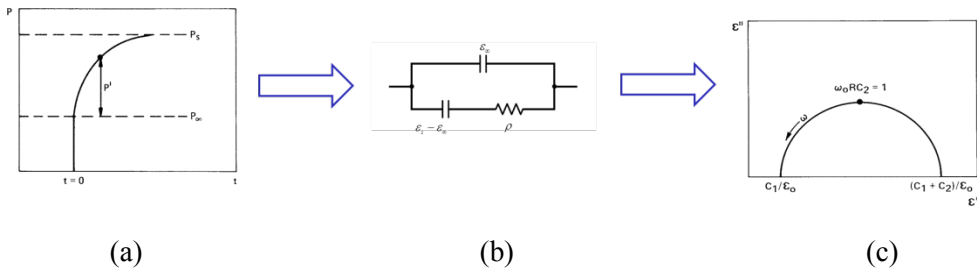


**Figure 2.4** (a) Time dependence of the polarization, (b) Debye equivalent circuit (c) complex plan plot of the complex permittivity

Cole and Cole extended this Debye's concept further to the concept of distributions of relaxation times. This assumes that the permittivity of each material is widely distributed around a mean of distributed time constants [43]. Equation (2.2.5) is represents the Debye's infinite sum of the distributed dielectric relaxation

$$\varepsilon - \varepsilon_\infty = \int_0^\infty \frac{(\varepsilon_s - \varepsilon_\infty) G(\tau) d\tau}{1 + j\omega\tau} \quad (2.2.5)$$

where  $G(\tau)$  is the fraction of the total dispersion ( $\epsilon_s - \epsilon_\infty$ ). And Equation (2.2.5)

can be represent as

$$\epsilon = \epsilon_\infty + \frac{(\epsilon_s - \epsilon_\infty)}{1 + (j\omega\tau)^{\psi_\epsilon}} \quad (2.2.6)$$

Where  $\psi_\epsilon$  is the constant lead to a depressed arc in complex plane of  $\epsilon$ , and when

$\psi_\epsilon = 1$ , it yields a Debye 's single relaxation constant. This equation is the well-

known Cole-Cole dielectric dispersion response function.  $A_0(j\omega)^{\psi_\epsilon}$  is admittance

of constant phase element.

Figure 2.5 illustrates how time-dependent polarization is modeled by a circuit and

plotted on the complex plane.

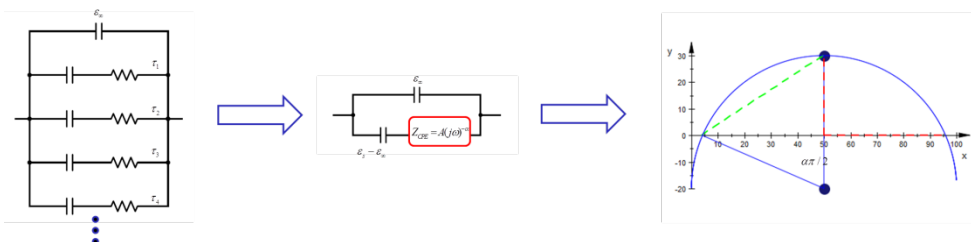


**Figure 2.5 (a) Distribution of relaxation times**

## 2.2.2 ZARC

Ampère's circuital law (with Maxwell's addition) can be written as

$$\mathbf{J}_{total} = \mathbf{J}_C + \mathbf{J}_D \quad (2.2.7)$$

The conductance and permittivity are as follows

$$\mathbf{J}_{total} = \sigma \mathbf{E} + \varepsilon \frac{d\mathbf{E}}{dt} \quad (2.2.8)$$

If conductance and permittivity are functions of position

$$\mathbf{J}_{total} = (\sigma(x) + \varepsilon(x)) \frac{d\mathbf{E}}{dt} \quad (2.2.9)$$

With Laplace transform

$$j(j\omega) = (\sigma(j\omega) + j\omega\varepsilon(j\omega))E(j\omega) \quad (2.2.10)$$

Thus

$$j(j\omega) = j\omega \left( \frac{\sigma(j\omega)}{j\omega} + \varepsilon(j\omega) \right) E(j\omega) \quad (2.2.11)$$

If total of the permittivity including the electric conductivity is represented by  $\varepsilon_c$  and the permittivity is expressed by the complex permittivity, the following is obtained.

$$\varepsilon_c = \varepsilon(j\omega) - j \frac{\sigma(j\omega)}{\omega} \quad (2.2.12)$$

If you try to configure it as a general circuit, it will have the same dimensionless configuration as the high frequency component circuit among the circuits mentioned in the Randel[44].

$$I = \frac{d}{A} \left( \frac{1}{\sigma + j\omega\varepsilon} \right) V \quad (2.2.13)$$

Where d is the length of the device and A is the area of the device. Thus, any dielectric with charge transfer characteristics is expressed as

$$Z_c = \frac{d}{A} \left( \frac{1}{\sigma + j\omega\varepsilon} \right) = \frac{1}{\frac{1}{R} + j\omega C} \quad (2.2.14)$$

Using similar results to Debye 's equation of transplantation, Macdonald generalized the charge transfer characteristics through transplantation [45].

$$\sum Z = \frac{A_1}{1 + j\tau_1} + \frac{A_2}{1 + j\tau_2} + \frac{A_3}{1 + j\tau_3} \dots = \int Z_n = \frac{1}{1 + (j\omega\tau)^{\nu_c}} \quad (2.2.15)$$

Figure 2.6 shows the impedance when the materials with various permittivities are connected in series. At this time, the charge transfer of each layer is expressed as a resistance, and each dielectric constant can be expressed by a capacitance. It is also expressed as a constant phase element when the change in the material at each interface is continuous. At this time, this impedance becomes a depress circle with the center of the circle down the x axis in the complex plane of Z.

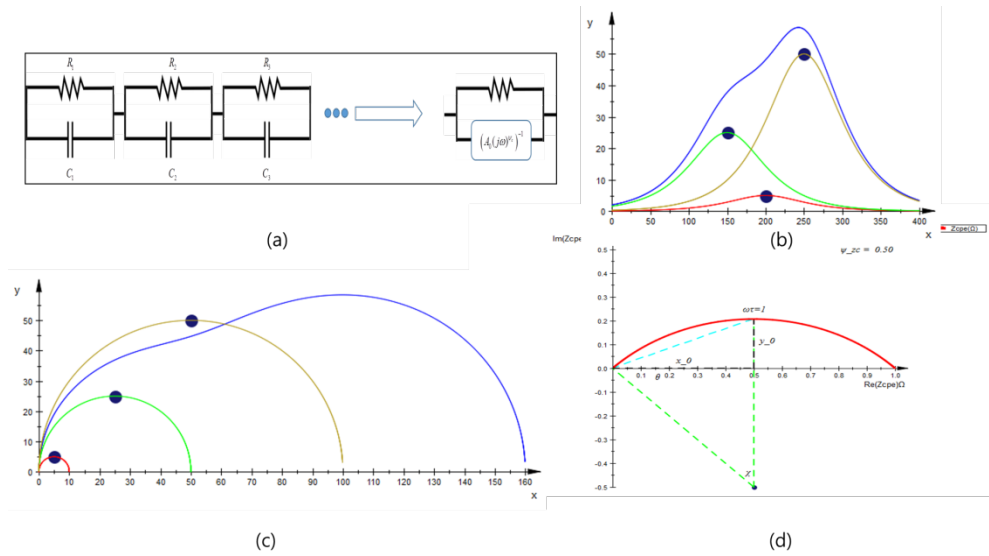


**Figure 2.6** Equivalent circuit when interface is formed perpendicular to current direction (a) And the reactance value (b) and complex plane plot of Z(c) for the three components on the left side of the equivalent circuit (d).

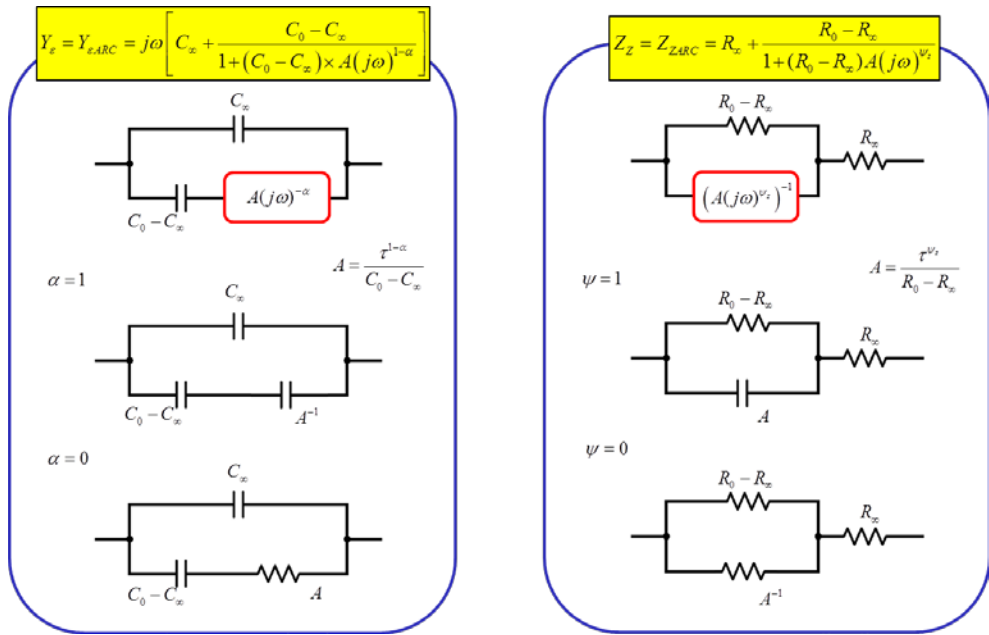


**Figure 2.7** Comparison of Equivalent Circuit Representation of eARC (a) and Equivalent Circuit Representation of ZARC. It shows that according to changes in  $\alpha$  and  $\psi$  value how to change CPE value.

Figure 2.7 compares the equivalent circuit representation of eARC and ZARC. In the eARC, when the  $\alpha = 1$ , the CPE acts as an ideal capacitance and the permittivity almost simultaneously becomes polarization. On the other hand, if  $\alpha = 0$ , the polarization is delayed by the time constant  $\tau = (RC)^{-1}$ . In the ZARC, when  $\psi = 1$ , it acts as an ideal capacitance, and the overall permittivity is integrated into one. On the other hand, when  $\psi = 0$ , it acts as a perfect conductor.

### 2.2.3 Negative Capacitance

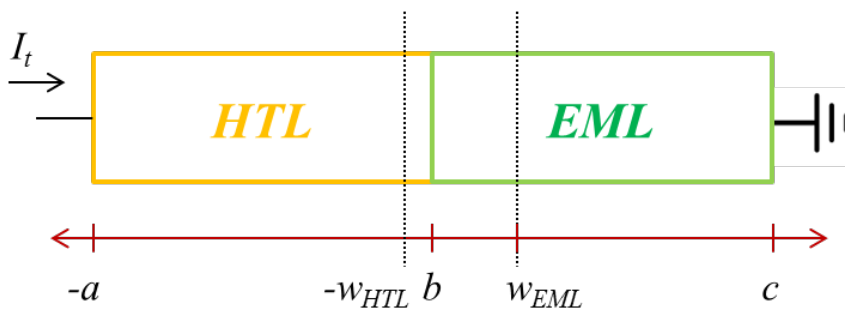
Negative capacitance is a phenomenon often observed in high voltage and low frequency band of OLEDs. Laux and Hess have successfully introduced and successfully proved a new model[1], denying the fatal defects of conventional diode models, that is the diffusion capacitances, which increase infinitely in proportion to the current. This has a negative contribution to reducing the internal capacitance, which means that the time-dependent recombination rate and the amount of carrier exiting to the outside cause this capacitance to decrease, and even negative values when certain conditions are met.

Figure 2.8 briefly shows one-dimensional double layered OLEDs. The continuity equation at position b and the current expression using Gauss' law are as follows [1]

$$\begin{aligned}
 J_t &= J_n(b) + J_p(b) + J_d(b) \\
 &= \underbrace{e \int_{-a}^c U_s dx}_1 + \underbrace{e \int_{-a}^b \frac{\partial n}{\partial t} dx + e \int_b^c \frac{\partial p}{\partial t} dx}_2 \\
 &\quad + \underbrace{e \int_b^c \frac{\partial(n-p)}{\partial t} dx}_3 + \underbrace{J_n(-a) + J_p(c)}_4 + \underbrace{J_d(c)}_5
 \end{aligned} \tag{2.2.16}$$

At this time, the current equation of (2.2.16) is divided into five terms, where term1 is the recombination term of the whole device, term 2 is the amount of carrier

increasing inside the device, term 3 is deplete capacitance, term 4 is the amount of current flowing out of both electrodes, term 5 represent for the displacement current at c.



**Figure 2.8** The one-dimensional double layered OLEDs, The depletion width is  $W = w_{HTL} + w_{EML}$ . The total diode length is  $c+a$ . Hole is injected at  $-a$  and electron is injected at  $c$ .  $b$  is chosen to be the location where  $n(b)=p(b)$

Here, terms 2 and 5 lead to an increase in capacitance due to the increase in the internal carriers. On the other hand, it can be seen that the term 1 and 4 indicate that the amount of internal carriers decreases. 2.5.1 When expressed as  $dV / dt$  through the chain law in the equation, it can be summarized into five capacitances and expressed as follows.



Term 1:

$$J_r = e \int_{-a}^b -\frac{\partial \delta p}{\partial V} dx \frac{\partial V}{\partial t} + e \int_b^c -\frac{\partial \delta n}{\partial V} dx \frac{\partial V}{\partial t} = -C_r \frac{\partial V}{\partial t} \quad (2.2.17)$$

Term 2:

$$J_{diff} = \int_{-a}^b \frac{\partial n}{\partial V} dx \frac{\partial V}{\partial t} + \int_b^c \frac{\partial p}{\partial V} dx \frac{\partial V}{\partial t} = (C_n + C_p) \frac{\partial V}{\partial t} \quad (2.2.18)$$

Term 3:

$$J_{depl} = C_{depl} \frac{\partial V}{\partial t} \quad (2.2.19)$$

Term 4:

$$J_n(-a) + J_p(c) = -\frac{\int_0^t J_n(-a) dt'}{\partial V} \frac{\partial V}{\partial t} - \frac{\int_0^t J_n(-a) dt'}{\partial V} \frac{\partial V}{\partial t} = -C_{out} \frac{\partial V}{\partial t} \quad (2.2.20)$$

Term 5:

$$J_d(c) = C_d \frac{\partial V}{\partial t} \quad (2.2.21)$$

It can be roughly expressed as :

$$J_t = (-C_r + C_p + C_n - C_{out} + C_d) \frac{\partial V}{\partial t} \quad (2.2.22)$$

Here, it is possible to estimate what the negative capacitance value can represent within the device. Equation (2.2.22) also suggests that each capacitance is connected in parallel. Considering the dielectric relaxation time of each capacitance here, the entire equivalent circuit model can be thought of as a parallel combination of series connection of R and C divided represented five terms.

Figure 2.10 shows the impedance response at low frequencies (100 Hz) of the two-layered OLEDs (ITO/HTL/ EML/LiF:Al). At low voltage ( $V_{op} < V_{bi}$ ), OLEDs behave as if they are insulators because they have almost no current contribution, and because the resistance of HTLs in OLEDs decreases at medium voltage ( $V_{Bi} < V_{op} < V_{on}$ ), only capacitance value of EML measured so that the total capacitance increase. Then at high voltage ( $V_{op} > V_{Peak}$ ), the negative capacitance increases because of the increase of current contribution. Figure 2.11 shows the variation of the band diagram in each case. When analyzing the impedance of OLEDs, it is very important to know that the measured impedance of OLEDs is what state of the OLEDs operating. Understanding how the OLEDs operate physically can help you extract accurate device information from the impedance response information.

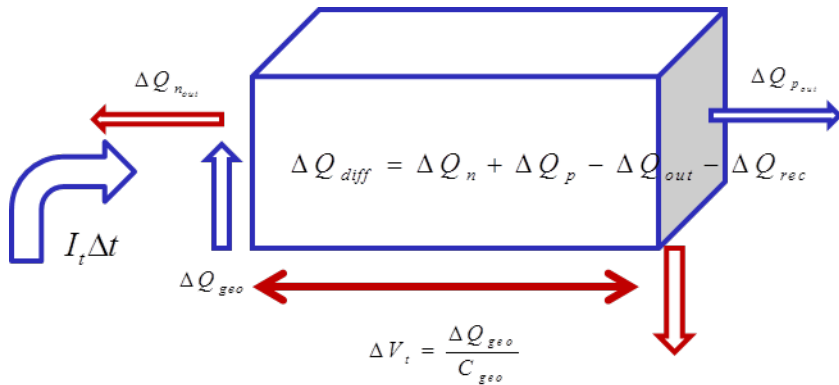


**Figure 2.9** The charge injected into the diode affects the depletion capacitance and diffusion capacitance. At this time, the charges that are discharged to the outside in the unit time and the recombination charge cause the decrease of the capacitance.

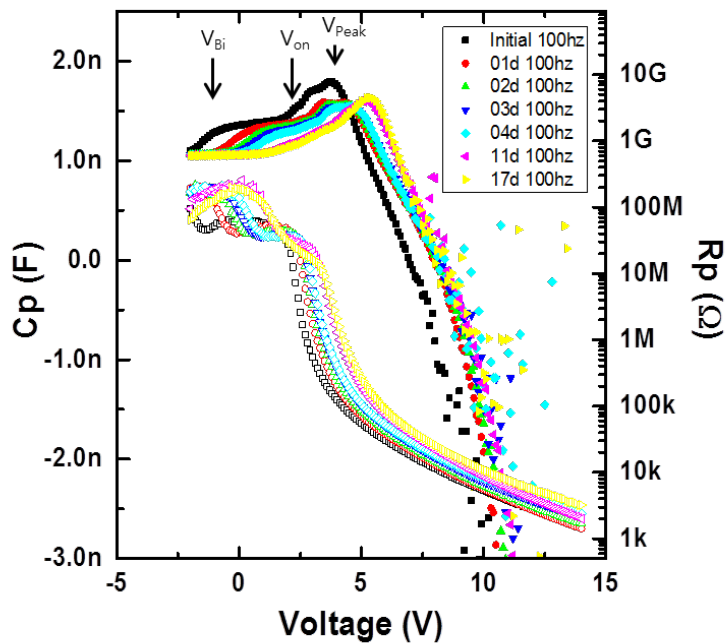


**Figure 2.10** Graph of C-V characteristics of OLEDs

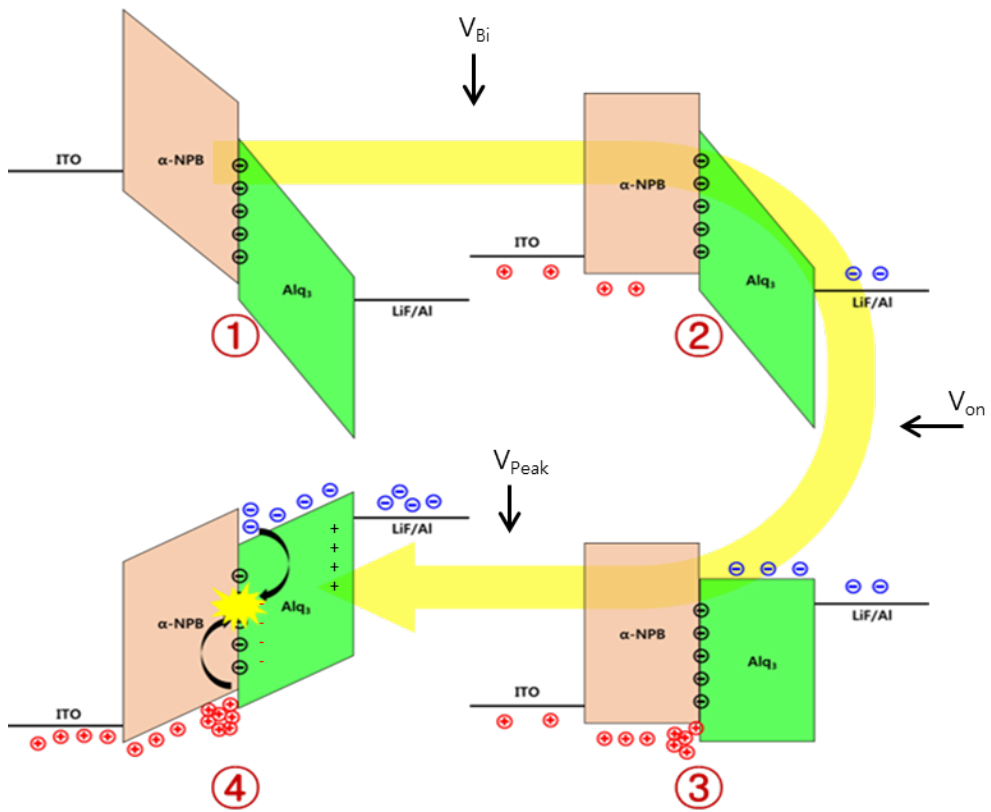


**Figure 2.11** Energy band diagram which explain the negative capacitance phenomenon of OLEDs

## 2.2.4 Equivalent circuit strategy for OLEDs

In the low-frequency region, the capacitance of OLEDs is modeled as inductance because of the negative capacitance. But this is not physically fit. Also, if the negative capacitance value described in the Laux & Hess model is described as

an inductor, it is cannot explained the fact that this negative capacitance value only affects the low frequencies. Therefore, this  $C$  is a typical capacitance whose component becomes zero at a high frequency, that is, a capacitance whose sign is negative.

We integrated the Maxwell model and the voigt model to integrate the three models into one. To incorporate charge transfer under this integration, the terms with capacitive dielectric effects are divided into three: the internal charge increase term, the charge recombination term, and the charge external term.

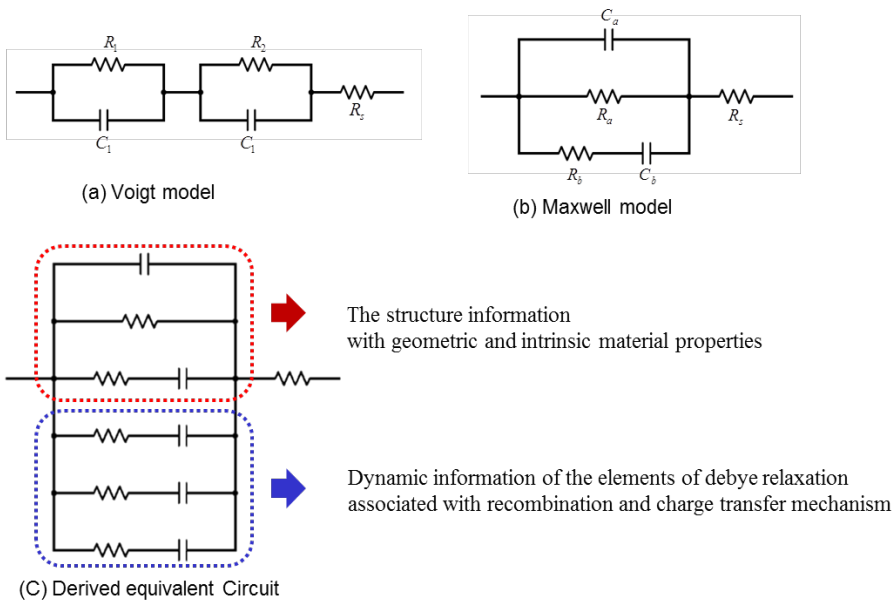


**Figure 2.12** Equivalent circuit model combining charge transfer model and interface model

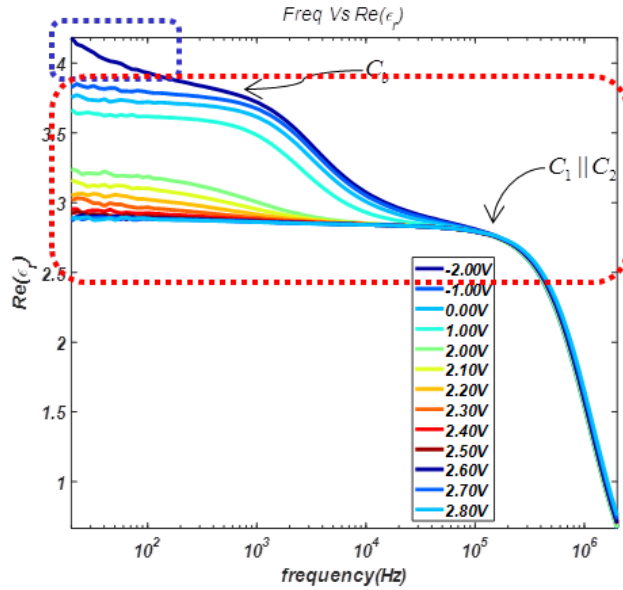


**Figure 2.13** Capacitance graph of OLEDs. The role of each equivalent circuit model is explained by dividing the area.

## 2.3 Theory

### 2.3.1 Impedance Spectroscopy

Impedance spectroscopy is particularly characterized by the measurement and analysis of some or all of the four impedance-related functions  $Z$ ,  $Y$ ,  $M$ , and  $e$  and the plotting of these functions in the complex plane[46]. It can be usefully used

small-signal ac response analysis of the electrode-material system. It uses a more generalized concept than a classical electrical engineering analysis that analyzes the response of an electrical circuit composed of ideal passive elements (R, L, C). Therefore, in impedance spectroscopy analysis, element of R, L, and C is no more ideal, and includes response of dependencies on frequency and potential or dynamic motion with time passed. The small signal impedance response, represented in the complex plane, represents a physicochemical value that includes the characteristic of the device.


In 1941, Cole and Cole first tried to plot  $\varepsilon'$  and  $\varepsilon''$  of dielectric systems in the complex plane, known as a Cole-Cole plot [43]. And from at least 1947, various researchers(i.e., Randles[44](1947), Jaffé [47](1952), Macdonald[48] (1953), and Friauf[49](1954)) have begun the theoretical treatment of semiconductor and ion systems using  $Z'/Z''$  or  $Y'/Y''$  in the complex plane.

Complex plane plots are sometimes referred to as Nyquist diagrams because they use the real and imaginary axes as the basis. However, since Nyquist diagrams generally represent transfer function responses of a time-invariant system with 3 or 4 terminals while conventional complex plane plots include 2-terminal input immittances, this is an invalid name, It is better to use complex plane or Cole-Cole plot rather than the name of Nyquist diagram.

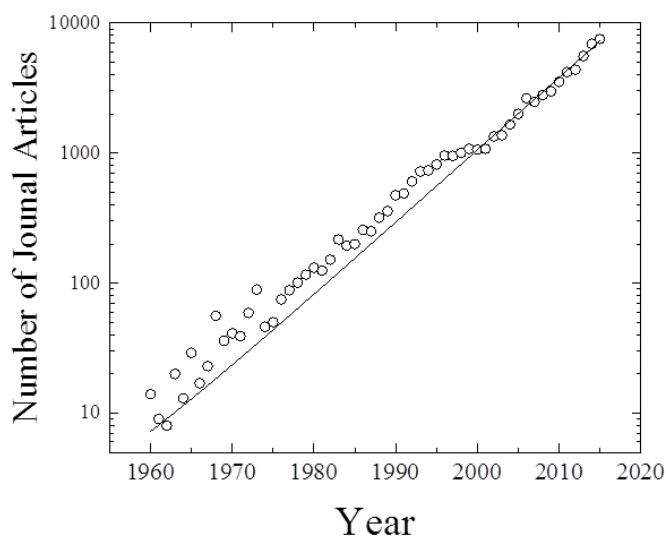



**Figure 2.14** Number of journal articles on impedance spectroscopy identified on October 3, 2016 using <http://www.sciencedirect.com/> search engine In Elsevier(Journal article only)


- Oliver Heaviside create the foundation of IS (1872)
- Nernst employ IS for measurement of dielectric properties and the resistance of galvanic cells.(1897)
- Warburg introduce Warburg diffusion element (ZW) which is a constant phase element (CPE)
- In the 1920s, impedance was applied to biological systems.
- In the 1940s, Grahame introduce fundamental understanding of the structure of the electrical double layer.
- Brother Cole and Cole introduce complex dielectric constant formula.
- In the 1950s, impedance began to be applied to more complicated reaction.
- In the 1970s, Nonlinear complex regression techniques were applied to IS by Macdonald.
- EIS conference was launched In 1989.
- Current key issues is heterogeneity of electrode and the correspondence to the use and misuse of CPE




Oliver Heaviside




Walther Hermann Nernst



Prof. Dr. Warburg  
Emil Warburg



Kenneth Stewart Cole



J. Ross Macdonald

**Figure 2.15** A brief history summary of Impedance spectroscopy



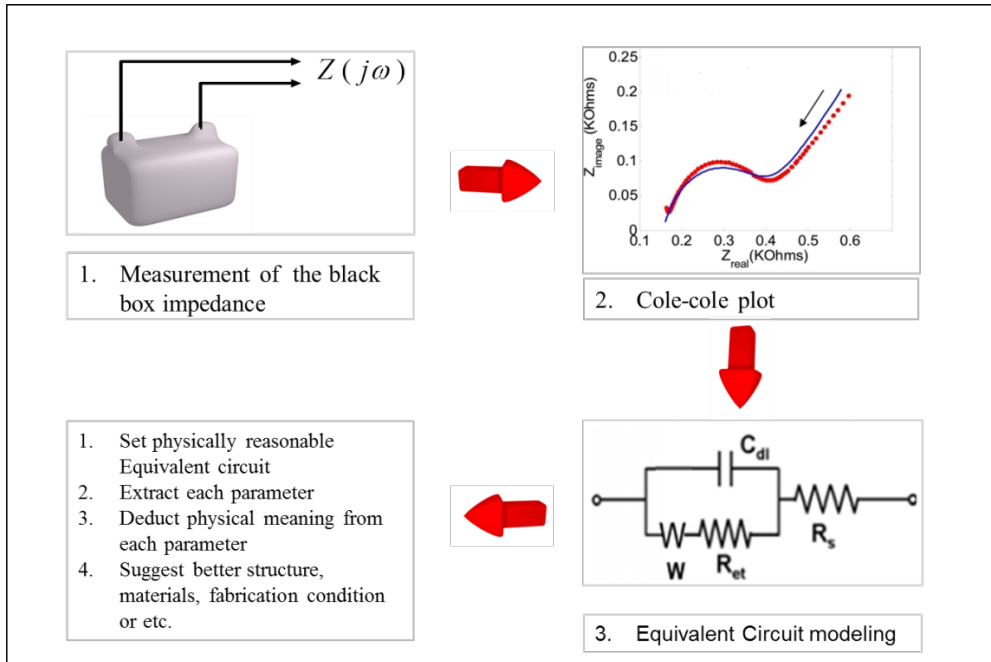


**Figure 2.16** Schematic flow process for impedance spectroscopy measurement process

**Table 2.1** Relations Between the Four Basic Immittance Functions<sup>a[46]</sup>

	<b>M</b>	<b>Z</b>	<b>Y</b>	<b>ε</b>
<b>M</b>	M	$\mu Z$	$\mu Y^{-1}$	$\epsilon$
<b>Z</b>	$\mu^{-1} M$	Z	$Y^{-1}$	$\mu^{-1} \epsilon^{-1}$
<b>Y</b>	$\mu M^{-1}$	$Z^{-1}$	Y	$\mu \epsilon$
<b>ε</b>	$M^{-1}$	$\mu^{-1} Z^{-1}$	$\mu^{-1} Y^{-1}$	$\epsilon$

<sup>a</sup>  $\mu \equiv j\omega C_c$  where  $C_c$  is the capacitance of the empty cell

### 2.3.2 Small-Signal Model

Generally, the impedance is the ratio of the complex representation of correlation with the resulting steady-state current  $i_{ac}(t) = I_m \sin(\omega t + \theta)$  after applying a monochromatic signal  $v_{ac}(t) = V_m \sin(\omega t)$  to the cell. Where  $\theta$  the phase is difference between voltage and current and  $\omega$  is the angular frequency of each signal. Unlike the ideal passive elements, most of the practical electronic device cells are rigorously non-linear device depending on the difference of the potential between electrodes. Small-signal modeling refers to the technique which replace non-linear device to linear device using time-varying currents and voltages (AC signals which have a small magnitude compare to the DC bias currents and voltages). The voltage applied to the device is expressed by the sum of  $V_{DC}$  and  $v_{ac}(t)$ , the current applied to the device is same, as follows.

$$\begin{aligned} v(t) &= V_{DC} + v_{ac}(t) \\ i(t) &= I_{DC} + i_{ac}(t) \end{aligned} \tag{2.3.1}$$

If the small-signal current of the response to the small-signal voltage satisfies the linearity, the dc component can be ignored and a differential equation is as follows.

$$i_{ac}(t) = \Psi(t) * \frac{dv_{ac}(t)}{dt} \tag{2.3.2}$$

In the case of an ideal diode, the small signal amplitude should be less than twice the thermal voltage ( $V_{th} = kT / q$ ) to apply the small signal model. Using Fourier transformation to simplify significantly the mathematical treatment of treatment of this system,

$$I(j\omega) = Y(j\omega)V(j\omega) \quad (2.3.3)$$

The real part and the imaginary part of the admittance  $Y(j\omega)$  in equation (2.3.3) can be expressed simply by conductance  $g_d$  and capacitance  $C$ .

$$Y(j\omega) = g_d + j\omega C \quad (2.3.4)$$

In equation(2.3.4), strictly speaking, the capacitance value and conductance are not a constant but also real number. These values are frequency dependent complex function. Here is why we use impedance spectroscopy. It is most desirable to interpret this using the impedance spectroscopy analysis on the complex plane diagram.

### 2.3.3 Complex Plane Diagram

Cole and Cole[43] showed that the expression of the impedance including the device relaxation can be represented by the sum of the semi-circles in the complex plane. To understand Cole and Cole methodology, it is required to know how to intuitively interpret the shape of the impedance seen in the complex plane. In this section, it is introduced how complex equations expression with one pole are displayed in the complex plane. If a complex equation expression is

$$Z = \frac{1}{A + jB} \quad (2.3.5)$$

where one of A or B is a constant and the other is a function of frequency. Equation 2.7.1 may be rewritten to the relation of real value  $\Re(Z)$  and imaginary value  $\Im(Z)$  as

$$\Re(Z)^2 + \Im(Z)^2 = \begin{cases} \frac{1}{A} \Re(Z) & \text{(if A is constant and B is function of } \omega) \\ \frac{1}{B} \Im(Z) & \text{(if A is function of } \omega \text{ and B is constant)} \end{cases} \quad (2.3.6)$$

This is the equation of a circle with radius  $1/(2A)$  or  $1/(2B)$  having its center

at  $(1/(2A), 0)$  or  $(1/(2B), 0)$ , respectively. This make to finding each parameter in complex plane easily. Depending on the sign of A or B, each semicircle is placed in one part of the first, second, third, and fourth quadrants, and the plot of this equation is shown in Figure 2.17.

Furthermore the greatest advantage of such a Cole and Cole expression in complex plain is that it allows predicting the overall parameters of the equation through only the maximum value of the real or imaginary part. That is, since maximum value of real or imaginary part is located at  $|A|=|B|$ , even if the maximum value of only one part is known, the other component value is obtained without any effort.

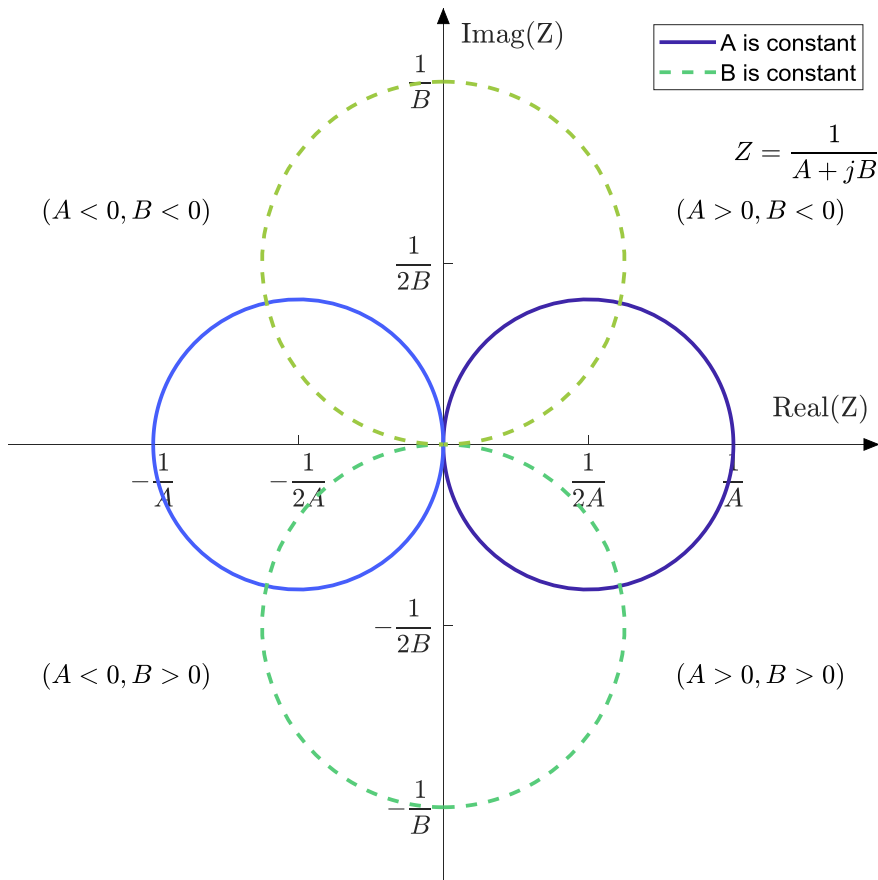


**Figure 2.17** Complex Plane Diagram of a complex equation(2.3.6). The diameter of the semicircle is determined by the reciprocal values of A and B, and the position of the center of the semicircle is determined by the sign of A and B.

### 2.3.4 Equivalent Circuit Modeling

In section 2.3.3, it is suggested that most common passive elements appear in a semicircular form on the complex plane. In impedance spectroscopy analysis of any devices, it is very important to learn how each passive circuit is expressed in which domain.

If you find a semicircle in the complex plane of  $Z$ , this circuit is a RC circuit that is connected in parallel which have the resistance value as a diameter of semicircle and capacitance value as minimum value of imaginary part. If you find a semicircle in the complex plane of  $Y$ , you will get an RC circuit that is connected in series in the same way as above.

In case RC in parallel circuit:

$$Z_{R||C} = \frac{1}{R^{-1} + j\omega C}; \quad \omega_{\max} = \tau_{\max} = \frac{1}{RC} \quad (2.3.7)$$

In case RC in series circuit:

$$Y_{R+C} = \frac{1}{R + (j\omega C)^{-1}} \quad \omega_{\max} = \tau_{\max} = \frac{1}{RC} \quad (2.3.8)$$

In case RL in parallel circuit:

$$Z_{R\parallel L} = \frac{1}{R^{-1} + (j\omega L)^{-1}} \quad \omega_{\max} = \tau_{\max} = \frac{R}{L} \quad (2.3.9)$$

In case RL in series circuit:

$$Y_{R+L} = \frac{1}{R + j\omega L} \quad \omega_{\max} = \tau_{\max} = \frac{R}{L} \quad (2.3.10)$$

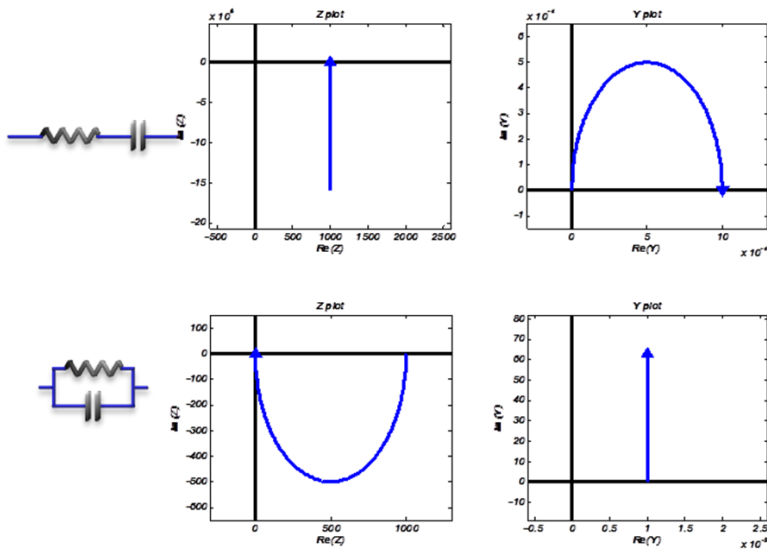


**Figure 2.18** Complex plane of Z and Y of resistance and capacitance circuits.



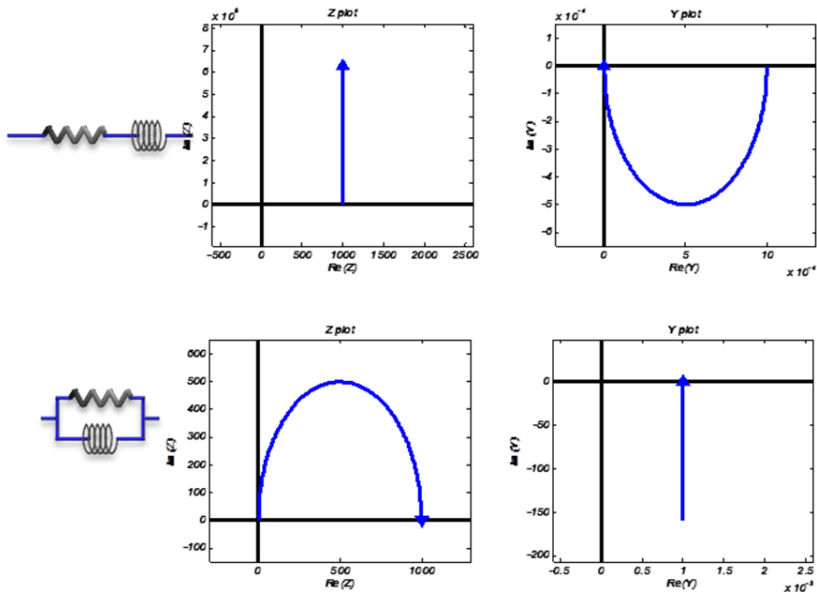


**Figure 2.19** Complex plane of  $Z$  and  $Y$  of resistance and capacitance circuits

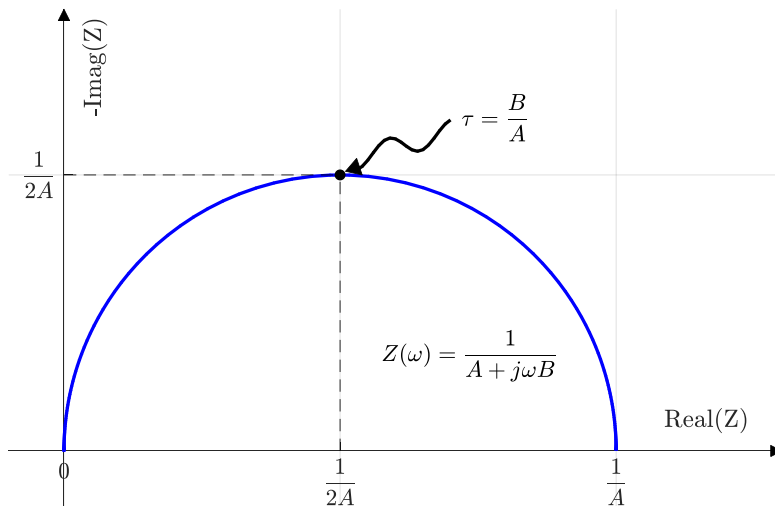


**Figure 2.20** Cole-cole plot of impedance( $Z$ ) of parallel circuit compound with resistance and capacitance.

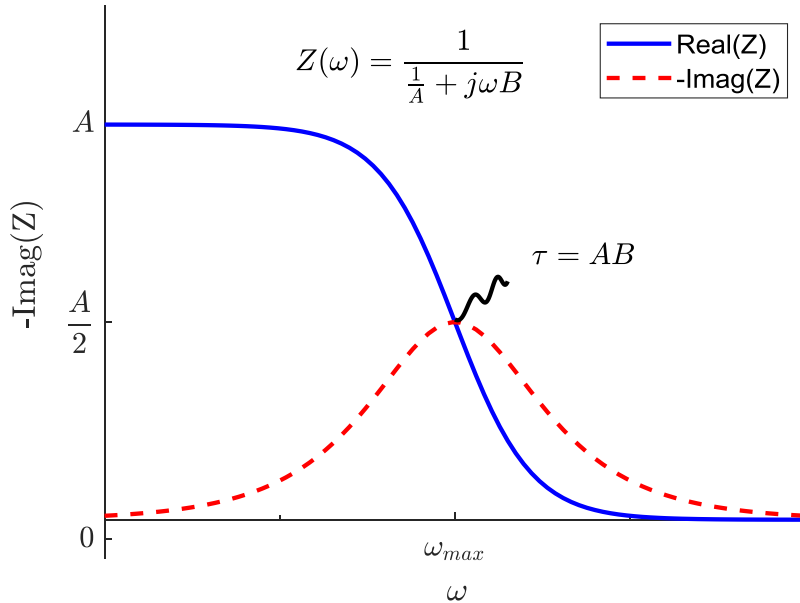


**Figure 2.21** Real(blue line) and imaginary(red dot line) value of impedance

Figure 2.20 shows the impedance shape in the complex plane when the capacitance and the capacitance are connected in parallel. In many documents, this is referred to as the Cole-cole plot. Generally, we use a complex plane with the y-axis reversed. It is possible to estimate the shape of the entire impedance from a part of the impedance measurement value through the same point (the maximum value of the imaginary part) at the same point of the real part and the imaginary part. In order to analyze more easily, it is better to transform the domain into a shape like Figure

2.21, which shows the imaginary axis and the real axis as a function of the frequency, and then find  $\omega_{max}$  from the maximum value of the imaginary value and a value from the maximum value of the real value.

### 2.3.5 Superposition of various Impedance Component

Actually, the practical impedance of the device is different from that in the previous section, which is superimposed when there are two or more relaxation time constants of polarization. Depending on each modeling strategy, different equivalent circuit models can be drawn, but the model can be inversely modeled from function shape on the complex plane. The most common assumption is that the impedance is superimposed when there are several internal interfaces. The equation of superposition impedance may be as

$$Z(\omega) = \sum_n \frac{1}{\frac{1}{A_n} \pm jB_n(\omega)} \quad (2.3.11)$$

Figure 2.22 shows the case where the time constant is divided into two in the form of Equation(2.3.11). Intuitively, if a semicircle seems to be split into two and a material with different time constants (or different dielectric constants) in the device

is placed vertically in the electric field, the separation of each layer is known and the physical Properties can be estimated. This is the best model for OLEDs analysis because it is suitable for the analysis of stacked layer devices consisting of junctions of different materials. However, there are difficulties in the case of two call analyzes with possible duplication. This can minimize errors with a method of nonlinear least squares (CNLS). A much more common and powerful method of complex nonlinear least squares is first applied to IS in Macdonald and Garber's study [50](1977), and Macdonald, Schoonman and Lehnen [51](1982), Macdonald [52](1991) proposed the methods for high resolution and accuracy [46].

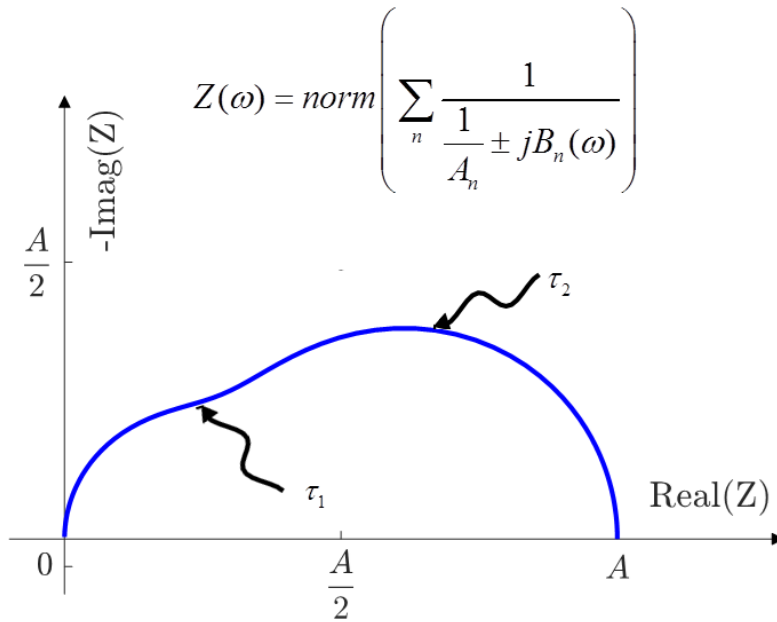


**Figure 2.22** Superposition of the impedance. Impedance response with a parallel combination of capacitance and capacitance connected in series. The shape of the impedance response appears as overlapping sub-circles and the parameters can be extracted in the minimum error range using the complex nonlinear least squares (CNLS) algorithm[50].

### 2.3.6 Debye relaxation plot( $\epsilon$ -plot)

When an electric field is applied to a substance, the polarization of the substance does not react immediately but flows to a certain average time and then

converges to a specific polarization value (Figure 2.23). In general, there are electronic polarization, atomic polarization, dipolar polarization, and ionic polarization in the order of the well-known dielectric constant reaction sequence. Thus, all materials have a dielectric relaxation time to polarize (Figure 2.24).

The best explanation of the retardation response of this polarization is the Debye relaxation theory[53]. Debye defines dielectric relaxation time is the average time it takes for completing the polarization, and the permittivity is treated as a function of the complex number through the Fourier theorem as

$$\varepsilon - \varepsilon_{\infty} = \frac{(\varepsilon_s - \varepsilon_{\infty})}{1 + s\tau} \quad (2.3.12)$$

Thus the real part of the complex dielectric constant can be regard as the dielectric constant of dc condition and the imaginary part of the complex dielectric constant are related to the amount of energy loss to make the polarization. The complex function of this dielectric is well described as an equivalent circuit (Figure 2.25). When this equivalent circuit is expressed as a complex permittivity in a complex plane, it also has a semicircular appearance as one can see Figure 2.26.

The author named this plot of expression in the complex plane of this dielectric constant as  $\varepsilon$ -plot and used it to define the diffusion capacitance by current in OLEDs.

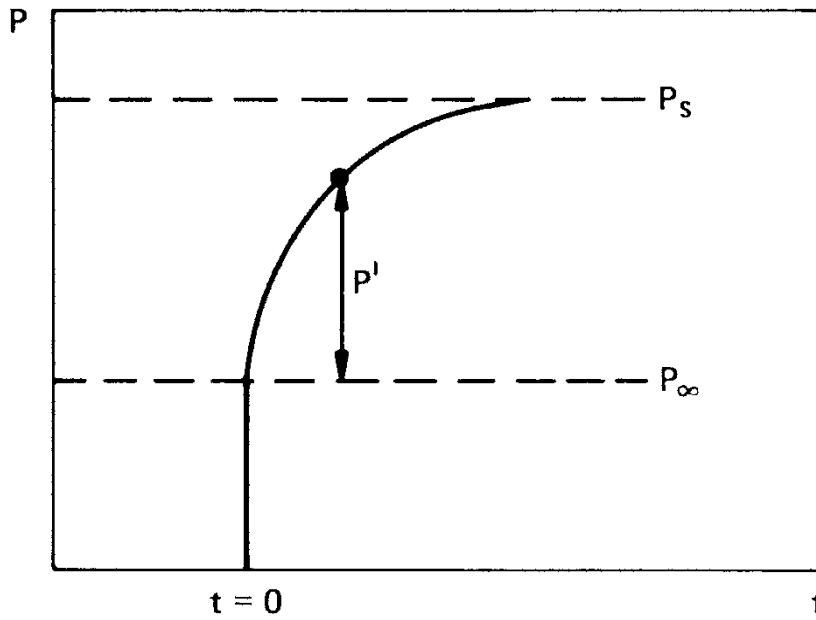


**Figure 2.23** Time dependence of the polarization after the application of an electric field to an insulator at  $t=0$  [46].

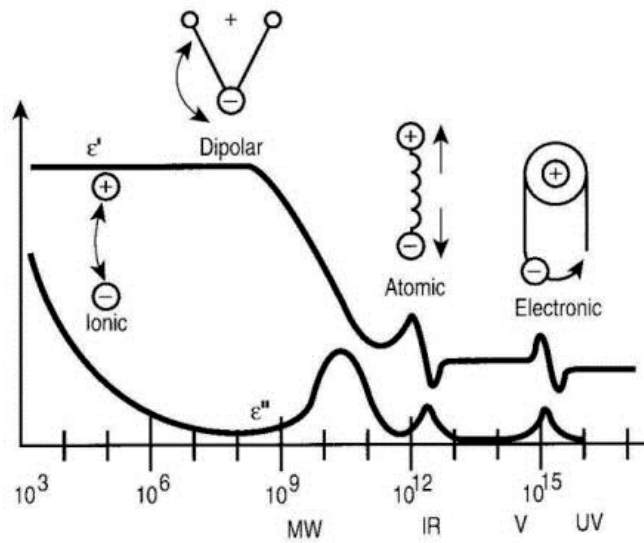


**Figure 2.24** Frequency response of dielectric mechanisms. (ref : Application Note

1217-1, "Basics of measuring the dielectric properties of materials," Hewlett Packard literature number 5091-3300E, 1992.)

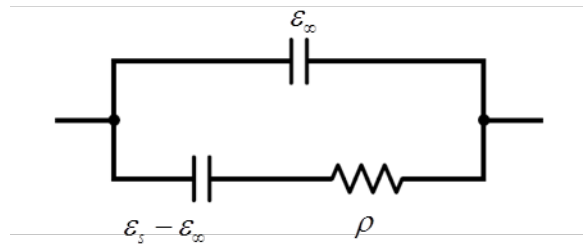


**Figure 2.25** The Debye equivalent circuit

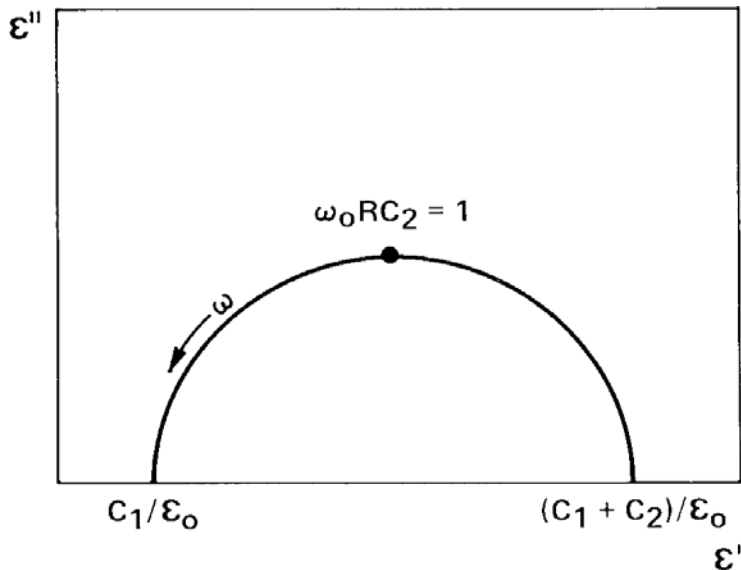


**Figure 2.26** Complex plane plot of the frequency dependence of the complex permittivity modeled by the circuit of Figure 2.1.2.[46]



## **2.4 How to extract reasonable parameter from impedance spectroscopy**

Section 2.2.4 presents an equivalent circuit model that combines the structural and charge transfer models of OLEDs. This model may be an ideal model or a model with distributed elements. Therefore, CPE (constant phase element) must be considered in all elements. However, it is difficult to accurately separate the CPE from the overlapping impedance response. Of course, the solution proposed by Macdonald's CNLS(Complex Non-linear least squares) fitting program(from : <http://jrossmacdonald.com/levmlevmw/>) can be a solution, but the residue between the actual impedance response and the equivalent circuit model varies greatly depending on what domain you are looking at. A more sophisticated approach than the Macdonald approach is needed. We present an empirical methodology that best represents the impedance response of OLEDs. First, we use the method of filling the variable of the equivalent circuit from the element of the impedance response with the smallest variation in the external variable at all frequencies. The order of determining the equivalent circuit parameters with the figure is as follows.

1. The  $C_{\text{geo}}$  is determined at the inflection point of the highest frequency.
  - ✓ Ensure that the  $C_{\text{geo}}$  value at high frequencies has a value close to the dielectric constant of the material.
2. The  $C_b$  is determined at the inflection point of the second highest frequency
  - ✓ Must be extracted in series with the  $C_b$  value at the previous voltage which reduces confusion at the ambiguous inflection point.
3.  $C_{\text{diff}}$  is modeled as a CPE in which the time constants of electrons and holes are dispersed.
4.  $C_{\text{rec}}$  is distributed at  $10^4 \sim 10^5$  frequencies, but is not large here and is therefore invisible at this scales
  - ✓ OLED carrier life time is lower than OLED recombination life time
5.  $C_{\text{out}}$  is the flux of charge exiting at the terminal at the lowest frequency.
  - ✓ OLED carrier life time is lower than OLED recombination life time
6.  $R_s$  can be derived precisely through Y-plot.
  - ✓  $R_s$  is the sum of the contact resistance and some of buck resistance.
7.  $R_1+R_2$  is derived precisely through Cole-cole plot.
  - ✓ The entire term of the structure is constructed, and if converted to a Voigt equivalent circuit, the geometry impedance can be accurately derived.

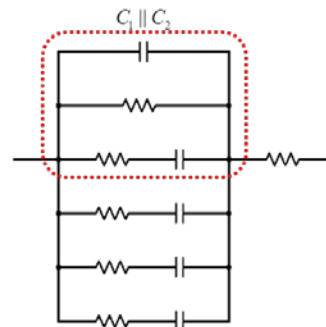
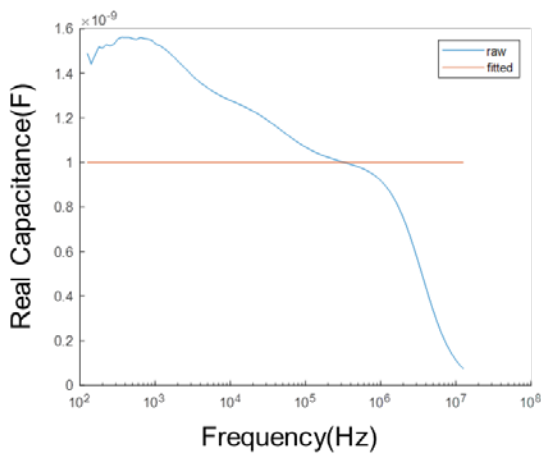
8. The contribution of the parasitic inductance component can be seen through M-plot.

✓ Effectively distinguishes parasitic inductance

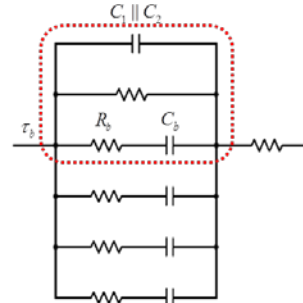
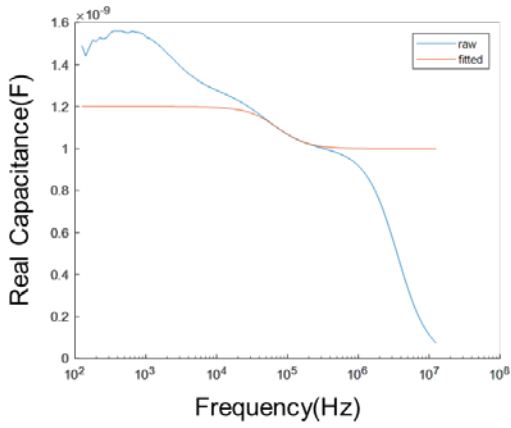
9. The contribution of the parasitic inductance component can be seen through M-plot.

✓ Effectively distinguishes parasitic inductance

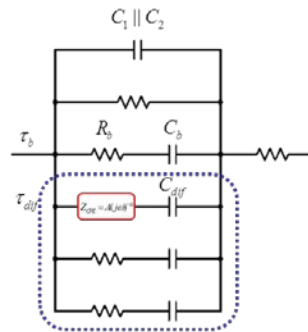
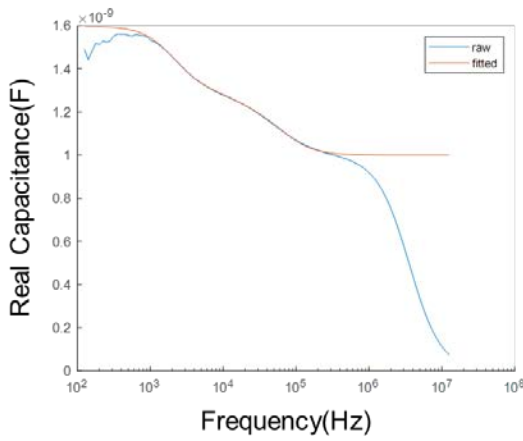
10. Verification data with CNLS fitting



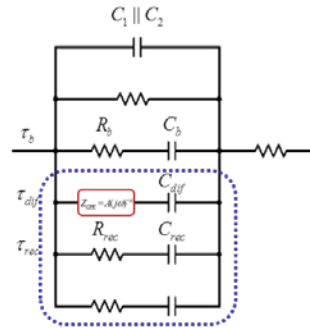
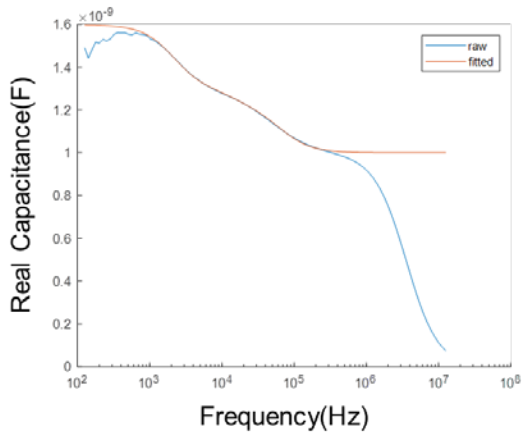
1. The  $C_{geo}$  is determined at the inflection point of the highest frequency.
  - Ensure that the  $C_{geo}$  value at high frequencies has a value close to the dielectric constant of the material.



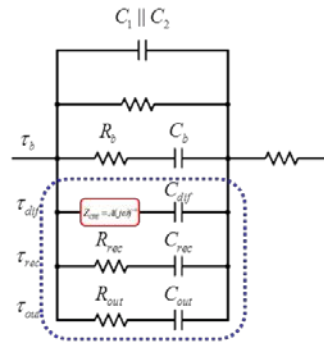
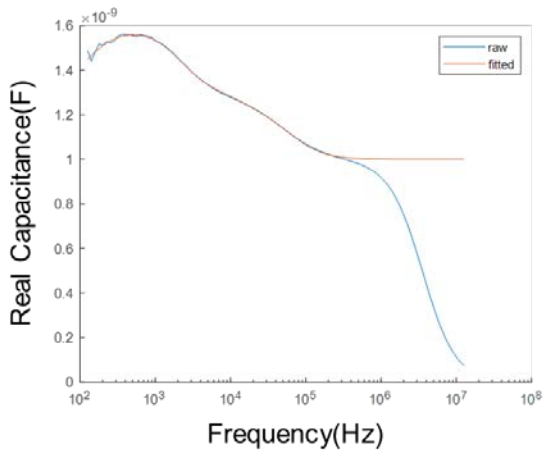
2. The  $C_b$  is determined at the inflection point of the second highest frequency
- Must be extracted in series with the  $C_b$  value at the previous voltage which reduces confusion at the ambiguous inflection point.



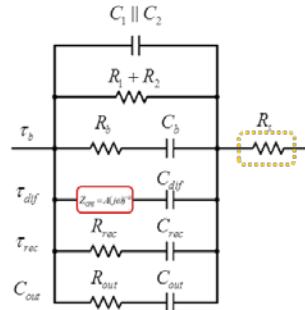
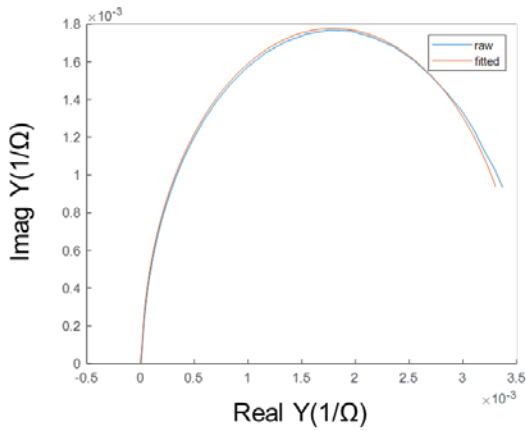
3.  $C_{diff}$  is modeled as a CPE in which the time constants of electrons and holes are dispersed.
- OLED carrier life time is lower than OLED recombination life time



4.  $C_{rec}$  is distributed at  $10^4 \sim 10^5$  frequencies, but is not large here and is therefore invisible at this scales
- OLED carrier life time is lower than OLED recombination life time

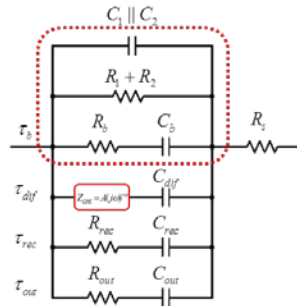
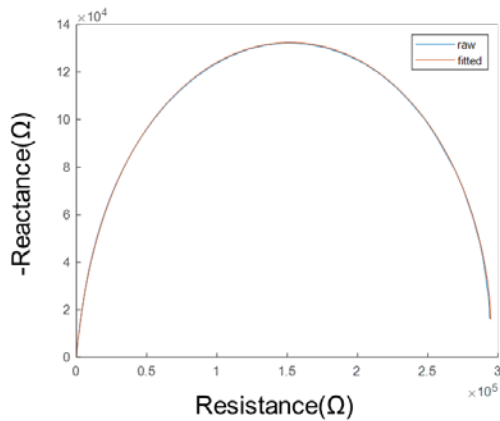


5.  $C_{out}$  is the flux of charge exiting at the terminal at the lowest frequency.
- OLED carrier life time is lower than OLED recombination life time



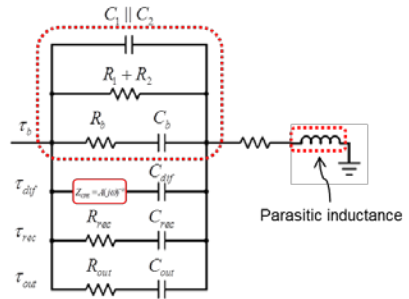
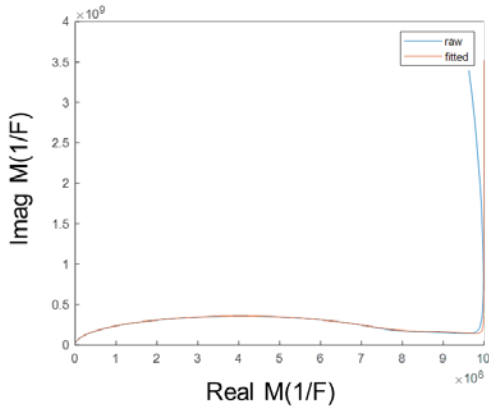
6.  $R_s$  can be derived precisely through Y-plot.

- $R_s$  is the sum of the contact resistance and some of buck resistance.

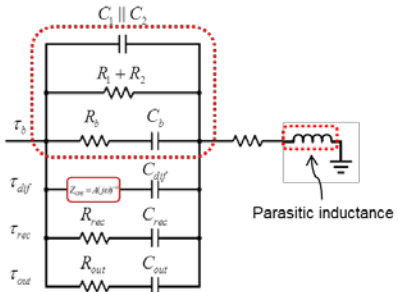
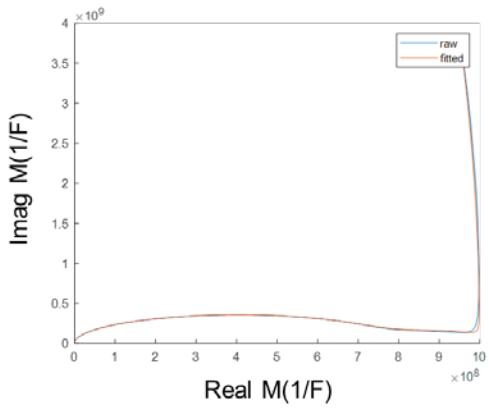


7.  $R_1+R_2$  is derived precisely through Cole-cole plot.

- The entire term of the structure is constructed, and if converted to a Vogit equivalent circuit, the geometry impedance can be accurately derived.



8. The contribution of the parasitic inductance component can be seen through M-plot.
- Effectively distinguishes parasitic inductance



9. The contribution of the parasitic inductance component can be seen through M-plot.
- Effectively distinguishes parasitic inductance

# Chapter 3

## Experiments

Several structures of OLEDs were analyzed using the impedance spectroscopy described in Chapter 2. First, to verify the impedance analysis method, OLEDs with different thicknesses were investigated. This makes it possible to examine changes in the impedance response caused by the structural difference of the OLEDs. Secondly, OLEDs with the ratio of the layer's thickness differently were investigated to closely examine at what each layer means. Also, the phenomenon that the interface collapses at the time of degradation can be confirmed by the Modulus plot, and the influence of the degradation on the interface is quantitatively examined. Third, we examine the change in impedance depending on the position of the doping. The doping was examined by changing the position of doping in the light emitting layer using DCM with about 5% doping of Alq3. The purpose of the



experiment of this Chapter is to verify the analytical theory described in Chapter 2 and to discuss the verification in Chapter 4.

### **3.1 Thickness modification OLEDs**

When analyzing OLEDs composed of stacked layers of different materials, it is necessary to examine where the corresponding impedance represents the layer in order to analyze each layer component. Therefore, the impedance was measured while changing the thickness of the HTL layer and the EML layer. Figure 3.1 shows the structure of the device. HTL selected 30n and 60n, EML selected 70n and 100n, and made four devices by combining them.

I-V-L characteristics were measured using the HP 4155C prior to each impedance measurement. The graph for this is shown in Figure 3.2. The current level of NPB: Alq3 was the highest at 30n: 70n, and decreased with thickening of each layer. This is a natural result because the resistance of the bulk increases with the length. In the case of NPB: Alq3 having 60n: 70n and 30n: 100n with similar thicknesses, the current level is similar but the HTL ratio is higher. This means that the rate of injection into Alq3 should be slower to increase efficiency. Therefore, in

order to increase the probability of recombination at relatively fast Alq<sub>3</sub>, it means that the resistance of NPB should be increased. The thickness of Alq<sub>3</sub> also affects the efficiency, because the electron transmission path becomes longer, so the efficiency decreases as the thickness increases.

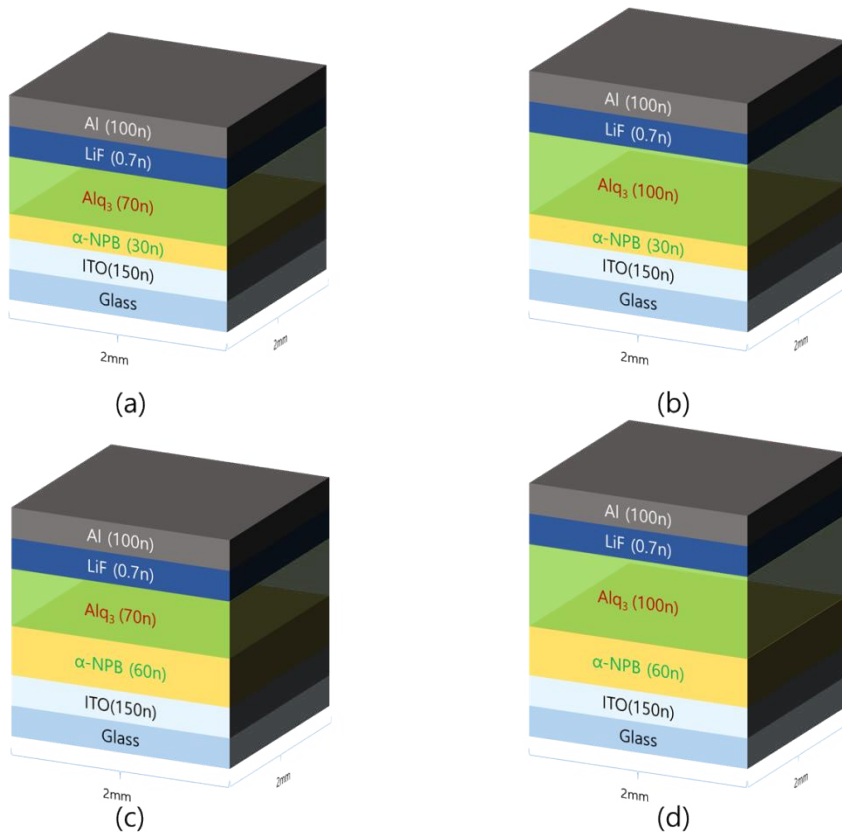


**Figure 3.1** Schematic diagram of OLEDs Structures used in this section

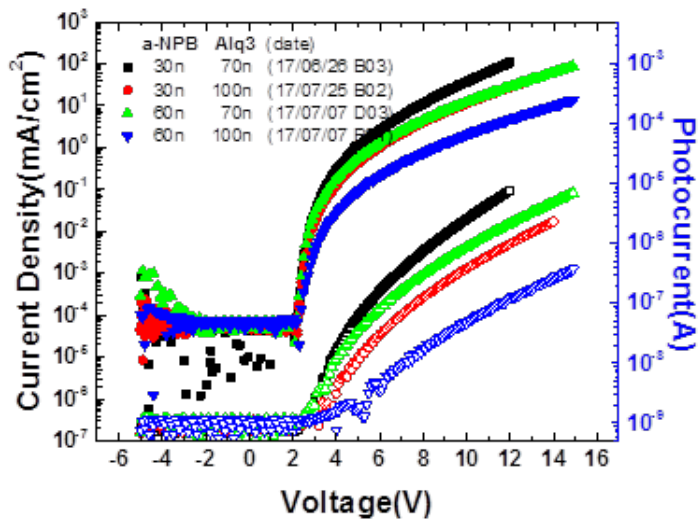


Figure 3.2 I-V-L characteristic of the OLEDs

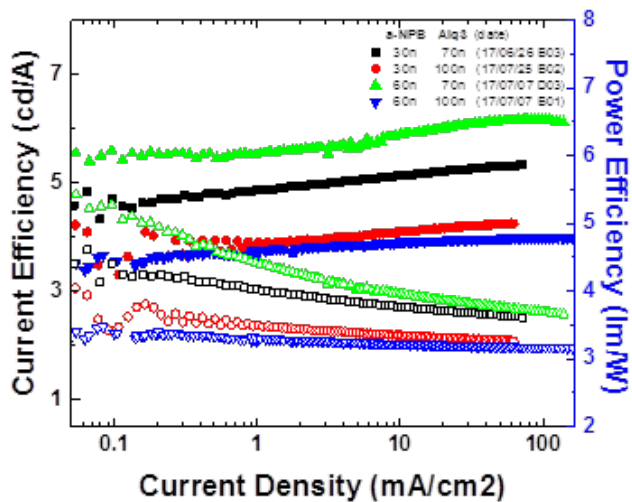


Figure 3.3 Current Efficiency and Power Efficiency characteristic of the OLEDs

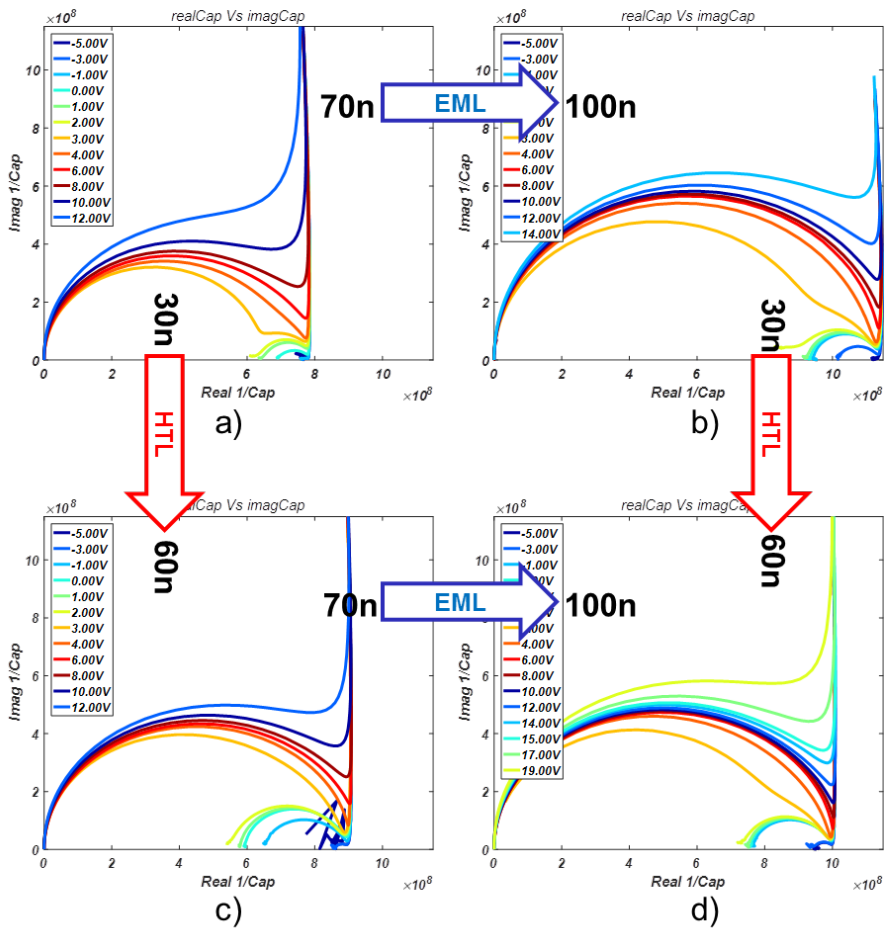


Figure 3.4 Response of Complex plane of M plot

### 3.1.1 Analysis of the Interface of the OLEDs

Figure 3.4 shows the Modulus plot for each OLED element. Modulus plots are sometimes referred to as M-plots, which plots the real and imaginary values of  $Y_{OLEDs} / j\omega$  and the radius of the circle represents the reciprocal of the capacitance in each layer.

$$\frac{Y}{j\omega} = \frac{1}{C - j\frac{1}{\omega R}} \quad (3.1.1)$$

As shown in Figure 3.4, in the low-voltage region, the layers are separated and the actual capacitance of HTL and EML can be identified. Of course, if the thickness of the layer is small, the capacitance becomes large and the radius of the circle becomes small. Therefore, this M-plot shows the thickness information of each layer. The sub circle of each circle represents the thickness information of the HTL, and it can be confirmed that the value of the cap gradually increases according to the voltage. This is because the number of charges existing inside due to the barrier in the device increases. The increase lasts until the barrier eventually collapses. This increase increases until just before turn-on, and the rate of increase is the largest at the most efficient HTL (60n)/ EML (70n). It can be seen that doubling the length of the HTL doubles the diameter of the small semicircle and increases the

diameter of the small semicircle about 1.5 times as the length of the EML increases 1.5 times. These semi-circles are clearly separated from the turn-on and are combined into a semicircle at high voltage. This fact is expected to be useful for determining the error of the product in the actual mass process.

Figure 3.5 shows the Response of complex capacitance of  $\varepsilon$ -plot plain. This is suitable for the analysis of the charge transfer model proposed by the authors. Here, each semi-circle represents the geometry capacitance of each layer of Maxwell Model (see Chapter 2). In terms of efficiency of OLEDs, the greatest increase in the degree of right-hand circularity is that there are many holes in the HTL, so it exists for a long time before the barrier is passed. The vertical line above shows the charge transfer, and as the voltage increases, it shifts to the left. When the degree of parallel movement is measured, it is expected that the most moving (a) is the largest current, and it can be proved that it is true when compared with Figure 3.2. In addition, the size of the left semicircle represents the capacitance of the geometry at both ends of the electrode.

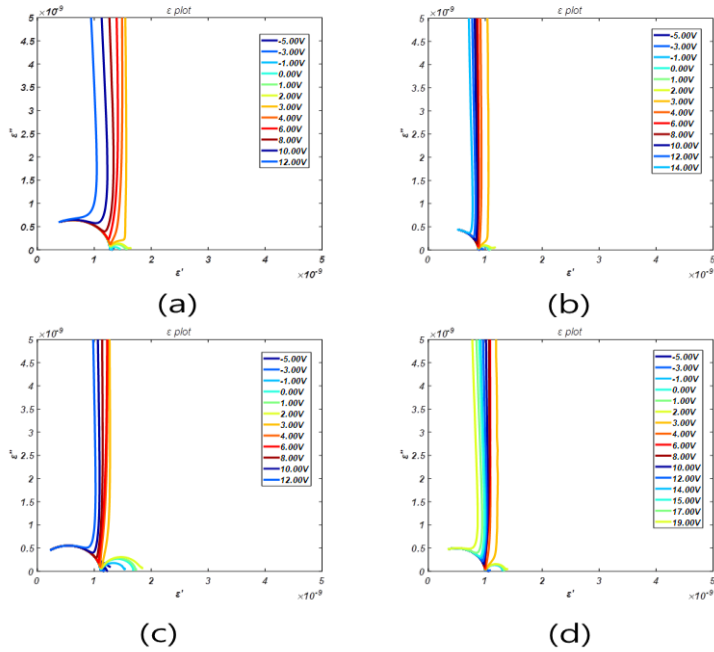


**Figure 3.5** Response of Complex capacitance of  $\epsilon$  plot plain

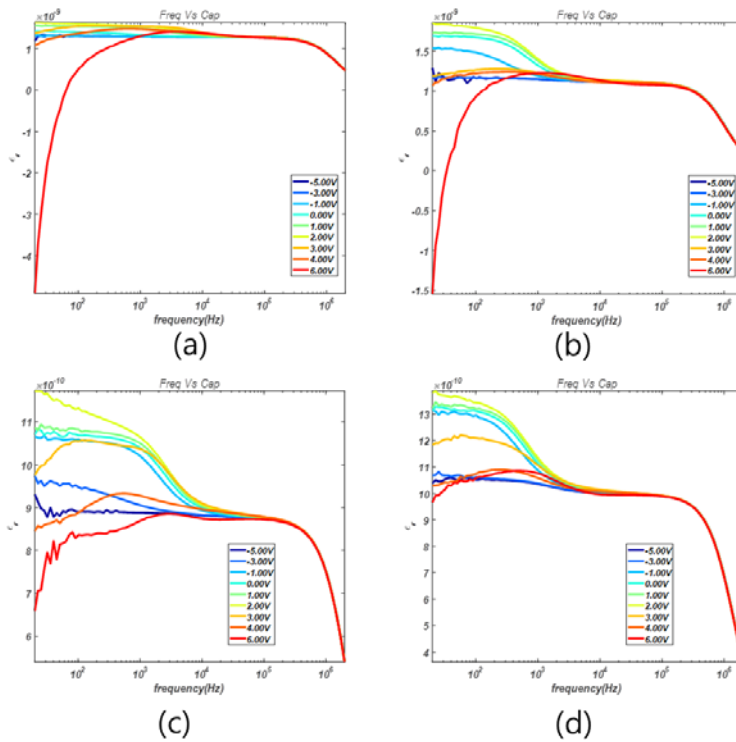
### 3.1.2 Analysis of the Carrier Distribution of OLEDs

Figure 3.6 shows the capacitance response versus frequency. This means the amount of pure capacitance measured when measuring capacitance in OLEDs. This is complicatedly changed according to the frequency, but the effect of the interface at high frequency and the effect of charge transfer at low frequency.

At low voltage, two hills are visible, with capacitance representing the

respective interface as a whole. Comparing this value with the actual thickness of the device, each represents the thickness of HTL and EML. However, what we are looking at in this graph is rather a reduction in the capacitance of the low frequency band. Comparing the low-frequency capacitance values at the same current, it means that the larger the values of the capacitance, the more carriers are distributed in the inside. From the voltage and current characteristics, it can be seen that the samples with the highest efficiency (c) and the samples with the same efficiency (a) and (c) have almost the same values at the same current. On the other hand, the low efficiency (d) shows the lowest amount of negative capacitance at the same current.





**Figure 3.6** Capacitance response of the OLEDs with Frequency Sweep

### 3.2 Thickness ratio modification

In order to better understand the change of the impedance with respect to the thickness, the effect of the degradation on the interface was examined by fixing the total thickness and changing the ratio of each HTL / EML to the degradation process. Figure 3.7 shows the structure of each device fabricated. The total thickness was

fixed at 70n and the HTL and EML portions were changed to 1:6, 2:5, 3:4, 4:3, 5:2. The reason for adjusting the thickness ratio is that the electron-hole balance can be relatively easily changed. Therefore, the change in impedance response was observed when the electron-hole balance was changed.

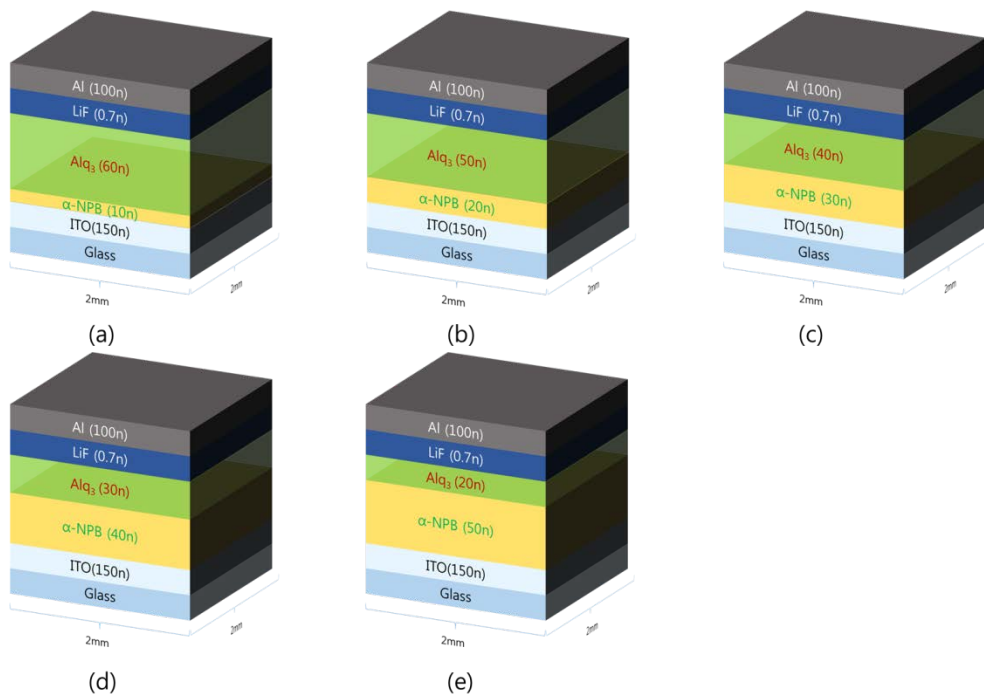


**Figure 3.7** Schematic diagram of OLEDs Structures used in this section

Sample#	Anode	a-NPB	Alq <sub>3</sub>	LiF	Cathode	Current Efficiency
OLED#1	150n	10n	60n	0.7n	100n	2.3 cd/A
OLED#2	150n	20n	50n	0.7n	100n	2.2 cd/A
OLED#3	150n	30n	40n	0.7n	100n	2.4 cd/A

<b>OLED#4</b>	<b>150n</b>	<b>40n</b>	<b>30n</b>	<b>0.7n</b>	<b>100n</b>	<b>2.1 cd/A</b>
<b>OLED#5</b>	<b>150n</b>	<b>50n</b>	<b>20n</b>	<b>0.7n</b>	<b>100n</b>	<b>1.5 cd/A</b>

**Table 3.1** Information on fabricated OLEDs

### **3.2.1 Relation between efficiency and M-plot**

Table 3.1 shows that the HTL: EML thickness ratio of 3: 4 is the highest. In chapter 3.1, HTL: EML thickness ratio was the highest at the ratio of 6: 7, which is a reasonable result. That is, the electron-hole balance is considered to be the highest at a ratio of about 6: 7 to 8.

Figure 3.8 is a graph showing the M-plot response of the above five samples. The size of each semicircle represents almost exactly the thickness ratio of HTL and EML. In addition, (c) shows the smallest change in the rate of change from the moment when the class members are not distinguished. This actually means that the C value in the C-V graph is maintained above  $V_{peak}$ . Therefore, in the actual M-plot, the factor that rapidly drops of negative capacitance above  $V_{peak}$  means that the size of the semicircle increases sharply. This means that the carriers that do not participate in the recombination with the OLEDs are also eliminated. As explained

in Chapter 2, this leads to a reduction in efficiency.

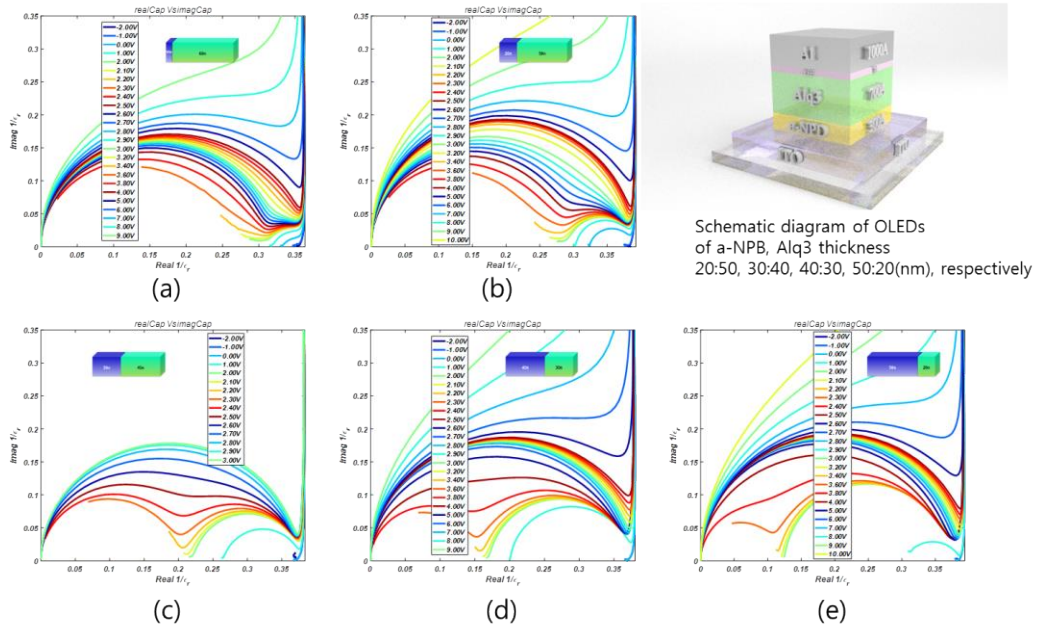


**Figure 3.8** M-plot representation for each device. It can be seen that the ratio of the thickness ratio to the diameter of the sub-semicircle coincides.

### **3.3 DCM doping ration Modification**

To understand the effect of doping, DCM doping was inserted in the middle of the Alq3 layer. The reason for this doping is that the doping itself can control the effects on the interface and the amount of charge recombination. Indeed, many experiments with doping locations have been done previously and were used to determine recombination sites. In this section, you can see the degree of recombination or the mobility characteristics of the bulk itself and the effect of doping.

#### **3.3.1 Correlation between Current-Voltage-Efficiency and Impedance Response**

The structure of the OLED was designed with NPB of 30n Alq3 at 70n and doped with 5 vol% DCM at an interval of 20n near NPB. Figure 3.9 shows the structure of the device and confirms that orange light is emitted as a result of doping of DCM (Figure 3.10). The luminescence gradually became greenish as the position of the doping layer in the NPB layer was increased, because the amount of luminescence was increased by Alq3. The color coordinates for the color are shown

in Figure 3.11 in the CIE coordinate system. The farther the DCM is from the interface between EML and HTL, the lower the current characteristic, while the higher the efficiency. This is similar to the basic assumption derived from Ching Tang's DCM doping experiment. Once doped with impurities of DCM in the interface of HTL and EML, it is greatly influenced by the state of the interface. Hence, the leakage current component becomes large, and hole injection is not performed properly at the homo level. Therefore, a large amount of non-luminescent charge carriers that do not participate in luminescence appear although the current is large. On the other hand, the device with DCM doped to the cathode side without a large defect at the interface seems to have higher probability of recombination in both Alq<sub>3</sub> and DCM. As shown in the right figure of Figure 3.14, the device (a) in which DCM is near the interface actually has the largest  $V_{on}-V_{bi}$  and more negative charge at the interface, which seems to act as a non-luminescent recombination center as an impurity. Also, it can be seen that the increase in internal carrier is greatest after  $V_{bi}$ , which means that the recombination component is less. The closer the DCM is doped to the cathode side, the more (c) it can be seen that the device is recombining more efficiently as a low-level implant. Also, the device with the slowest negative capacitance at higher voltages is also the device with the DCM closest to the cathode (c), which means that the number of recombining charges lasts even higher voltages. On the other hand, the element (a) has a very sudden negative

capacitance value.

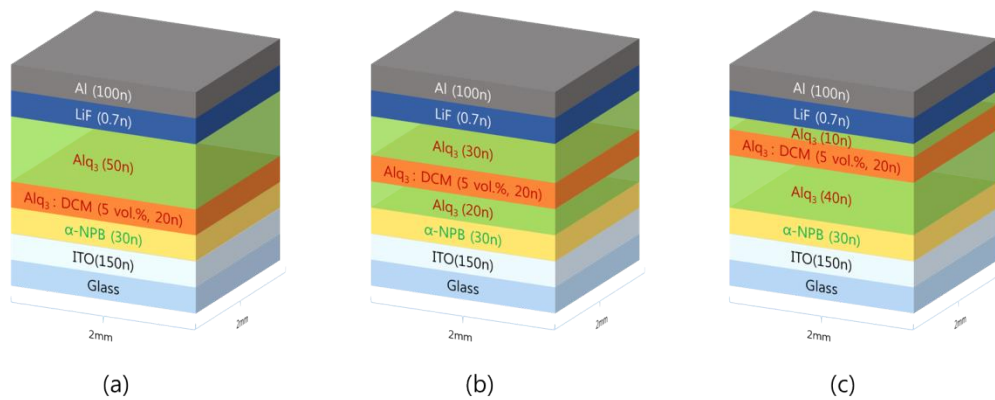


**Figure 3.9** Schematic diagram of OLEDs Structures used in this section

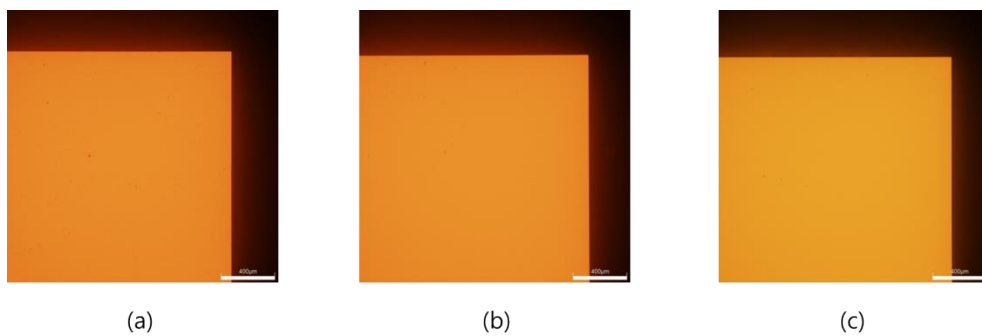


**Figure 3.10** Microscope image of the DCM doped OLEDs

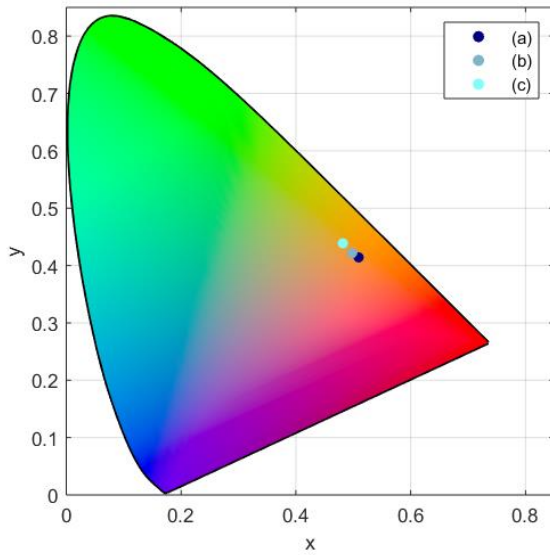


Figure 3.11 CIE x, y value of the chromaticity diagram DCM doped OLEDs

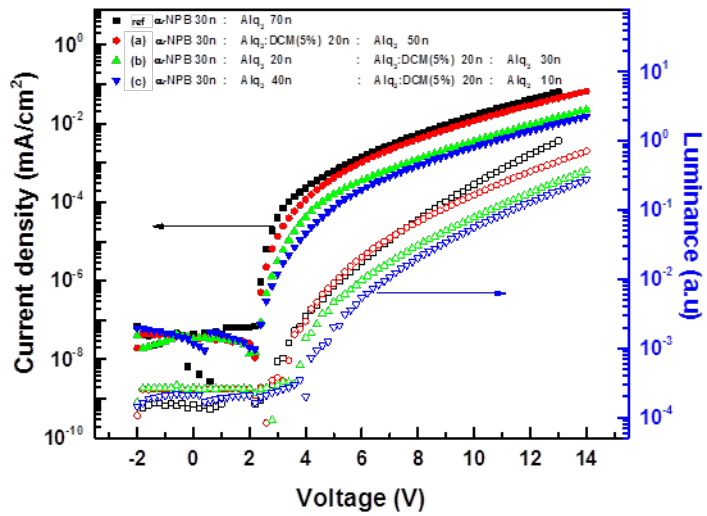
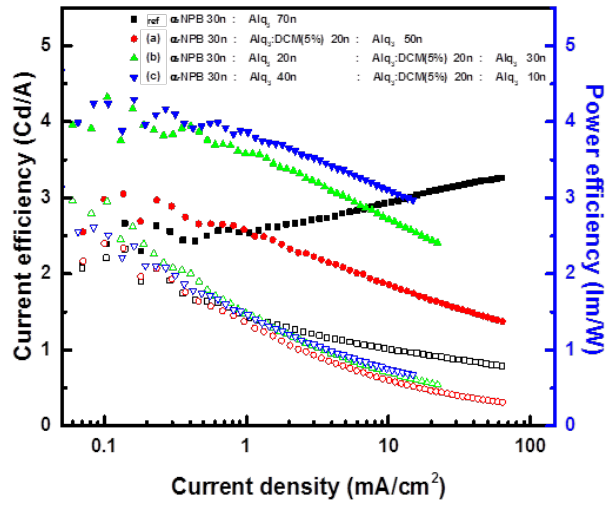
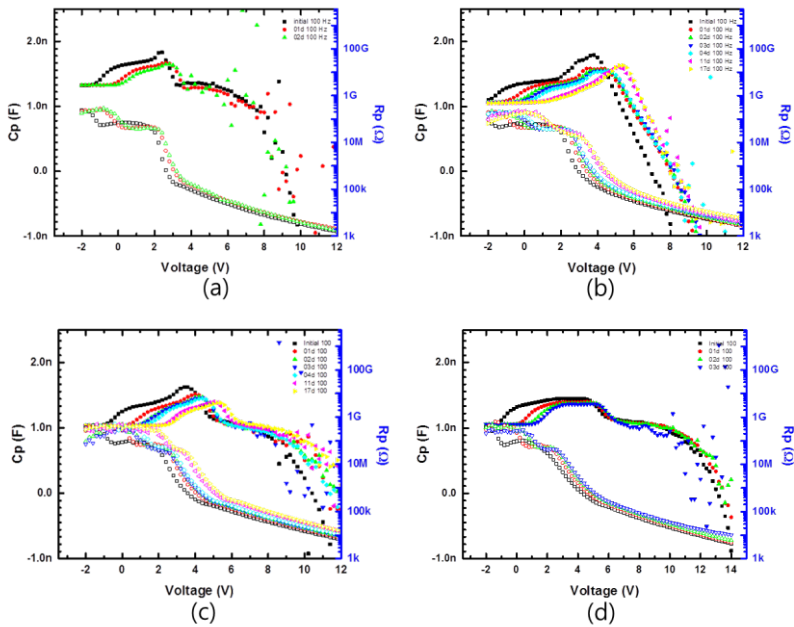


Figure 3.12 I-V-L characteristic of the DCM doped OLEDs





**Figure 3.13** Current Efficiency and Power Efficiency characteristic of the DCM doped OLEDs



**Figure 3.14** C-V characteristic of OLEDs (a) not doped (b) doped near HTL/EML interface (c) intermediate EL (d) near cathode

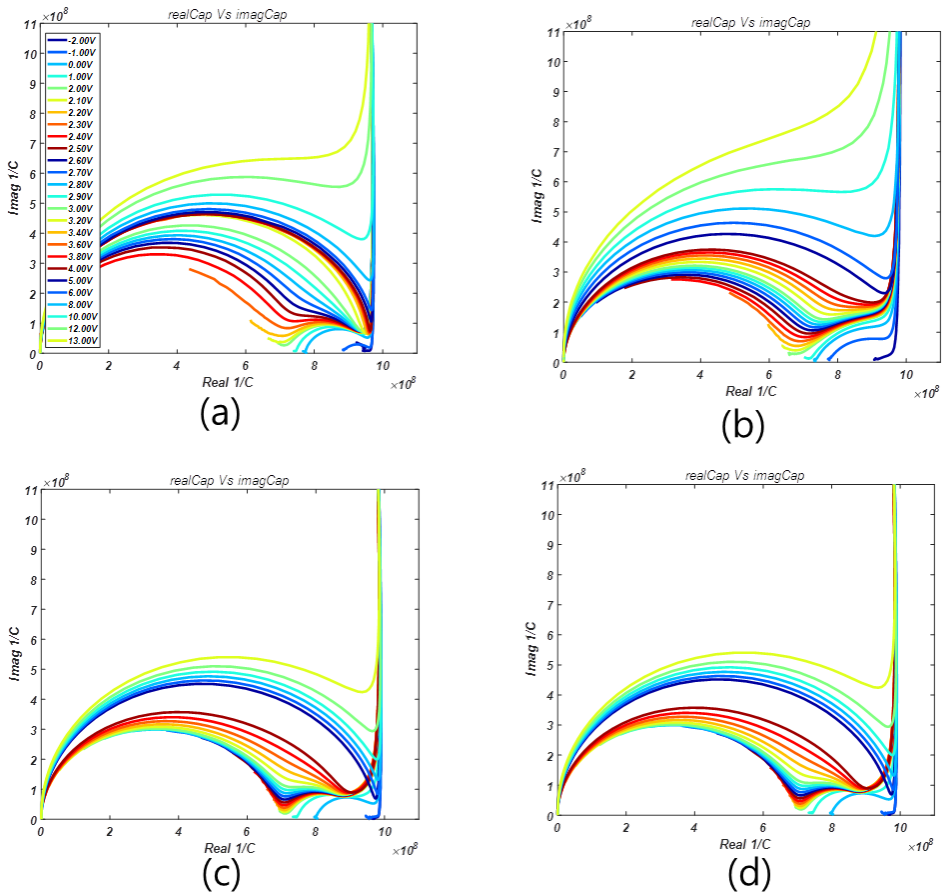


**Figure 3.15** The structure of the device is maintained through the M-plot characteristics, but it can be seen that different layers appear in the intermediate frequency band. (a) Not doped (b) doped near HTL/EML interface (c) intermediate EML (d) near cathode.

# Chapter 4

## Discussion

### 4.1 Consideration of Effects of Interface Properties

The interface characteristics are largely divided into organic/organic and organic/metal characteristics. At this time, the field distribution due to the relocation of the space charge created by the potential barrier due to the energy band difference can be approximated by the RC circuit of the tunneling current characteristic which determines the capacitance and crosses the space. Here, the value of the fixed charge existing in the interface affects the capacitance and the resistance value. The interface charge of the organic/organic interface is usually present as a negative charge[54], which changes the field distribution per layer. It is possible to estimate

the amount of the interface charge by the potential difference between  $V_t$  and  $V_{bi}$  in the low frequency capacitance graph. Figure 4.1 shows how the values of  $V_t$ ,  $V_{bi}$ , and  $V_{peak}$  at low frequencies (100 Hz) are determined.  $V_{bi}-V_t$  decreases with degradation, which decreases the electron-hole balance by increasing the amount of holes injected from the HTL to the EML, thereby decreasing the efficiency. It can be seen that this reduction of the fixed charge leads to a reduction in the amount of carriers present in the EML and that the capacitance reduction due to the recombination becomes noticeable at higher voltages.

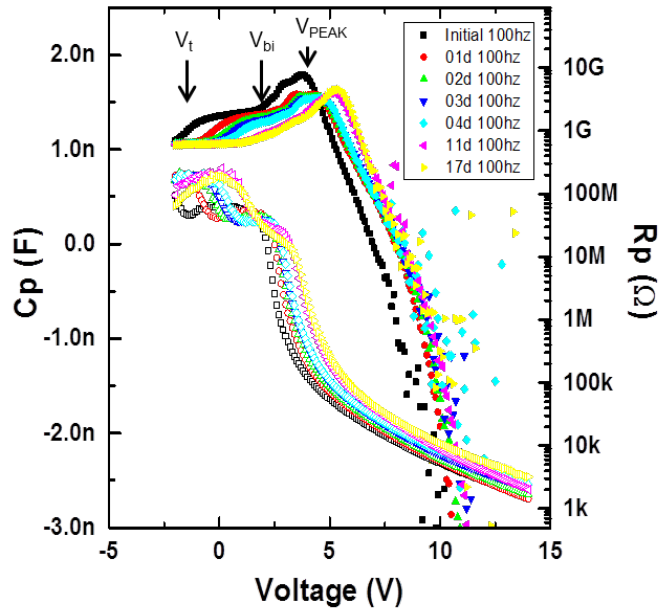


**Figure 4.1** C-V graph showing the decrease in fixed charge of organic / organic interface at low frequency (100Hz) and the resulting decrease in efficiency

## 4.2 Consideration of Effects of Bulk properties

Bulk properties can be obtained by obtaining  $R_s$ . This  $R_s$  value can be found at the inflection point of the slope where the capacitance rapidly drops to zero at high frequencies. The  $R_s$  value at low voltage is generally increased as the voltage goes up, but it is also possible to reduce it from the structural factor. At this time,  $R_s$  value is as follows.

$$R_s = 1 / \omega C_{geo} \quad (4.2.1)$$

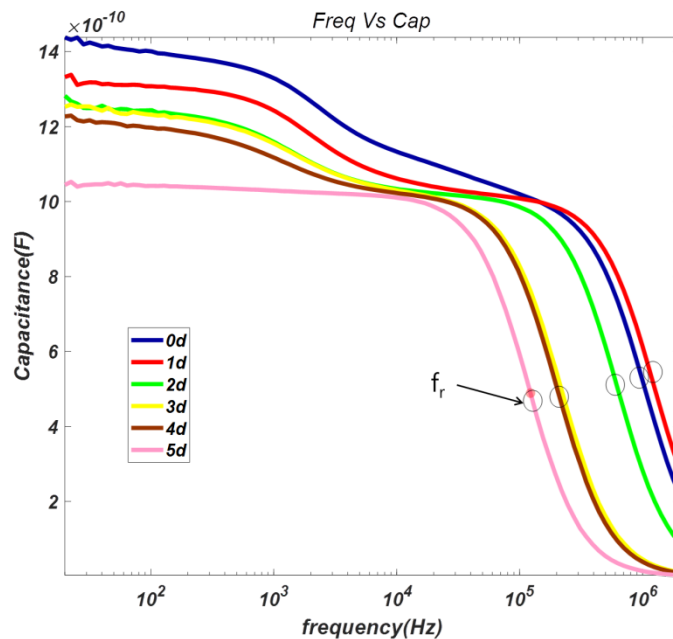


**Figure 4.2** Capacitance response at 2V near turn on voltage.  $R_s$  can be read at transient frequency ( $f_r$ ).

Generally, when stress is applied, this resistance tends to decrease at first time and then increase soon. This can explain the general phenomenon that OLEDs initially have a temporary increase in current-voltage characteristics. That is, the resistance to bulk is gradually relaxed while electrical stress is applied rather than the initial OLEDs. However, if the stress continues, hopping conductance decreases due to the change of physical properties of the bulk resistance increase. Figure 4.2 clearly shows that the inflection point frequency of the high frequency increases during the first day and then decreases. In the case of the same sample, the amount of change in bulk can be deduced from the comparison of the reduction amount.

### **4.3 Negative Capacitance relation with efficiency analysis**

The main cause of NC(negative capacitance) is related to the charge disappearing inside the injected charge. In the Laux and Hess study, the material with the PN junction has negative capacitance values due to the charge dissipated by the recombination and the injected carrier due to the short distance of the diode which outflow from OLEDs. Thus, this reduction in capacitance means a recombination or quenching factor. The former is associated with increasing efficiency and the latter with lower efficiency. However, it is not easy to distinguish

between the two because they appear overlapping. A typical example is shown in Figure 4.2. This sample is an ITO (150nm) / NPB (30nm) / Alq3 (40nm) / LiF (0.7nm) / Al (100nm) sample manufactured on different days. The OLEDs of these two OLEDs can be seen to have almost the same structure when judged by the M-plot shown in the sub-plot of Fig. 4.2 (a) and (b). However, the efficiency of these two samples was significantly different. The device (E02) manufactured on December 12, 2017 had a higher efficiency than the device (C03) manufactured on January 17, 2018. The reason for this is thought to be that there is a difference in the material or interface due to precisely unknown reasons in the process. As shown in Figure 4.2 (d), the difference between  $V_t$  and  $V_{bi}$  is constant. However, when the amount of capacitance decreasing in the region of 4 V or more after  $V_{peak}$  is observed, it can be seen that the E03 device exhibiting a higher efficiency has a smaller capacitance than the C03 device. It is presumed that the carrier injected from the electrode stays in the EML for a longer time and increases the recombination probability. Immediately after  $V_{peak}$ , the capacitance of the device C03 is seen as a flat layer, so the amount of internal carriers appears to be larger in the region between 3 and 4 V, but considering that the reduction in capacitance due to recombination is 2/3 of the actual capacitance, Background capacitance appears to have appeared.

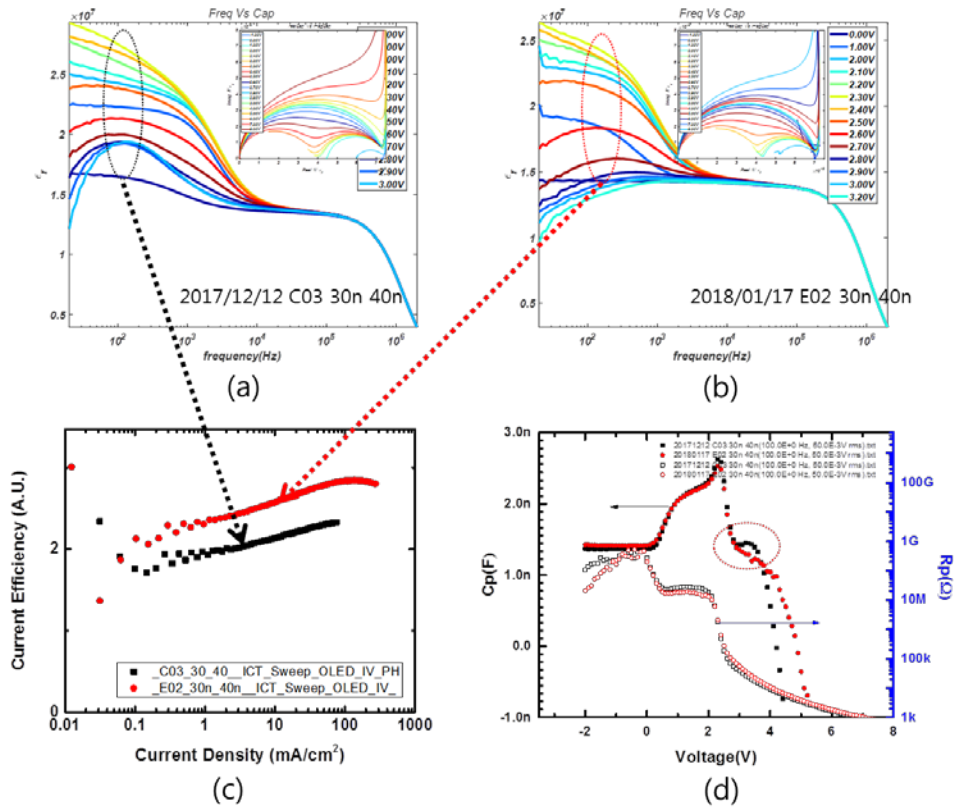


**Figure 4.3** OLEDs of the same structure made of the same process with different electrical properties. The M-plot shows that the device structure is the same, but the efficiency is different. This can be understood in advance through the low-frequency analysis of the negative capacitance value.



## 4.4 Mobility Measurement Using Impedance analysis

Aldert van der Ziel, in Solid State Physical Electronics [1957], found that the mobility of a single injection space charge diode can be obtained by the Laplace transform of a SCL diode current equation with a small signal applied [55].

$$\begin{aligned}
 J(t) &= J_0 + J_1 \exp(j\omega t), & F &= F_0 + F_1 \exp(j\omega t) \\
 J_0 &= -\frac{9}{8} \varepsilon \varepsilon_0 \mu_n \frac{V_a^2}{L^3} \\
 J_1 &= -g_0 \frac{\frac{1}{6} (j\omega\tau)^3 V_1}{1 - j\omega\tau + \frac{1}{2} (j\omega\tau)^2 - \exp(-j\omega\tau)} \\
 Y &= -\frac{J_1}{v_{a1}} = g + j\omega C = g_0 \frac{\frac{1}{6} (j\omega\tau)^3}{1 - j\omega\tau + \frac{1}{2} (j\omega\tau)^2 - \exp(-j\omega\tau)}
 \end{aligned} \tag{4.4.1}$$

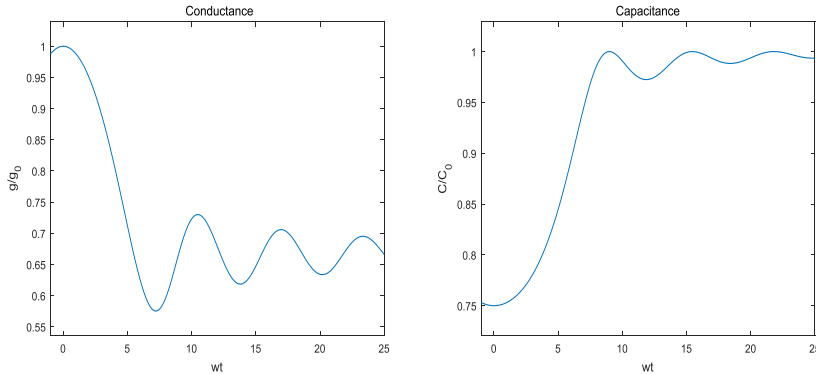


**Figure 4.4** Mobility extraction from SCLC current characteristics. By adding a small signal to the SCL current, mobility can be obtained from the minimum value of the admittance value

Naito's team of Japan showed that mobility can be extracted accurately from the value obtained by multiplying the time constant by a constant when the B method and the G method are applied when the actual disorder is a substance [56, 57]. This can be a mobility extraction method of an approach different from the methods of actual TOF and transient EL, transient SCLC, and the like. In this study, the mobility value of Alq3 was successfully extracted using EOD and results similar to those in the literature were derived.

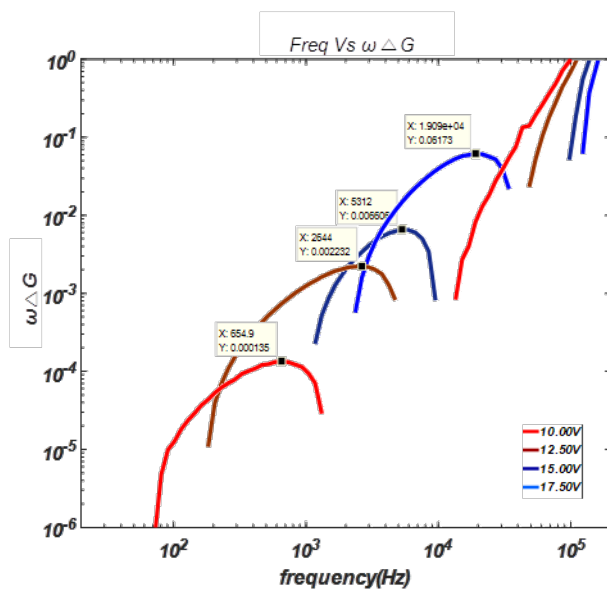


**Figure 4.5** Maximum frequency per voltage for mobility extraction using  $\Delta G$  method

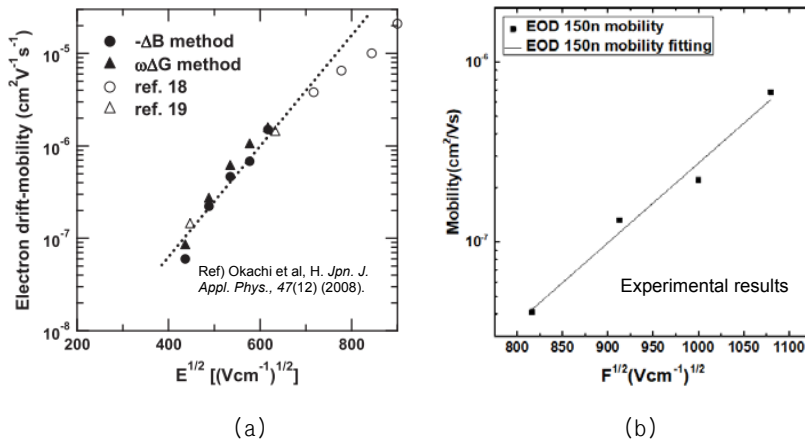


**Figure 4.6** Mobility extraction value using  $\Delta G$  method. Mobility proportional to square of field extracted

As shown in Figure 4.3(d), when the capacitance value is measured at low frequency ( $<100$  Hz), the capacitance value that has increased at the turn on vicinity rapidly decreases at high electric field ( $> 5.0 \times 10^7$  V/m).

Negative capacitance (NC) phenomenon is typically observed on high disorder material via impedance analysis. It used to be thought to be mainly caused by a measurement error. However, as the measurement technology becomes more precise, NC is considered to be one of the important physical properties in materials with low mobility and hopping conduction[58]. In particular, the negative capacitance phenomenon in organic light-emitting diodes (OLEDs) has been

reported steadily[29, 59]. NC values are known to increase at low frequencies under high electric fields[60].

In this paper, we show that the average transition time ( $\tau_{tr}$ ) from a hopping site to another hopping site can be expressed as the phase difference ( $\Theta$ ) of between lagging alternative current (AC) current and the applied small signal AC voltage with frequency of  $\omega_s$ . That is,  $\tau_{tr} = \tan \theta / \omega_s$ . OLEDs with relatively simple structure of ITO/ $\alpha$ -NPB/Alq<sub>3</sub>/LiF/Al, which have varied thickness ratio, were fabricated and their average transition time were analyzed. When this transition time is applied to the mobility relation of ( $\mu = 4d^2 / (3\tau_{tr}V)$ ), it can be seen that it reflects the mobility value relatively accurately. As shown in Fig. 2, since the mobility of hole transport layer (HTL) material is larger than that of emissive layer (EML) material, it can be seen that the composite mobility value becomes smaller as the thickness ratio (thickness\_Alq<sub>3</sub>/thickness\_ $\alpha$ -NPB) increase while the composite mobility value increases as the thickness ratio decreases. These values are summarized in Table 4.1.

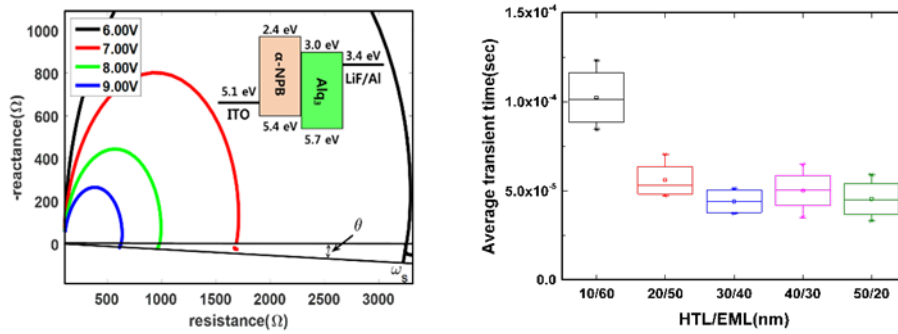


**Figure 4.7** The lag phase shift of the negative capacitance

**Table 4.1** The average transient time value and the composite OLED SCLC mobility

Thickness ratio(nm)	Average transition time (Experimental value)	Transient SCLC mobility
10/60	1.02E-04	3.78E-07
20/50	5.61E-05	6.87E-07
30/40	4.42E-05	8.71E-07
40/30	5.02E-05	7.67E-07
50/20	4.06E-05	9.49E-07

# Chapter 5

## Conclusion

So far, we have investigated the impedance spectroscopy of OLEDs and analyzed the electrical properties and degradation mechanism of OLEDs using impedance response. As mentioned in the text, OLED parameters are not extracted by simple circuit model alone, but must be measured by voltage and current with various strategies. Therefore, complexity is added here. In particular, the impedance response of OLEDs should be analyzed by separating the carrier transport characteristics and the structural characteristics. The purpose of this paper was to examine how OLEDs can interpret physical phenomena through impedance representation. This requires an attempt to analyze the impedance as accurately as possible. Unfortunately, not only the instability of the OLEDs, but also experimental errors has led to very difficulties in this analysis.

So I tried to analyze more OLEDs, but unfortunately I had to experiment with the simplest structure of the device as stable as possible. However, the simpler the structure, the clearer it is to have a closer look.

We have tried to automate everything from production to measurement for the accuracy of extraction, and this has been solved through Labview. To analyze the impedance of the measured device, we extracted the parameters through recursive constant non-linear least square (CLNS) method using MATLAB. Basically you can see the structure of OLEDs better at low voltage injection and high frequency. Once the structure of OLEDs at the high frequency is determined, the charge transfer characteristics can be analyzed in more detail at low frequencies. The domain in which the structure is well visible is the domain of the M-plot. At this time, the resistance and capacitance information of HTL and EML are extracted from the low voltage until the current is injected into the EML. In general, the remaining layers except the EML are planarized by the fixed charge at the interface. This point is where the capacitance of the EML is extracted, and it looks as if the parallel plate capacitance exists as thick as the EML. This allows the stack structure of OLEDs to be extracted. Also, in the e-plot, the small semicircle in the high frequency range means the capacitance of the OLEDs over the voltage across the device, which can indicate the state of the interface.

Therefore, when analyzing OLEDs using impedance spectroscopy, it is

necessary to measure the impedance sequentially while changing the voltage or changing the frequency and it is necessary to have the ability to read the continuous change value. Actual device capacitance may also require a decentralized capacitance value that is different from the ideal capacitance value. Therefore, the introduction of CPE (constant phase element) is also very important. These CPEs are particularly suited to models in which carriers are injected in the charge transfer model. Each carrier is hopping conduction between states near the homo or lumo level of the OLEDs, so its dielectric relaxation time is more likely to be more dispersive. This can explain the behavior of a somewhat unusual capacitance in the low frequency range.

After the turn-on voltage, injected carriers accumulate inside the device, indicating a typical diffusion capacitance and increasing rapidly. However, this is negative due to the current component flowing out of the electrode during the recombination and the internal carriers are in equilibrium. This is the origin of the negative capacitance appearing at low frequencies, and the capacitance of these two negatives is an important factor in determining the probability of recombination and the efficiency of the device. Therefore, we have studied the role of negative capacitance in OLED devices, which are short, low mobility and relatively long carrier lifetime by taking advantage of the results of Laux and Hess. In some papers, negative capacitance has often modeled with inductance, but we concluded that



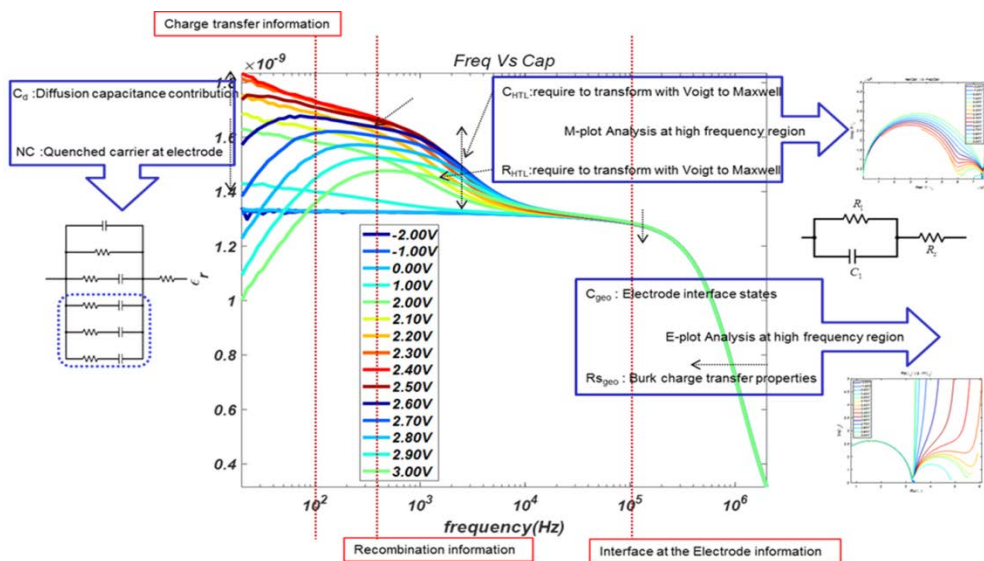
modeling with inductance is not good at any thin film devices. In addition, we have used the results of HESS and LAUX to study the role of cathode capacitance in OLED devices with short, low mobility and relatively long carrier lifetimes. I often modeled this negative capacitance with the inductance of an existing model, but I concluded that modeling with inductance is not good for my model. This is because if the inductance is included in the equivalent circuit modeling, it is contradictory that the magnetic field must be formed electromagnetically. In addition, the inductance extracted from the inductance model is very large. Also, in direct current, the impedance value due to the diffusion capacitance due to the internal carrier must be zero, so it is reasonable to consider this as a capacitance. Therefore, the capacitance associated with charge transfer appears as a path connected in parallel to the RC circuit representing the entire structure, which has positive and negative values to represent an increasing carrier and a decreasing carrier.

Figure 5.1 shows the frequency band and equivalent circuit that can be used to find out all OLED characteristics mentioned in this paper. The intermediate frequency connected to the frequency recombination delay time of the low frequency band in which the charge transfer information is known, and the high frequency band in which the electrode interface is known are separately displayed, and the equivalent circuit is also shown. In addition, the transition frequency can be clearly seen through the M-plot of the intermediate frequency, and the thickness of

each layer can be seen intuitively only by the picture. With the  $\epsilon$ -plot, you can see more details of the geometry of OLEDs and the change in the mobility of the bulk. It can be seen that the charge transfer model is located at the low frequency, and it becomes simple at the high frequency and represents only the interface between the electrodes. The shape of vertically cut-off line becomes a voltage-capacitance graph and the state of the interface and the characteristics of the bulk can be determined by changing through the line. The carrier transfer model in the low frequency domain can be represented by CPE, and Chapter 2 describes in detail how to extract it. Figure 5.2 illustrates where to select the frequency and voltage region to obtain desired characteristics of OLEDs. The length of the ellipse tells the sweep range, which means that the longer the ellipse, the larger the voltage range must be swept. Table 5.1 shows the effect of degradation, the observation method and the domain which easily informs characteristic according to degradation factor.

This study investigated how to identify the elemental characteristics of OLEDs as impedances, and succeeded in proving them in part. However, the impedance response is very sensitive, so there is a possibility that the changes due to unknown variables will overlap. Therefore, it is necessary to systematically analyze and verify a lot of big data by finely manufacturing the device. If the standardization of the impedance analysis method is made through this study, not only the device characteristics and degradation factors can be identified by only analyzing the

impedance response of the OLEDs, but also it can reduce trial and error and cost in determining the optimal structure and materials needed to design high efficiency and durable OLEDs. We expect impedance spectroscopy to be widely used as a benchmark for evaluating OLEDs in the near future.



**Figure 5.1** An equivalent circuit model and extraction strategy for which frequencies should be observed in frequency - capacitance graph

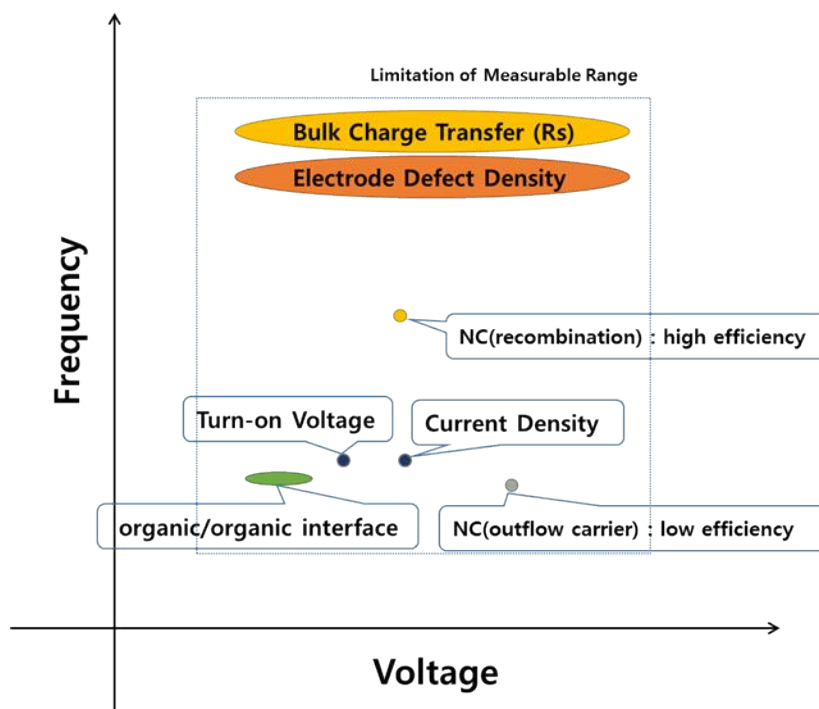


**Figure 5.2** The voltage and frequency range that should be measured to determine the characteristics of OLEDs. The length of the ellipse tells the sweep range, which means that the longer the ellipse, the larger the voltage range must be swept.

<b>Degradation Factor</b>	<b>Effects of Degradation</b>	<b>Observation method</b>	<b>Measuring Domain</b>
<b>Organic material denaturation</b>	Increase of impurities in organic matter	Rs of Increase / decrease at high frequency	$\epsilon$ -plot, C-V
<b>Electrode/Organic interface</b>	defect increase at the interface	C with voltage sweep at high-frequency	$\epsilon$ -plot, C-V
<b>HTL/EML fixed charge</b>	Hole-electron balance	Flatue region except EML In C-V, at low-frequency	M-plot,C-V
<b>Turn-on Voltage</b>	Increase EML injection barrier	The highest rate of change of Rp in the C-V at low-frequency	C-V
<b>External quenching carrier</b>	Charge flux outward from electrode during injection carrier	C-V at high-frequency in high-level injection	C-V, C-f
<b>Injection barrier increase</b>	Current level reduction	C increase immediately after turn-on	C-V
<b>Efficiency decrease</b>	Non-radiation recombination increase	Intermediate voltage at the intermediate frequency	C-V

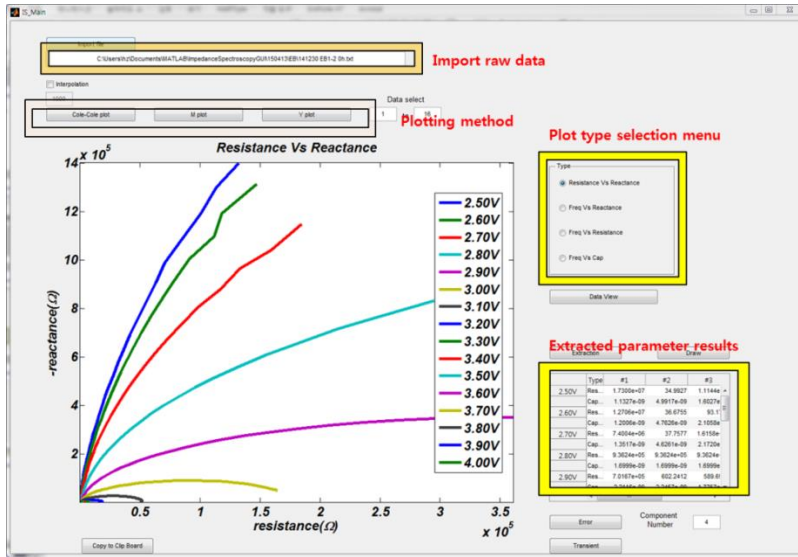
**Table 5.1** The effect of degradation, the observation method and the domain which easily informs characteristic according to degradation factor

# Appendix

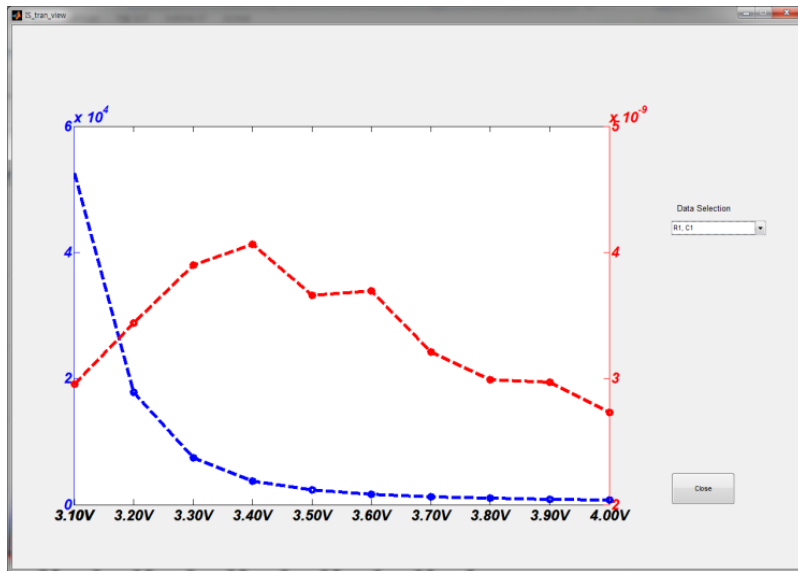
## **Solutions Programs Tools to Assist Impedance Analysis of OLEDs**

There are many commercial programs that analyze impedance in the electrochemical field, but the focus is on electronic devices with electrolytes rather than solid electronic devices such as OLEDs. Therefore, the authors have developed a tool that can directly extract the impedance rather than using the existing program. In order to extract the impedance of the OLEDs, the voltage that satisfies the characteristic condition of the layer at various voltages is extracted, and the impedance according to the voltage is extracted. At the same time, the impedance is checked using the complex non-linear square Least Squares (CNLS) and the residue can be extracted.

The author designed an automated process using Labview to measure the impedance value of 200 frequencies from 20 voltages over one sample per sample.



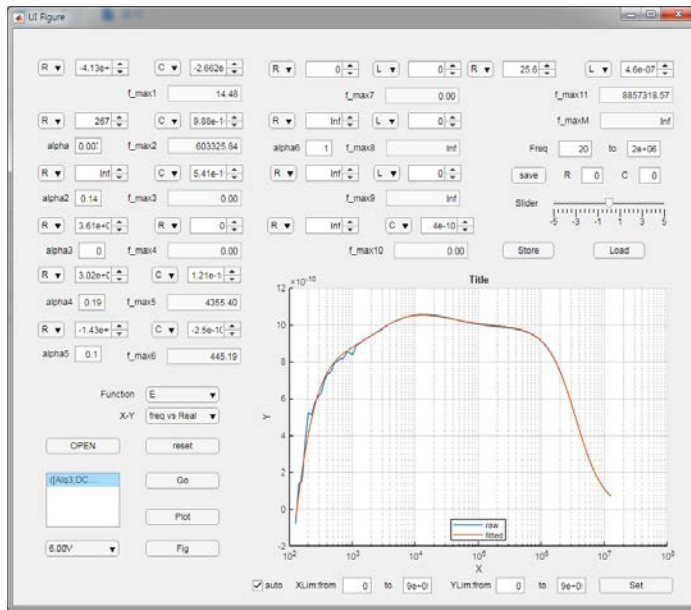
(a)



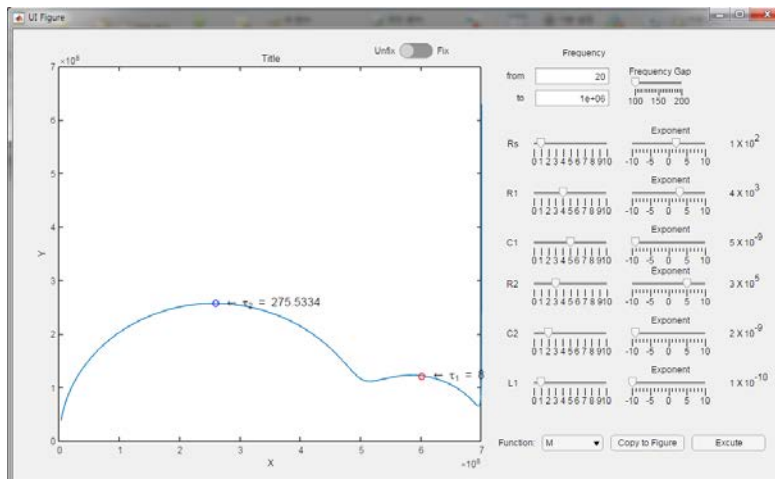
(b)

**Figure A.1** Impedance spectroscopy Analyzer by Hyunjong (a) main interface (b)

transient window of each parameter



(a)



(b)

**Figure A.2** Impedance constructor with CPE by Hyunjong (a) main interface (b)

CPE time constant extractor



### **Fitting algorithm using MATLAB**

Since each parameter of the impedance affects each other, when extracting a new parameter, the previous parameter is affected. It is not easy to take all of these effects into account with the simple CLNS approach. Therefore, a new algorithm is developed and the flowchart for the algorithm is written as figure A.5.

Find the most easily found RC element at first. Then, at the impedance that removed the first RC element, find the next dominant RC element in a similar way. When you combine these two things, an error will always appear. Again compensates for errors in the first RC element. It then repeats this in the second and third elements and recursively repeats until the overall impedance error is the smallest. These algorithms find the closest RC component value to the measured impedance response.

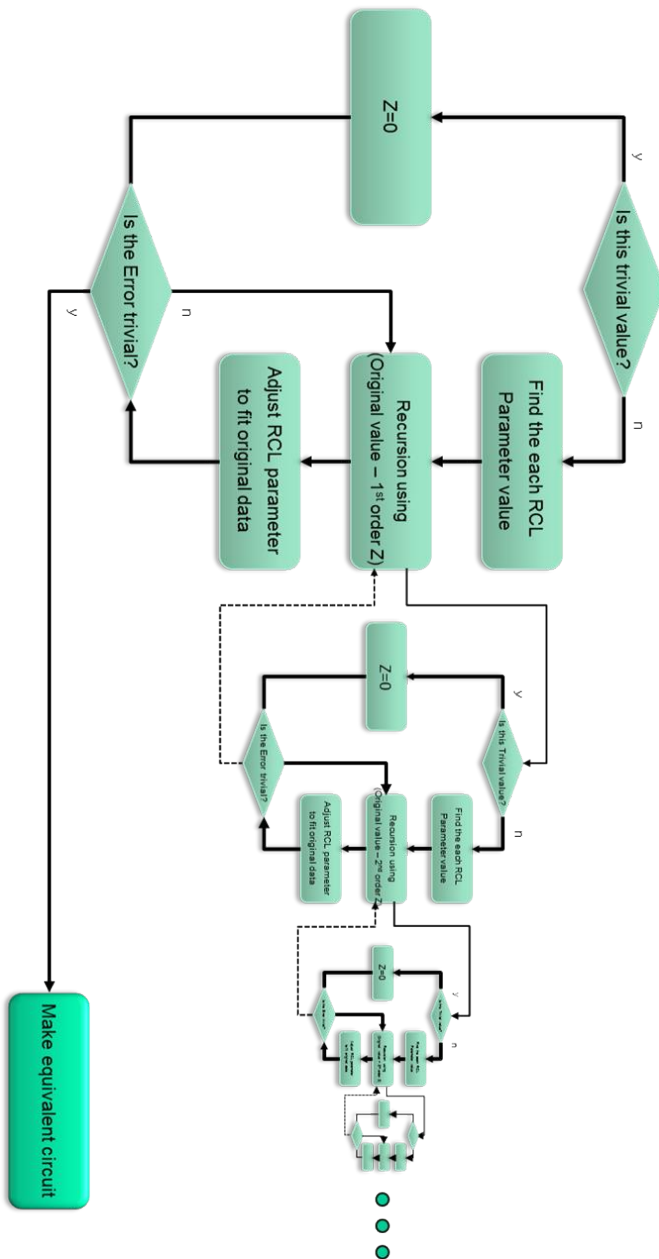


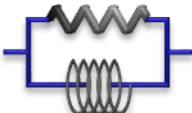


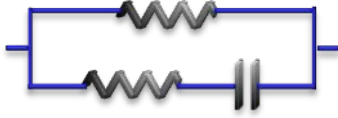
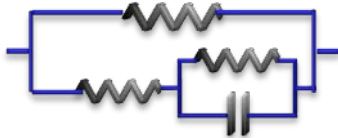
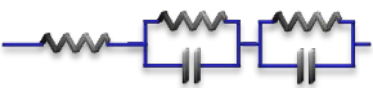
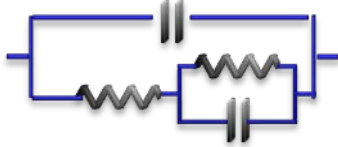


Figure A.5 Recursion programming flow chart to extract more precise

**Passive parametric representations of equivalent circuits expressed in impedance**

	$Z_{1st} = R \parallel \frac{1}{sC} = \frac{1}{\frac{1}{R} + sC} = \frac{A}{s + \alpha} \quad \dots (A = 1/C, \alpha = 1/RC)$
	$Z_{2nd} = R + \frac{1}{sC} = \frac{sRC + 1}{sC} = A \frac{s + \alpha}{s} \quad \dots (A = R, \alpha = 1/RC)$
	$Z_{3rd} = R \parallel sL = \frac{1}{\frac{1}{R} + \frac{1}{sL}} = \frac{As}{s + \alpha} = A - \frac{A\alpha}{s + \alpha} \quad \dots (A = R, \alpha = R/L)$
	$Z_{4th} = R + sL = A(s + \alpha) \quad \dots (A = 1/L, \alpha = R/L)$

**Table A.1** Impedance response formula of basic circuit for complex plane analysis

	$Z_{5th} = R + Z_{1st} = A' + \frac{A}{s + \alpha} = A \frac{s + \beta}{s + \alpha}$
	$Z_{6th} = R \parallel Z_{2nd} = \left( A' + A \frac{s}{s + \alpha} \right)^{-1} = A \frac{s + \beta}{s + \alpha} = A' + \frac{A}{s + \alpha}$
	$Z_{7th} = R \parallel Z_{5st} = \left( R^{-1} + A \frac{s + \alpha}{s + \beta} \right)^{-1} = \left( A \frac{s + \alpha}{s + \beta} \right)^{-1}$ $= A \frac{s + \beta}{s + \alpha} = A' + \frac{A}{s + \alpha}$
	$Z_{8th} = R + Z_{1st} + Z_{1st} = A' + \frac{A}{s + \alpha} + \frac{B}{s + \beta}$
	$Z_{9th} = 1/sC \parallel Z_{5st} = \left( sC + A \frac{s + \alpha}{s + \beta} \right)^{-1} = \left( A \frac{s^2 + \alpha s + \beta'}{s + \beta} \right)^{-1}$ $= A \frac{s + \beta'}{(s + \alpha)(s + \beta)} = \frac{A}{s + \alpha} + \frac{B}{s + \beta}$

**Table A.2** Impedance response formula of complex circuit for complex plane analysis

# Bibliography

- [1] Laux, S.E. and K. Hess, *Revisiting the analytic theory of pn junction impedance: Improvements guided by computer simulation leading to a new equivalent circuit*. IEEE Transactions on Electron Devices, 1999. **46**(2): p. 396-412.
- [2] Tang, C.W. and S.A. VanSlyke, *Organic electroluminescent diodes*. Applied Physics Letters, 1987. **51**(12): p. 913-915.
- [3] Bernanose, A., M. Comte, and P. Vouaux, *A new method of emission of light by certain organic compounds*. J. Chim. Phys, 1953. **50**: p. 64-68.
- [4] Bernanose, A. and P. Vouaux, *Organic electroluminescence type of emission*. J. Chim. Phys, 1953. **50**: p. 261.
- [5] Bernanose, A., *The mechanism of organic electroluminescence*. Journal of Chemical Physics, 1955. **52**: p. 396-400.
- [6] Pope, M., H. Kallmann, and P. Magnante, *Electroluminescence in organic crystals*. The Journal of Chemical Physics, 1963. **38**(8): p. 2042-2043.
- [7] Helfrich, W. and W. Schneider, *Recombination radiation in anthracene crystals*. Physical Review Letters, 1965. **14**(7): p. 229.
- [8] Tsujimura, T., *OLED display fundamentals and applications*. 2017: John Wiley & Sons.
- [9] Schlaf, R., H. Murata, and Z. Kafafi, *Work function measurements on indium tin oxide films*. Journal of Electron Spectroscopy and Related Phenomena, 2001. **120**(1-3): p. 149-154.
- [10] Koch, N., et al., *Conjugated organic molecules on metal versus polymer*

- electrodes: Demonstration of a key energy level alignment mechanism.* Applied Physics Letters, 2003. **82**(1): p. 70-72.
- [11] Ishii, H., et al., *Energy level alignment and interfacial electronic structures at organic/metal and organic/organic interfaces.* Advanced materials, 1999. **11**(8): p. 605-625.
- [12] Campbell, I., et al., *Controlling Schottky energy barriers in organic electronic devices using self-assembled monolayers.* Physical Review B, 1996. **54**(20): p. R14321.
- [13] Hamada, Y., et al., *Blue-light-emitting organic electroluminescent devices with oxadiazole dimer dyes as an emitter.* Japanese journal of applied physics, 1992. **31**(6R): p. 1812.
- [14] Hung, L. and C. Chen, *Recent progress of molecular organic electroluminescent materials and devices.* Materials Science and Engineering: R: Reports, 2002. **39**(5-6): p. 143-222.
- [15] Shen, J., et al., *Degradation mechanisms in organic light emitting diodes.* Synthetic metals, 2000. **111**: p. 233-236.
- [16] Burrows, P., et al., *Reliability and degradation of organic light emitting devices.* applied physics letters, 1994. **65**(23): p. 2922-2924.
- [17] Zardareh, S.Z. and F.A. Boroumand, *Degradation in organic light emitting diodes.* World Academy of Science, Engineering and Technology, 2009. **38**: p. 274-277.
- [18] Chou, H.H. and C.H. Cheng, *A highly efficient universal bipolar host for blue, green, and red phosphorescent OLEDs.* Advanced Materials, 2010. **22**(22): p. 2468-2471.
- [19] Mitschke, U. and P. Bäuerle, *The electroluminescence of organic materials.* Journal of Materials Chemistry, 2000. **10**(7): p. 1471-1507.
- [20] Rajan, G., et al., *Study of injection and transport properties of metal/organic interface using HAT-CN molecules as hole injection layer.* Vacuum, 2017. **146**: p. 530-536.
- [21] Qi, Y., et al., *A molybdenum dithiolene complex as p-dopant for hole-*

- transport materials: a multitechnique experimental and theoretical investigation*. Chemistry of Materials, 2009. **22**(2): p. 524-531.
- [22] Tang, C.W., S.A. VanSlyke, and C. Chen, *Electroluminescence of doped organic thin films*. Journal of Applied Physics, 1989. **65**(9): p. 3610-3616.
- [23] Nicollian, E.H., J.R. Brews, and E.H. Nicollian, *MOS (metal oxide semiconductor) physics and technology*. Vol. 1987. 1982: Wiley New York et al.
- [24] Heiman, F.P. and G. Warfield, *The effects of oxide traps on the MOS capacitance*. IEEE Transactions on Electron Devices, 1965. **12**(4): p. 167-178.
- [25] Huang, C.-L. and G.S. Gildenblat, *MOS flat-band capacitance method at low temperatures*. IEEE Transactions on Electron Devices, 1989. **36**(8): p. 1434-1439.
- [26] Hoffmann, K., *System integration: From transistor design to large scale integrated circuits*. 2006: John Wiley & Sons.
- [27] Ehrenfreund, E., et al., *Negative capacitance in organic semiconductor devices: Bipolar injection and charge recombination mechanism*. Applied physics letters, 2007. **91**(1): p. 012112.
- [28] Bisquert, J., et al., *Negative capacitance caused by electron injection through interfacial states in organic light-emitting diodes*. Chemical Physics Letters, 2006. **422**(1-3): p. 184-191.
- [29] Pingree, L., et al., *Negative capacitance in organic light-emitting diodes*. Applied Physics Letters, 2005. **86**(7): p. 073509.
- [30] Gommans, H., M. Kemerink, and R. Janssen, *Negative capacitances in low-mobility solids*. Physical Review B, 2005. **72**(23): p. 235204.
- [31] Gommans, H., et al., *Charge transport and trapping in Cs-doped poly (dialkoxy-p-phenylene vinylene) light-emitting diodes*. Physical Review B, 2004. **69**(15): p. 155216.
- [32] Hulea, I., et al., *Effect of dye doping on the charge carrier balance in PPV light emitting diodes as measured by admittance spectroscopy*. Applied

- physics letters, 2003. **83**(6): p. 1246-1248.
- [33] Martens, H., *HCF Martens, JN Huiberts, and PWM Blom, Appl. Phys. Lett. 77, 1852 (2000)*. Appl. Phys. Lett., 2000. **77**: p. 1852.
- [34] Kim, S.H., et al., *Conduction mechanism of organic semiconductor AlQ3: Impedance spectroscopy analysis*. Current Applied Physics, 2005. **5**(1): p. 35-37.
- [35] Park, H., et al., *Impedance spectroscopy analysis of organic light-emitting diodes fabricated on plasma-treated indium-tin-oxide surfaces*. Journal of Korean Physical Society, 2007. **51**: p. 1011.
- [36] Kowal, J., D. Hente, and D.U. Sauer, *Model parameterization of nonlinear devices using impedance spectroscopy*. IEEE Transactions on Instrumentation and Measurement, 2009. **58**(7): p. 2343-2350.
- [37] Nam, E., et al., *Electroluminescence and impedance analyses of organic light emitting diodes using anhydride materials as cathode interfacial layers*. Thin Solid Films, 2009. **517**(14): p. 4131-4134.
- [38] Nowy, S., et al., *Impedance spectroscopy as a probe for the degradation of organic light-emitting diodes*. Journal of Applied Physics, 2010. **107**(5).
- [39] Okachi, T., et al., *Equivalent circuits of polymer light-emitting diodes with hole-injection layer studied by impedance spectroscopy*. Thin Solid Films, 2008. **517**(4): p. 1327-1330.
- [40] Pingree, L., et al., *Field dependent negative capacitance in small-molecule organic light-emitting diodes*. Journal of applied physics, 2006. **100**(4): p. 044502.
- [41] Mora-Seró, I., et al., *Implications of the Negative Capacitance Observed at Forward Bias in Nanocomposite and Polycrystalline Solar Cells*. Nano Letters, 2006. **6**(4): p. 640-650.
- [42] Pingree, L.S.C., et al., *Negative capacitance in organic light-emitting diodes*. Applied Physics Letters, 2005. **86**(7).
- [43] Cole, K.S. and R.H. Cole, *Dispersion and absorption in dielectrics I. Alternating current characteristics*. The Journal of chemical physics, 1941.



- 9(4): p. 341-351.
- [44] Randles, J.E.B., *Kinetics of rapid electrode reactions*. Discussions of the faraday society, 1947. **1**: p. 11-19.
- [45] Macdonald, J.R. and L.D. Potter Jr, *A flexible procedure for analyzing impedance spectroscopy results: Description and illustrations*. Solid State Ionics, 1987. **24**(1): p. 61-79.
- [46] Barsoukov, E. and J.R. Macdonald, *Impedance spectroscopy: theory, experiment, and applications*. 2018: John Wiley & Sons.
- [47] Chang, H.C. and G. Jaffe, *Polarization in electrolytic solutions. Part I. Theory*. The Journal of Chemical Physics, 1952. **20**(7): p. 1071-1077.
- [48] Macdonald, J.R., *Theory of ac space-charge polarization effects in photoconductors, semiconductors, and electrolytes*. Physical Review, 1953. **92**(1): p. 4.
- [49] Friauf, R.J., *Polarization effects in the ionic conductivity of silver bromide*. The Journal of Chemical Physics, 1954. **22**(8): p. 1329-1338.
- [50] Macdonald, J.R. and J. Garber, *Analysis of impedance and admittance data for solids and liquids*. Journal of the Electrochemical Society, 1977. **124**(7): p. 1022-1030.
- [51] Macdonald, J.R., J. Schoonman, and A. Lehnen, *Applicability and power of complex nonlinear least squares for the analysis of impedance and admittance data*. Journal of Electroanalytical Chemistry and Interfacial Electrochemistry, 1982. **131**: p. 77-95.
- [52] Macdonald, D., et al., *The Electrochemical Impedance of Porous Nickel Electrodes in Alkaline Media II. Nonuniform Transmission Line Analysis*. Journal of The Electrochemical Society, 1991. **138**(5): p. 1359-1363.
- [53] Debye, P.J.W., *collected papers of Peter JW Debye*. 1954.
- [54] Berleb, S., W. Brütting, and G. Paasch, *Interfacial charges and electric field distribution in organic hetero-layer light-emitting devices*. Organic Electronics, 2000. **1**(1): p. 41-47.
- [55] Van der Ziel, A., *Fluctuation phenomena in semi-conductors*. 1959:

Butterworths scientific publications.

- [56] Ishihara, S., et al., *Demonstration of determination of electron and hole drift-mobilities in organic thin films by means of impedance spectroscopy measurements*. Thin Solid Films, 2014. **554**: p. 213-217.
- [57] Okachi, T., et al., *Determination of Charge-Carrier Mobility in Organic Light-Emitting Diodes by Impedance Spectroscopy in Presence of Localized States*. Japanese Journal of Applied Physics, 2008. **47**(12): p. 8965-8972.
- [58] Jonscher, A.K., *The physical origin of negative capacitance*. Journal of the Chemical Society, Faraday Transactions 2: Molecular and Chemical Physics, 1986. **82**(1): p. 75-81.
- [59] Ershov, M., et al., *Negative capacitance effect in semiconductor devices*. IEEE Transactions on Electron Devices, 1998. **45**(10): p. 2196-2206.
- [60] Nowy, S., et al. *Impedance spectroscopy of organic hetero-layer OLEDs as a probe for charge carrier injection and device degradation*. in *SPIE Photonic Devices+ Applications*. 2009. International Society for Optics and Photonics.

# Publications

## Journal Papers (SCI)

- [1] **H. Kim**, S. Kim, and Y. Hong\*, "Frequency Dependency of Multi-layer OLED Current Density-voltage Shift and Its Application to Digitally-driven AMOLED", Journal of the Optical Society of Korea, 16, 181 (2012) (SCI-E)
  
- [2] J. Byun†, B. Lee†, E. Oh, **H. Kim**, S. Kim, S. Lee, and Y. Hong\*, "Fully printable, strain-engineered electronic wrap for customizable soft electronics", Scientific Reports, 7, 45328 (2017)
  
- [3] S. Kim, S. Choi, E. Oh, J. Byun, **H. Kim**, B. Lee, S. Lee, and Y. Hong\*, "Revisit to three-dimensional percolation theory: Accurate analysis for highly

stretchable conductive composite materials", Scientific Reports, 6, 34632

(2016)

[4] Y. Joo, J. Byun, N. Seong, J. Ha, **H. Kim**, S. Kim, T. Kim, H. Im, D. Kim, Y.

Hong\*, "Silver Nanowire-embedded PDMS with Multiscale Structure for Highly Sensitive and Robust Flexible Pressure Sensor", Nanoscale, 7, 6208

(2015)

[5] **H. Kim**, G. Kim, and Y. Hong\*, "OLED Operation Analysis via Voltage and

Frequency Sweep Impedance Spectroscopy", in preparation

[6] **H. Kim**, G. Kim, and Y. Hong\*, "OLED Operation Analysis via Bias-Stress

Impedance Spectroscopy", in preparation

## International Conference

- [1] **H. Kim**, J. Yang, S. Ye, C. Lee, and Y.Hong\*, “OLED degradation mechanism study using impedance spectroscopy,” IMID/IDMC/Asia Display, Oct. 13-17, 2008. (oral)
  
- [2] **H. Kim**, S. Kim, S.W. Chang, D. Lee, D.S. Jeong, H.K. Chung, and Y.Hong \*, “Frequency dependence of OLED voltage shift degradation,” IMID '07, Aug. 2007 (oral)
  
- [3] **H. Kim** and Y.Hong \*, “Degradation Behavior of OLED under Analog and Digital Driving Conditions,” The 4th International Workshop on Nanoscale Semiconductor Devices, Apr. 5-6, 2007. (poster)
  
- [4] Y. Hong\*, B. Lee, J. Byun, E. Oh, J. Yoon, **H. Kim**, S. Choi, H. Cho " Strain-engineered Platform Technology for Stretchable Hybrid Electronics", SID Display Week 2018, Los Angeles, May (2018)

- [5] Y. Hong\*, B. Lee, J. Byun, E. Oh, **H. Kim**, S. Kim, S. Lee, D. Kim, and J. Yoon, "Key Enabling Technology for Stretchable LED Display and Electronic System ", SID Display Week 2017, Los Angeles, May (2017)
- [6] **H. Kim**, S. Kim, S. Choi, J. Byun, B. Lee, E. Oh, and Y. Hong\*, "Chip mounting technology for stretchable electronic system", The 16th International Meetings on Information Display (IMID 2016), Jeju, Korea, August (2016)
- [7] B. Lee, J. Byun, E. Oh, **H. Kim**, S. Kim and Y. Hong\*, "All-Ink-Jet-Printed Wearable Information Display Directly Fabricated onto an Elastomeric Substrate", SID Display Week 2016, San Francisco, May (2016)
- [8] J. Byun, B. Lee, E. Oh, S. Kim, **H. Kim**, S. Choi and Y. Hong\*, "Stretchable and Deformable LED Configurations Based on Inkjet-Printed Chip-Bonding Technology", The 15th international Meetings on Information Display (IMID 2015), Daegu, Korea, August (2015)

## Domestic

- [1] 홍용택 \*, 김현중, 양지훈, 전기적 분석법을 이용한 유기 발광 다이오드의 특성 연구,” 광전자 및 광통신 학술대회, May 13-15, 2009 (초청논문)
- [2] 김현중, 노승욱, 이창희, 홍용택, “주파수에 따른 임피던스 변화를 이용한 OLED 소자의 열화 분석,” 대한전자공학회 추계 학술대회, Nov. 24 2007 (oral)
- [3] H. Kim, G. Kim, Y. Hong\*, “Relations between Average Transition Time and Negative Capacitance”, The 19th Korea Liquid Crystal Conference (KLCC 2018), January (2018) (poster)

# 초 록

본 논문은 임피던스 분광법을 이용한 유기 발광 다이오드의 특성 분석 방법에 대한 연구이다. 일반적으로 유기 발광 소자는 TCO (Transparent Conductive Oxide)와 금속 전극 사이에 발광에 필요한 유기 물질이 얇게 적층된 구조를 갖는다. 유기 물질의 화학적 취약성과 헤테로 접합의 복잡성으로 인해 파괴적인 방식 보다는 비파괴 방식으로 제조된 유기 발광 다이오드의 특성을 조사해야 한다. 고전적으로, 전류-전압계를 사용하여 전류-전압 곡선을 측정하고 휘도 계를 사용하여 발광을 측정하는 방법이 OLEDs의 특성을 평가하는데 사용된다. 그러나 OLEDs의 인터페이스 상태 또는 캐리어 동역학에 대한 세부 사항을 조사하기 위해서는 작동 조건 하에서의 임피던스 응답을 측정해야 한다

일반적인 고체 물리에서의 임피던스 분석 방법은 커패시턴스에 주로 초점을 맞추고 있는 반면에, 임피던스 분광법 (IS)은 miliherz 에서 megahertz의 주파수 범위에서 모든 임피던스 응답을 다루는 것이 특징이다. 이를 통해 분해능이 높은 등가 회로를 구성하고 각각 측정된 임피던스를 면밀히 분석 할 수 있다. 각 임피던스는 작동 직류 전압을 결정한



후 교류 소신호를 인가하여 측정되는데, 이 작동 직류 전압과 교류 소신호는 소자의 동작을 적절히 설명하기 위해 전략적으로 선택되어야 한다.

제 1 장에서는 임피던스 분광 분석의 개요를 소개하고 임피던스 측정 방법의 배경을 설명한다. 그리고 임피던스 분석 방법을 OLEDs에 적용하려는 동기에 대해서 설명하고 임피던스 분광학을 통해 OLEDs의 특성을 분석하는 다양한 방법들이 논의된다.

제 2 장은 OLEDs의 임피던스 분석 방법에 대해 이전에 보고된 논문을 검토하고 이들 논문의 한계를 설명한다. 특히, 이전에 과소평가된 확산 캐패시턴스의 기여는 OLEDs의 특성을 결정할 때 오류를 방지하는데 매우 중요하다는 것을 보여줄 것이다. 이러한 확산 용량을 설명하기 위해 Laux & Hess 모델이 적용되었다. 이 모델은 잔류 전류에 대한 임피던스 응답을 매우 잘 설명 할 수 있고 심지어 음의 캐패시턴스 현상도 잘 설명해 준다. Laux & Hess 모델을 사용한 분석 결과는 작동 중의 OLEDs의 특성을 잘 묘사 하고 있음을 보였고 이 모델의 분석 방법을 위한 근사 프로세스를 제안하였다.

제 3 장에서는 ITO/a-NPD[N,N' -Bis(naphthalen-1-yl)-N,N' -bis(phenyl)-2,2' -dimethylbenzidine]/Alq3[Tris-(8-hydroxyquinolato)aluminum]/LiF/Al 형 OLED를 제작하여 제 2 장에서 제안된 개선된 임피던스 분석법을 사용하여 조사하였다. 먼저, 구조적 (두께) 변화에 따른 임피던스 응답의 변화를 측정하여 물리적, 정량적 해

석이 수행되었다. 높은 주파수에서 측정된 임피던스는 OLEDs의 인터페이스 및 버크 특성을 나타내며 저주파수에서의 임피던스는 OLEDs의 캐리어의 동적 이동을 설명한다.

또한 OLEDs의 열화로 인한 임피던스 변화를 분석하였다. 본 논문에서 제안된 Impedance Spectroscopy Analysis 방법을 사용하면, 열화의 원인으로서 계면과 버크의 상태 변화가 정확하고 효과적으로 분리될 수 있다. 결과는 HTL/EML의 인터페이스 트랩 효과에 대한 기존 해석을 강화하는 것으로 나왔고 추출된 임피던스 값의 변화율을 추적할 수 있음을 보여 주었다.

4 장에서는 이 논문에서 사용된 OLEDs를 분석하기 위한 프로그램 도구를 간략하게 소개하고 수식에 대한 부록을 첨부했다. 그리고 향후 이 임피던스 분광학 분석을 산업에 적용시킬 가능성에 대해 논의하고 요약하도록 하겠다.

주요어 : 유기 발광 다이오드, 임피던스 분광 분석법(IS), 등가회로 모델링, 열화, 확산 캐패시턴스, 음의 캐패시턴스

학번: 2014-30311